RSNA 2023 Edition

UNITED IMAGING

Issue Highlights

Deep Learning-Based Reconstruction of Coronary CT Angiography in Patients with Diverse Anatomical and Pathological Complexities

Dijia Wu, et al.
Page 08

Clinical Evaluation of Advanced Algorithms for CCTA: A Focus on High BMI and Elevated Heart Rate Populations

John Osborne, et al.
Page 24

A Vision for Magnetic Resonance Imaging to Assess Cardiotoxicity

Mary P. Watkins, et al.
Page 47

Expert Interview: Cardiac Imaging, Inc. Interview with Jens Huettges

Jens Huettges
Page 63

Disclaimer

The articles contained in this magazine are provided solely by the authors, and the author(s) of each article appearing in this magazine is/are solely responsible for the content thereof as well as personal data, which is used anonymously or in compliance with applicable data privacy laws or regulations. United Imaging Healthcare makes no representation or warranties, expressly or impliedly, with respect to the accuracy, timeliness, reliability, legitimacy, applicability, fitness, originality, or completeness of the contents of this magazine. United Imaging Healthcare assumes no legal responsibility or liability for any error, omission, or illegality with respect to the material contained within.

All articles contained in this magazine only represent the opinions and views of the authors and do not implicitly or explicitly represent any official positions or policies, or medical opinions of United Imaging Healthcare or the institutions with which the authors are affiliated unless this is clearly specified. Discussions of any brand, services, or products in the magazine should not be construed as promotion or endorsement thereof.

Articles published in this magazine are intended to inspire further general scientific research, investigation, understanding, and discussion only and are not intended to and should not be relied upon as recommending or promoting a specific medical advice, method, diagnosis, or treatment by physicians for any particular individual, nor to replace the advice of a physician or other healthcare professional. Any individual wishing to apply the information in this magazine for the purposes of improving their own health should not do so without consulting with a qualified medical practitioner. All patients need to be treated in an individual manner by their personal medical advisors. The decision to utilize any information in this magazine is ultimately at the sole discretion of the reader, who assumes full responsibility for any and all consequences arising from such a decision. United Imaging Healthcare makes no representations or warranties with respect to any treatment, action, or application of medication or preparation by any person following the information offered or provided within or through the magazine.

The articles included in this magazine may contain work in progress, which represents ongoing research and development. Such technologies are not available for sale in China or the United States for clinical use and also may not be available for such sales in other countries.

Please note that the magazine is intended to be distributed within a limited scope.

If you have any questions about the magazine, or simply wish to reach out to us for any other reasons, you may contact us at: compliance@united-imaging.com

Editorial Board

Dr. Gregory Lanza, M.D., PhD
Guest Editor

Lingzhi (Lance) Hu, Ph.D.
Editor-in-Chief

Dileep Kumar, Ph.D.
Associate Editor

Adam Chandler, Ph.D.
Associate Editor

Editors/Reviewers

Akash Gandhamal, Ph.D.
Editor/Reviewer

Yongfeng Gao, Ph.D.
Editor/Reviewer

Morgan Wang, M.D., Ph.D.
Editor/Reviewer

Joshua H Wiley
Editor/Reviewer

Dharmesh Singh, Ph.D.
Editor/Reviewer

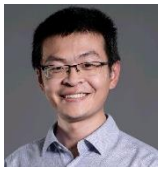

Shuheng Zhang, M.S.
Reviewer-MR

Yun Dong, Ph.D.
Reviewer-MI

Zhong Xue, Ph.D.
Reviewer-AI

Patrick Kling, Ph.D.
Reviewer-CT

Contributors

Legal & Compliance

Lina Sun

Cyndi Baily, J.D.

Marketing & Communication

Krista K. Stein

Norren C. Coombs

Brand Communication & visual Design

Xiaojing Cheng

Yang Zhong

Page 04

Editorial: Optimizing Advanced Imaging Technologies through Artificial Intelligence Innovations to Address the World-Wide Cardiovascular Disease Pandemic
Gregory M. Lanza

Page 08

Deep Learning-Based Reconstruction of Coronary CT Angiography in Patients with Diverse Anatomical and Pathological Complexities
Dijia Wu, et al.

Page 18

Clinical Significance of Coronary Artery Calcium Score in Predicting Coronary Artery Disease: A CT Coronary Angiography Study
Anand H. K., et al.

Page 24

Clinical Evaluation of Advanced Algorithms for CCTA: A Focus on High BMI and Elevated Heart Rate Populations
John Osborne, et al.

Page 32

Myocardial Perfusion Imaging by PET with Myocardial Blood Flow is Proving to be the Gatekeeper for Identifying Physiologic Severity of CAD by Guiding Treatment with Invasive Procedures and Revascularization – So Why is Adoption Limited?
Amanda Roby

Page 40

Role of Cardiac T1, T2 Mapping and Extracellular Volume in the Diagnosis of Clinical Cardiomyopathies
Kamal Aggarwal, et al.

Page 47

A Vision for Magnetic Resonance Imaging to Assess Cardiotoxicity
Mary P. Watkins, et al.

Page 54

Free-Breathing Simultaneous Cardiac Multi-Parametric Mapping: Technical Developments and Initial Clinical Experience
Haikun Qi, et al.

Page 63

Expert Interview: Cardiac Imaging, Inc. Interview with Jens Huettges
Jens Huettges

Optimizing Advanced Imaging Technologies through Artificial Intelligence Innovations to Address the World-Wide Cardiovascular Disease Pandemic

Gregory M. Lanza, M.D., Ph.D., FACC
Washington University Medical School, St. Louis, MO

We all die of something! Indeed, cardiovascular disease (CVDs) deaths have almost become normalized as a likely cause of death globally. Nearly 18 million people, 32% of all deaths worldwide, were related to CVD in 2019. In broad strokes, cardiac mortality can be attributed to ischemic (i.e., 85%) or nonischemic and arrhythmogenic causes, the latter broadly occurring among all categories of CV disease. Importantly, three-quarters of the victims of CV disease occur in populations of low- and middle-income countries. Clearly, cardiovascular diseases can be ameliorated by addressing behavioral risk factors such as tobacco use, unhealthy diet and obesity, physical inactivity and harmful use of alcohol, but the answer is not so straightforward as myriad genetics and epigenetic factors account for a substantial portion of the outcome variability. Consequently, our overarching goal as physicians is to detect and characterize the onset of cardiovascular disease as early possible to allow an opportunity to intervene with counselling and medicines as well as surgeries and device-related therapies when necessary.

Cardiovascular imaging is a cornerstone of cardiac diagnosis and management, with echocardiography becoming a screening gateway modality to advanced imaging techniques that provide further characterization to diagnose disease and to quantify therapeutic responses serially. Artificial Intelligence (AI)- and Deep-learning (DL) enhanced point-of-care ultrasound technologies are rapidly emerging to allow global assessments of myocardial health in emergency departments and at the bedside in hospitals, in rural communities and increasingly in remote regions of the world. Democratization of advanced imaging techniques has been stifled by imaging related costs, technologist training and availability, and image data processing resources. Extending the benefits of advance imaging beyond tertiary healthcare institutions to smaller hospitals and outpatient centers nationally and to middle- and low-income countries internationally is the fundamental unmet need to reduce global CV deaths. United Imaging Healthcare and United Imaging Intelligence have accepted this world CVD challenge, which is increasingly reflected in AI and DL-enabled innovations for computed tomography (CT), nuclear medicine (NM, PET/CT, PET/MR) and cardiac magnetic resonance imaging (cMRI).

Cardiovascular related deaths are dominated by vascular diseases of the heart (coronary and microvasculature), and the large great vessels. Diagnostic cardiac catheterization was introduced by André Cournand and Dickinson Richards in the 1940s, followed by selective coronary angiography by Mason Sones in the 1960s. With the advent of catheter-based interventions, pioneered by Andreas Gruentzig in the 1970s. In the last 50 years, there has been tremendous progress in the refinement and expansion of these techniques. Today, percutaneous coronary intervention (PCI) access is through the femoral and the radial arteries. Coincidently, never ending development of interventional technologies have emerged from discrete single coronary artery (CA) lesions procedures to left main CA interventions, and more recently to multivessel coronary disease cases with risks too high for surgical solutions.

Cardiac catheterization is traditionally compartmentalized into two phases: diagnostic and interventional procedures. Initially, diagnostic cardiac catheterization delineated the coronary vascular bed anatomy to assess the extent of atherosclerotic disease and to identify significant intervenable flow-limiting lesions. Over time eyeball assessments of lesions gave way to direct measurements of stenosis relative to adjacent “normal” segments. The development of wire based Doppler flow assessments

(Fractional Flow Reserve (FFR), and later Instantaneous wave - Free Ratio (iFR)) led to an anatomical – physiology based assessment of lesion significance and the potential for improvement after revascularization. These data, obtained on the cath lab table, informed referrals to interventional specialists and surgeons for subsequent revascularization. Diagnostic catheterization procedures are still performed in most interventional cardiology programs, but developments in Cardiac CT coronary angiography are rapidly becoming a preferred way to risk-stratify patients for revascularization.

In this issue of United Imaging uINNOVATION-GLOBAL 2023, Dijia Wu and Jiayin Zhang (UII Shanghai, China) describe the role of Deep Learning-based Reconstruction of Coronary CT Angiography (CCTA) for Patients with Diverse Anatomical and Pathological Complexities. As is the case for most advanced imaging techniques, CCTA image post-processing reconstruction is time-consuming and interpretation is complicated by complex anatomy, such as chronic total occlusion (CTO), anomalous coronary anatomy, by-pass grafts, stents and calcifications. Advanced multi-row CT detector arrays are now offered by all vendors. The uCT 960+ with its 320 row detector and 250msec full heart acquisition represents the penultimate CT scanner in the UIH line. These authors delineate the DL-assisted image processing model, uAI® Discover Coronary CT solution and its two main components: a Spatial Anatomical Dependency (SAD) module and the Hierarchical Topology Learning (HTL) module.

Coronary artery calcium scoring (CACS) is assessed noninvasively with cardiac CT to provide estimates of calcified plaque as a biomarker of atherosclerotic plaque build-up and cardiovascular risk. Endorsed by the American College of Cardiology, CACS can help guide the use cholesterol reducing medications as well as suggest the benefit for additional stress-testing. Drs. Anand, Ramachandra, Pooja, Raju, Gandhamal, and Kumar share results of a CTA study involving 153 patients to assess the Clinical Significance of CAC score in Predicting Coronary Artery Disease. They describe the clinical relevance of combination of CT-coronary angiogram and CACS calculations as an initial screening method for patients with mild to moderate symptoms and as a gateway to timely intervention.

While CCTA is a welcome front-end addition to coronary artery screening and disease management, patients who are obese or present with high heart rates are challenging. The diagnostic efficacy of CCTA in high base mass index (BMI) patients can be compromised by image noise, reduced spatial resolution, and diminished contrast-to-noise ratio. Also, high heart rates can lead to motion artifacts, blurring, and incomplete vessel opacification, which further compromise image data accuracy and precision. In this issue of uINNOVATION-GLOBAL 2023, Drs. Osborne, Surapeneni, Murdock, and Gao address these issues in their report entitled Clinical Evaluation of Advanced Algorithms for CCTA: A Focus on High BMI and Elevated Heart Rate Populations. This report describes three new and interrelated processes, Auto ALARA. CardioXphase and CardioCapture. Human exposure is constrained to as low as reasonably achievable (ALARA), which is the radiation safety standard for all X-ray and nuclear techniques. AutoALARA is an automatic exposure control algorithm to automatically adjust X-ray tube voltage and current to optimize image quality while minimizing radiation dose. CardioXphase algorithm adopts the best phase selection method for a multi-phase reconstruction step with a focus on coronary arteries using a small Field of View (FOV) and reduced matrix size. CardioCapture involves an innovative AI-driven motion correction module that is focused in the vicinity of the coronary arteries. An advanced imaging pilot study is reported that endorses the significance and potential of individually tailoring advanced algorithms to address specific challenges among high-risk atherosclerotic patients with coronary disease.

Advanced coronary interventions have evolved from an initial ocular reflexive phase, i.e., “see a lesion – stent a lesion”, to Doppler-enabled physiologic culprit lesion assessments, and to remodeling of complex coronary arterial plaque segments employing intravascular ultrasound, intravascular optical coherence tomography, intravascular lithotripsy, plaque atherectomy, balloon angioplasty, and stenting. CT angiography delineates the vascular lumen and provides an assessment of intramural calcifications, but it does not provide significant noninvasive insight into the intricacies of plaque disease.

uINNOVATION-GLOBAL 2023 highlights two discussions

regarding PET/CT. The first by Amanda Roby entitled Myocardial Perfusion Imaging by PET with Myocardial Blood Flow is Proving to be the Gatekeeper for Identifying Physiologic Severity of CAD by Guiding Treatment with Invasive Procedure and Revascularization – so Why is Adoption Limited? The author acknowledges the resource and skill barriers entailed in initiating an MPI patient care center and contends that the efficiency cost savings are possible with improved physician and technologist collaboration to achieve optimal benefit. The second article is an Expert Interview with Jens Huettges (CTO, Cardiac Imaging, Inc). In this discussion, Jens Huettges describes the mobile cardiac imaging business, the ability of mobility to reach communities with poor access to advanced PET/CT cardiovascular imaging, the attributes of PET perfusion needed for high quality images, and the future of the modality.

Finally but not least, three papers address cardiac MRI, which is among the most promising tools for cardiac imaging, not only for questions unresolved by technically challenged echocardiography studies and quantitative structure-function-strain data but also for myocardial texture analysis. Myocardial texture analysis is the key approach for assessing tissue infiltrating diseases, including myocarditis, amyloidosis, and now cardiac fibrosis. Drs. Qi and Lyu provide a paper entitled Free-breathing Simultaneous Cardiac Multi-parameter Mapping: Technical Developments and Initial Clinical Experience. In typical practice, T1 and T2 relaxation mapping require a breath hold for each slice. While a single slice does not overwhelm a patient, it introduces significant sampling error and relatively poor estimates. Pathology development is nonhomogeneous at first among and within slices. Nine slices are often needed to cover the entire heart, which requires 18 breath holds for full T1 and T2 mapping characterization. This is increased to 27 breath holds if extracellular volume is calculated (post-gadolinium contrast). Cardiology patients with heart failure, elderly patients with arthritic spines and joints, and individuals prone to claustrophobia are challenged by the breathing requirements, even if the breath holds are short. The important data buried in myocardial relaxation maps might best be brought forward with a free-breathing simultaneous method for multi-parameter mapping. As anticipated, correction for respiratory motion and mitigating mapping errors is the crux of the challenge discussed. Additionally, in the context of myocardial fibrosis, a T1 ρ sequence, typically used in musculoskeletal imaging, is studied to increase sensitivity to low-frequency interactions between macromolecules, such as collagen, and bulk water. It is an innovative application attacking a clearly unmet need in heart failure.

In concert with the myocardial texture analysis theme, Drs. Aggrwal, Singh, Anand, and Kumar discuss the Role of Cardiac T1, T2 Mapping and Extracellular Volume Measurements for the Assessment of Clinical Cardiomyopathies. The investigators present preliminary pilot data affirming the power of these metrics as a prognostic tool with diagnostic advantage. Although the techniques and images required are available on many scanners, the resources to process the data are a challenge. The path of these investigators is further embraced and extended in the report by Watkins, Atteberry, Innanje, Sun, X. Chen, T. Chen, Syed, Mitchell, Wang, and Lanza entitled A Vision for Magnetic Resonance Imaging to Assess Cardiotoxicity. This collaboration between WUMS and UIH has an overarching mission to address the barriers to cMRI use and democratization worldwide. The short article describes the anticipated workflow of concurrent image acquisition and data post processing that will allow readers to simultaneously receive the images and the post-processing reports. Intended to help address MR technologist dependency and enhance serial study consistency, a brief synopsis of EasyScan® and AIshim® is provided. Beyond this start, on-going development with feature-tracking strain analysis is in progress. MyoScan® (Myocardial Solutions, Inc). is used as the strain reference. The expectation is that both tagging and feature tracking techniques will be clinically equivalent. The segmentation masks derived from the FT strain procedures are passed to segment the colorized T1 and T2 relaxation maps, which are envisioned as intuitive colorized maps of abnormal myocardium voxels (i.e., 2 std deviations above or below the nominal values of T1 and T2) overlaid onto corresponding short-axis grayscale slices. The percent volumes of abnormal myocardium for each slice and the entire heart are calculated. For cardiac amyloid, the highly sensitive extracellular volume metric is calculated and used at a high threshold to differentiate amyloid from cardiac fibrosis.

Collectively, this issue of uINNOVATION-GLOBAL 2023 offers a vision into the diversified directions that CT, PET/CT, and MRI are taking to enhance the utility of advanced imaging in the US and worldwide. All of the development strategies heavily utilize optimized imaging hardware, innovative software and AI/DL neural network processes. In virtually all cases, imaging workflows are accelerated, simplified and enhanced with advanced image post-processing results achieved on the scanner computer complex. Eventually, physician readers, whether onsite or accessed by telemedicine, will be presented a greater depth of information from which to produce a report. The anticipated ultimate goal is that patient care, regardless of residence, is not compromised by a lack of access to informative imaging results that might improve their medical outcomes and longevity.

Editor's Biography

Dr. Gregory Lanza

Professor of Medicine,
Radiology, Biomedical
Engineering, and Biology
and Biomedical Sciences
Washington University
School of Medicine
St Louis, MO, USA

Dr. Gregory Lanza is a Cardiologist and Professor of Medicine, Biomedical Engineering, Radiology, Biology and Biomedical Sciences at the Washington University School of Medicine in St Louis. His clinical areas of interest include echocardiography and cardiac magnetic resonance imaging, with specific research interests in the development of novel nanotechnologies for biomedical molecular imaging and targeted drug delivery in cardiovascular, neurological, inflammatory, and oncological disease.

He obtained his Doctor of Philosophy from University of Georgia, Athens and his Doctor of Medicine from Northwestern University Medical School, Chicago; he did his residency and cardiology fellowship at Washington University School of Medicine in St Louis. He is also a recipient of numerous grants and prestigious awards.

Deep Learning-Based Reconstruction of Coronary CT Angiography in Patients with Diverse Anatomical and Pathological Complexities

Dijia Wu[a], Jiayin Zhang[b]
[a]United Imaging Intelligence (UII), Shanghai, China
[b]Shanghai General Hospital, Shanghai, China

1. Introduction

The utility of Coronary Computed Tomography Angiography (CCTA) as a non-invasive diagnostic tool for coronary artery disease (CAD), particularly in terms of its high sensitivity and negative predictive value, has been widely acknowledged [1]. European and American guidelines advocate for its employment as a primary approach in managing stable chest pain, especially in patients with an intermediate pre-test probability of CAD [2, 3]. Over the last decade, the application of CCTA has experienced a substantial surge [4]. Furthermore, the usage has risen by 14% in the aftermath of the COVID-19 pandemic, compared to the pre-pandemic phase [5].

The analysis of coronary computed tomography angiography (CCTA) is a laborious and time-consuming task due to the necessary reconstruction of major epicardial vessels in multiple formats and the detailed assessment of coronary atherosclerosis. A previous survey found that the median time for post-processing and interpretation of CCTA images was 15 and 18 minutes, respectively [6]. Furthermore, the presence of complex coronary lesions, such as chronic total occlusion (CTO), anomalies in vessel origin, bypass grafts, stents, and severe calcification, further complicates and extends the process of reconstruction and interpretation. Consequently, with the increasing number of CCTA cases being performed, the conventional manual reconstruction significantly restricts the daily capacity for practicing CCTA [7].

Over the past decade, significant progress has been made in the field of deep learning (DL)-assisted medical image processing, particularly in tissue segmentation, lesion detection, and disease characterization [8]. Deep learning approaches have shown promising results in vessel segmentation, primarily due to their ability to learn automatically and generalize well. These approaches have been successfully applied to various types of medical images, including retinal vessel fundus images [9], head and neck angiograms [10, 11], and cardiac CT angiograms.

The objective of this study is to evaluate the effectiveness of a deep learning-based segmentation model in automatically reconstructing coronary vessels in different complex clinical situations. These scenarios include CTO, anomalies in coronary vessel origin, bypass grafts, and stents.

2. Materials and Methods

2.1 Patient Data Sets

All three distinct hospital's (comprising two tertiary - 1. Shanghai General Hospital, Shanghai, 2. Shanghai Jiao Tong University Affiliated Sixth People's Hospital and one secondary institution - Shanghai General Hospital, Jiading Branch) ethics committee sanctioned this retrospective analysis, eliminating the need for informed consent. For our validation cohort, we amassed data on 1,023 patients who underwent CCTA across three distinct hospitals from January 2019 to June 2022. We excluded cases where CCTA image quality was severely compromised, specifically those with extreme artifacts that rendered the images non-diagnostic. To evaluate the effectiveness of reconstructing intricate coronary structures, our validation cohort included 211 chronic total occlusion patients with 240 CTO lesions, 105 with bypass grafts, 152 with stents, and 100 with origin anomalies, notably the anomalous origin of the coronary artery from the opposite sinus (ACAOS).

2.2 CCTA Image Acquisition

For the validation set, we included CCTA exams performed on six CT scanners from four vendors to validate the generalizability of developed model across varies CT equipment. These include: 1) third-generation dual source CT (SOMATOM Force, Siemens Healthineers); 2) 256-row wide detector CT scanner (Revolution, GE Healthcare); 3) 320-row wide detector CT scanner (uCT 960+, United Imaging); 4) dual-

layer detector spectral CT (IQon, Philips Healthcare); 5) 64-row multidetector CT (Definition AS+, Siemens Healthineers); and 6) 64-row multidetector CT (uCT 760, United Imaging). Retrospective ECG-gating acquisition was used for 128-slice multidetector CT and dual-layer detector spectral CT whereas prospective ECG-triggering acquisition was adopted for third-generation dual source CT and wide detector CT with automatic tube voltage and dose modulation.

2.3 DL Model Development

In this work, the automated CCTA coronary reconstruction was performed using uAI® Discover CoronaryCTA® solution (United Imaging Intelligence Inc., Shanghai, China). It employs a progressive learning framework consisting of two main components as shown in Figure 1 [12]: (a) the Spatial Anatomical Dependency (SAD) module and (b) the Hierarchical Topology Learning (HTL) module. The SAD module aims to perform an initial segmentation of both the heart chambers and coronary arteries. The segmentation outcomes from this module are then used to compute distance field maps that represent the spatial relationship between the artery and the heart. Meanwhile, the HTL module is engineered to further refine the initial coronary segmentation. This refinement is achieved through the multi-level learning of coronary topological features, encompassing key points, centerlines, and adjacent cube-connectivity. The integration of these two modules substantially enhances the accuracy and consistency of segmenting coronary arteries, accounting for their varied shapes, dimensions, and spatial orientations in different individuals.

2.4 Efficacy of DL-assisted and conventional CCTA reconstruction

From each study, the cardiac phase image showing optimal image quality (with the least motion artifact) was manually selected and processed by both the Discover CoronaryCTA® software and default commercially available workstations provided by CT vendors. The procedures are hereinafter referred as DL-assisted reconstruction and conventional reconstruction, respectively. All CCTA exams were randomly assigned to two junior cardiovascular radiologists (with 4-year and 6-year experience in cardiovascular imaging) and two radiology residents (in the third year and fourth year of residency) for coronary reconstruction. In instances where the software was unable to automatically achieve a successful segmentation of the coronary vessels, manual corrections were made using the built-in editing functions.

Each exam underwent both DL-assisted and conventional reconstruction by the same person, ensuring a one-month interval between the two reconstructions to mitigate memory biases. An independent senior cardiovascular radiologist, with 14 years of expertise in cardiovascular imaging and unaware of the reconstruction techniques employed, assessed the quality of the reconstructions. The assessment utilized a 5-tier scale as follows:

4 = All vessels are flawlessly segmented, with no interruptions, venous interferences, or centerline deviations.

3 = Vessels are displayed without interruptions, venous interferences, or centerline deviations, yet minor distal branches of less than 1mm in diameter were omitted.

2 = Vessels are displayed with minor interruptions, venous interferences, or centerline deviations, or omitting distal branches of less than 1mm in diameter.

1 = Vessels are shown with moderate interruptions, venous contaminations, or centerline deviations, or branches ranging from 1mm to 1.5mm in diameter were excluded.

0 = Vessels have severe interruptions, venous contaminations, or centerline deviations, or branches measuring 1.5mm or more in diameter were not represented.

A reconstruction was considered successful in this work when the post-processing of the vessels reached scores of 3 or 4 on the aforementioned 5-point scale and are applied to native coronary vessels, chronic total occlusions, bypass grafts, coronary stents, and origin anomalies.

The clinical efficiency of the two methods was evaluated based on the total post-processing duration. This duration was demarcated as the span from the commencement of image loading to the successful completion of all necessary reconstructions, encompassing any requisite manual edits. For cases involving CTO, this post-processing timeframe also incorporated the assessment of parameters related to the J-CTO score, including total occlusion length, CTO calcification burden, stump morphology (either blunt or tapered), and the tortuosity of the course.

2.5 Statistics Analysis

Statistical analysis was performed using IBM SPSS Statistics 22.0 (IBM Corporation) and MedCalc Statistical Software

20.019 (MedCalc Software Ltd). Continuous variables are presented as mean ± SD if normally distributed or as median and interquartile range (IQR) otherwise. Normal distribution was assessed using the probability-probability plot. Ordinal categorical variables are presented as median and IQR. Categorical variables are presented as the number and percentage of patients. Paired Samples Wilcoxon signed ranks test was used to compare the difference of image quality and total processing time. Successful rate of DL-assisted reconstruction and conventional reconstruction was compared using the McNemar test. A two-tail $p < 0.05$ was considered statistically significant.

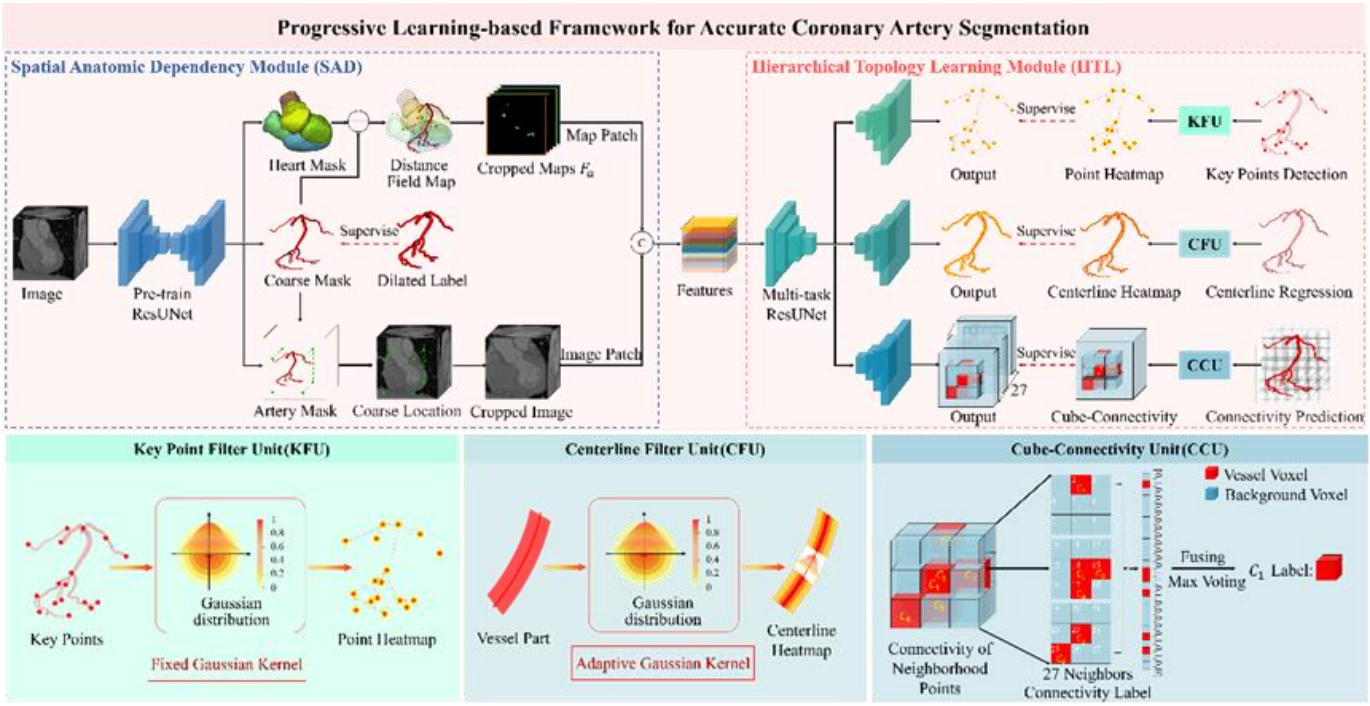

Figure 1. The progressive framework of the coronary segmentation model.

3. Results

3.1 Efficacy of DL-assisted reconstruction of CTOs

In the DL-assisted reconstruction, a remarkable 95% (228 out of 240) of CTO lesions were successfully segmented with no need for manual adjustments (see Figure 2). Of the 12 lesions necessitating manual intervention, 11 were amendable to further quantitative analysis following radiologist-led vessel editing. A single lesion remained uncorrectable. The primary factors prompting manual corrections for the DL model included the misidentification of contrast material–contaminated coronary veins as blocked arteries (five cases), the occlusion of diminutive vessels with diameters less than 2 mm (three cases), a tortuous trajectory (two cases), and mild artifact presence (two cases). By contrast, the traditional workstation automatically reconstructed occlusions in merely 48% (116 out of 240) of the lesions, markedly inferior to the DL-assisted method ($P < .001$). Predominant causes for manual revisions for the conventional workstation were extended occlusions with a length of 2 cm or more (57 cases), blockages in tiny vessels with diameters up to 2 mm (40 cases), mistaking contrast-contaminated veins for obstructed arteries (13 cases), sinuous pathways (12 cases), and minor artifact presence (two cases). The overall processing and evaluation duration utilizing the DL model was notably reduced compared to the standard manual method, with times recorded as 121 seconds ± 20 versus 456 seconds ± 68 for the junior radiologist ($P < .001$) and 106 seconds ± 14 versus 348 seconds ± 70 for the senior radiologist ($P < .001$).

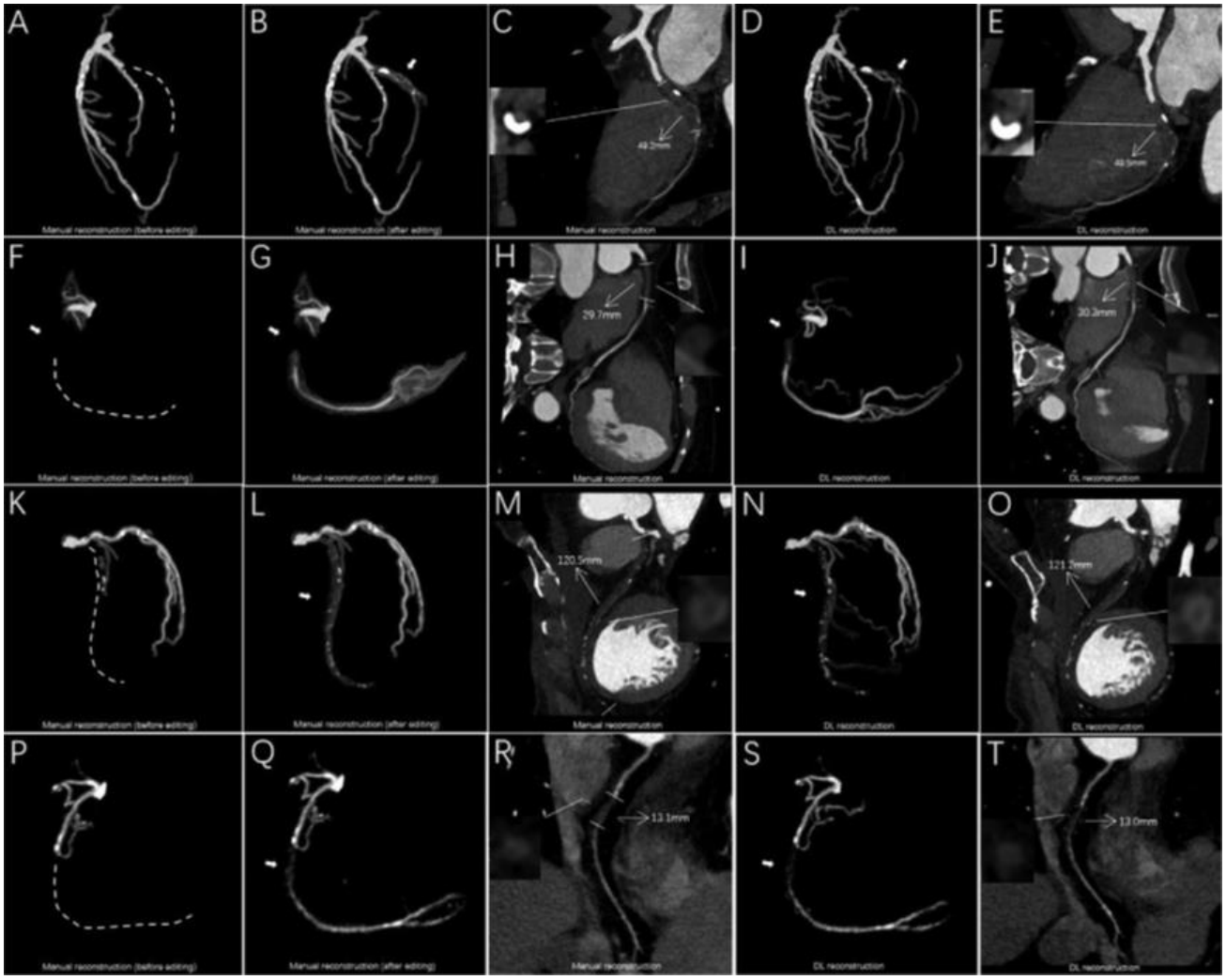

Figure 2. A comparison of example chronic total occlusion (CTO) lesion images utilizing DL-assisted reconstruction versus reconstruction with conventional workstations.

In a 49-year-old male with a CTO in the left circumflex artery, imaged with a third-generation dual-source CT scanner: (A) The standard workstation couldn't delineate the occluded segment (highlighted by dashed line). (B) Manual tracing of the CTO was conducted using the multiple-clicks vessel function (indicated by arrow), revealing a bend under 45°. (C) Conventional curved planar reformation (CPR) showed an occlusion length of 49.2 mm with a blunt termination. Calcium was found to constitute a minimum of 50% of the lumen area. Analysis duration: 423 seconds. (D) The DL model comprehensively identified the CTO trajectory, capturing several minor branches. (E) DL-based CPR displayed a CTO span of 49.5 mm, consistent calcium composition, and a reduced analysis time of 100 seconds.

In a 56-year-old female with a CTO in the right coronary artery (RCA), captured using a 128-section CT: (F-G) The standard platform struggled to identify both the occlusion and the distal lumen, later manually traced, indicating a CTO bend exceeding 45°. (H) Standard CPR illustrated an occlusion of 29.7 mm ending with a tapered stump, and no calcification. Analysis took 613 seconds. (I-J) In contrast, the DL model reconstructed the full CTO path and estimated its length at 30.3 mm in 105 seconds.

For a 74-year-old female with a CTO in the left anterior descending artery, using third-generation dual-source CT: (K-L) Initial extraction was unsuccessful for the occlusion and distal lumen. Post-manual tracing, the CTO bend was under 45°. (M) Traditional CPR depicted an extensive 120.5 mm CTO with a blunt end and no calcification, analyzed in 1077 seconds. (N-O) DL's efficacy was evident as it traced the complete CTO, estimating it at 121.2 mm in just 117 seconds.

For a 61-year-old female with an RCA CTO, analyzed with a 256-section wide detector CT: (P-Q) The conventional method missed the occlusion and distal lumen. After manual input, the CTO bend was seen to be under 45°. (R) Standard CPR indicated a 13.1 mm CTO with a blunt end and no calcification, taking 420 seconds. (S-T) The DL methodology precisely traced the CTO, gauging its length at 13 mm and concluding the process in 112 seconds.

Figure 3. Comparative display of DL-assisted versus conventional workstation reconstruction in patients exhibiting complex coronary anatomies.

3.2 Efficacy of DL-assisted reconstruction of native vessel, stents, bypass grafts, and origin anomaly

The DL-model demonstrated superior automatic segmentation capabilities when applied to intricate coronary anatomies, including stents, bypass grafts, and origin anomalies, as shown in Figure 3. Quantitative assessment revealed that the model consistently produced images of enhanced quality across all subgroup categories: stent (4 [IQR, 4 – 4] compared to 3 [IQR, 3 - 4]), bypass graft (4 [IQR, 3 – 4] versus 3 [IQR, 2 – 4]), and origin anomaly (4 [IQR, 4 – 4] in comparison to 4 [IQR, 3 – 4]), with all yielding p-values < .001 (Refer to Figure 4 for details). Moreover, a significant observation was the dominant presence of score 4 (indicating exemplary reconstruction image quality), which constituted 93.4%, 73.3%, and 91.0% of patients with stents, bypass grafts, and origin anomalies, respectively. In stark contrast, the conventional workstation reconstruction achieved this score in only 37.5%, 40.0%, and 52.0% of the cases, respectively, with all these instances presenting p-values < .001.

In most subgroups, the successful (score = 3 or 4) reconstruction rates by DL-model exceeded 97% except for the bypass graft (76.2%). The main reasons for failed reconstructions included inability to track the interarterial course of ACAOS (3 cases), occluded left internal mammary artery (LIMA) (9 cases) and saphenous venous graft (SVG) / radial artery graft (16 cases).

Panels A-H represent imaging from a 71-year-old male with a sequential SVG-LAD-OM-LCx-PDA graft captured using a third-generation dual-source CT scanner.

 A-D are images reconstructed through the DL model, characterized by an image quality score of 4. The overall processing duration was 11 seconds, obviating the need for manual intervention. Specifically, A depicts volume rendering (VR), B showcases maximal intensity projection (MIP), C presents curved planar reformation (CPR), and D provides a cross-sectional perspective, delineating the full course of the patent graft.

 E-H convey images rendered using traditional reconstruction techniques, also achieving an image quality score of 4. However, the processing time extended to 977 seconds. The illustrations are analogous in nature with E for VR, F for MIP, G for CPR, and H delineating the patent graft's full course.

Panels I-P present imaging from a 58-year-old female diagnosed with a subpulmonic anomalous origin of the LAD from the right coronary sinus, captured using a 64-row multidetector CT scanner.

 I-L are reconstructions via the DL model, exhibiting an image quality score of 4, and processed in merely 7 seconds without manual modifications. The illustrations include I for VR, J for MIP, K for CPR, and L offering a comprehensive perspective of the anomalous LAD.

 M-P highlight traditional reconstruction techniques, delivering an image quality score of 3, attributed to the omission of smaller distal branches (diameter <1mm). The process spanned 417 seconds. The sequence remains consistent with M for VR, N for MIP, O for CPR, and P displaying the anomalous LAD, albeit with fewer minuscule distal branches relative to the DL model reconstructions.

Panels Q-X detail imaging from a 68-year-old female with a stent in the first diagonal, obtained using a 256-row wide detector CT scanner.

 Q-T employ the DL model for reconstruction, resulting in an image quality score of 4 and a rapid processing time of 17 seconds without manual adjustments. The sequence comprises Q for VR, R for MIP, S for CPR, and T vividly presenting the full course of the stented vessel.

 U-X rely on traditional reconstruction, achieving an image quality score of 3. The process took 782 seconds. The series include U for VR, V for MIP, W for CPR, and X showing the stent, though lacking several smaller distal branches.

Relative to the conventional reconstruction, the median processing duration for DL-assisted reconstruction exhibited a substantial reduction, declining from 465.0 seconds (IQR, 337.5 – 656.0 seconds) to a mere 11.0 seconds (IQR, 8.0 – 31.0 seconds) across the patient cohort. This trend was consistently discernible in every subgroup, with each showing significant differences (P < .05) as depicted in Figure 5.

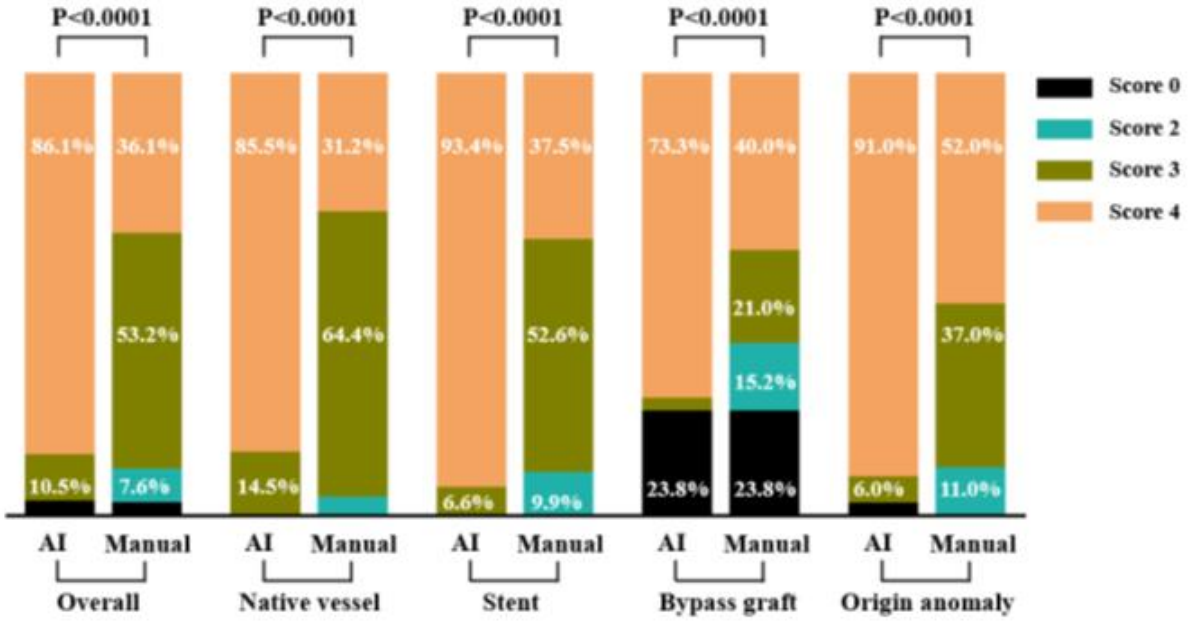

Figure 4. Comparative analysis of image quality between DL-assisted (AI) and conventional (Manual) reconstruction across diverse subgroups. Abbreviation: AI = Artificial Intelligence.

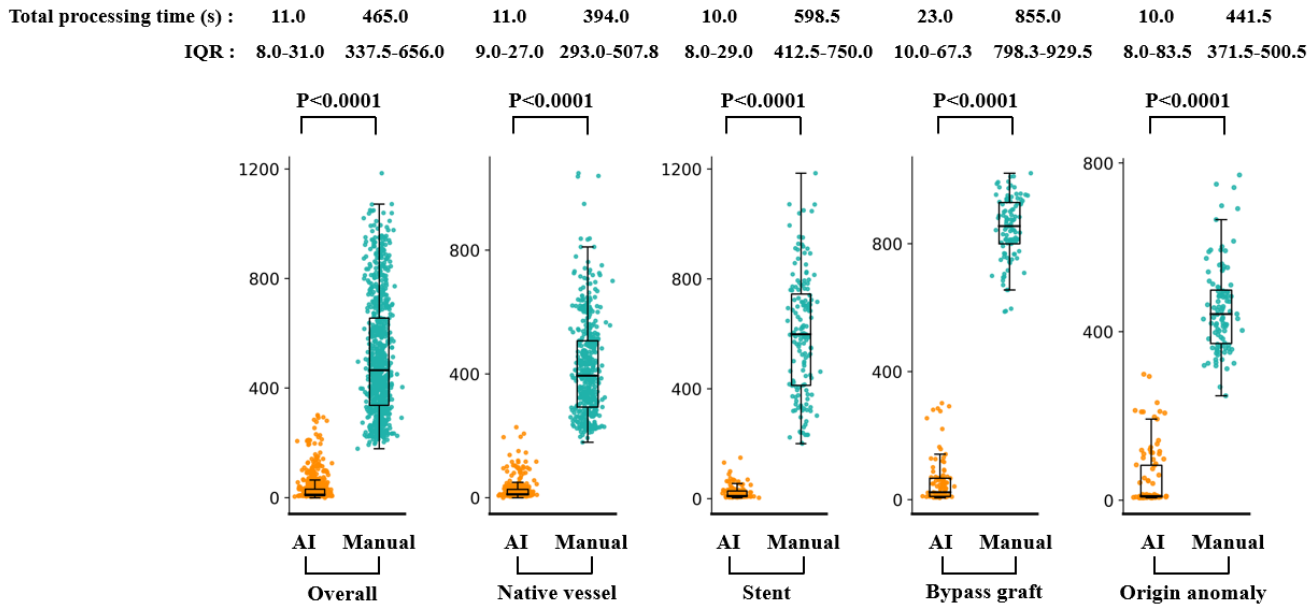

Figure 5. Comparative evaluation of total processing duration between DL-assisted (AI) and conventional (manual) reconstruction. The DL-assisted approach consistently yielded a markedly reduced processing time relative to the conventional method across all examined groups. Abbreviations: AI = Artificial Intelligence; IQR = Interquartile Range

4. Discussion

CCTA is a prevalent non-invasive imaging technique utilized in the clinical diagnosis of CAD. There has been a significant surge in the utilization of CCTA over recent decades, leading to an increased demand for post-processing. Contemporary research has explored the application of AI-driven models for the automated segmentation of CCTA, resulting in enhanced outcomes in native vessel reconstruction. Nonetheless, for patients presenting with anatomical and pathological intricacies, the automated reconstruction of coronary arteries continues to pose challenges due to inherent

technical difficulties.

Coronary CTO constitutes one of the most challenging lesions to address during coronary intervention. CCTA stands out as an instrumental tool for guiding CTO revascularization, given its distinct capability to provide an in-depth anatomical assessment of occlusion features. Nonetheless, the automated reconstruction of occluded vessel segments and the connection of distal interrupted arteries present technical hurdles. Consequently, manual adjustments are frequently necessary on conventional workstations.

The present study strongly supports the use of DL-assisted reconstruction to facilitate CTO evaluation in clinical practice. The uAI® Discover CoronaryCTA® provides fully automated vessel segmentation and a variety of reconstruction formats (maximal intensity projection, volume rendering, curved planar reformats, etc.) without need for manual adjustments. This process typically concludes within 2 minutes, remarkably quicker than conventional workstations. It will specifically benefit interventional cardiologists, who are usually not as experienced as radiologists in terms of performing CCTA post-processing.

Coronary stent is another hard entity for automatic reconstruction, especially in terms of accurate centerline tracing in CPR images. As stent strut has high attenuation value, it may sometimes be misidentified as contrast-enhanced lumen and therefore leads to deviated centerlines in the stented segment, which usually requires manual adjustment. However, this study demonstrates that DL-assisted reconstruction was able to generate CPR images with accurate centerline tracing in all patients studied, with an impressive 93.4% attaining a score of 4. In contrast, conventional workstations only achieved this score for 37.5% of the patients. Consequently, DL-assisted CCTA post-processing appears to be a promising approach for patients with coronary stents.

As for origin anomalies, the inter-arterial type of ACAOS predominates in the present cohort. This presents a heightened technical challenge for automatic reconstruction due to the anomalous artery's ostium typically being situated at a considerable distance from its usual location, coupled with the artery's proximal course navigating between the pulmonary trunk and the ascending aorta. Notably, findings from this study revealed that DL-assisted reconstruction adeptly segmented the anomalous coronary artery in 97.0% of the subjects. This positions the DL methodology as highly suitable for automatic reconstruction, offering a substantial reduction in post-processing time compared to traditional workstation techniques.

Finally, coronary bypass graft is probably the utmost challenging scenario for automatic reconstruction of CCTA. This is chiefly attributed to the substantial variability in the count and trajectory of SVGs or radial arteries across various surgical interventions.

Within the scope of this research, the entire trajectory of LIMA was precisely identified for all patients. Similarly, non-occluded SVGs or radial grafts exhibited a 100% identification rate, regardless of procedural discrepancies. Yet, a notable limitation was the model's inability to detect ostially occluded grafts. The primary reason is the indiscernibility of a collapsed graft lumen in CCTA. In comparison to arterial blockages where a thrombosed lumen is still visible on CCTA, a collapsed venous graft often displays no evident residual lumen. Tracing such grafts remains a persistent challenge, impacting both traditional workstation-based methods and DL-assisted reconstruction techniques. The findings from this study reveal that both methods struggled to accurately map the course of occluded grafts.

Our study has several limitations. Initially, while the DL-assisted reconstruction facilitates automated delineation and reconstruction of the coronary vasculature with commendable precision and efficiency, the reliability of DL-driven lesion identification - pertaining to stenosis severity and plaque characterization - remains unverified. Furthermore, the present model struggles to track bypass grafts exhibiting proximal anastomosis occlusions. Consequently, there is a risk of neglecting obstructed grafts without meticulous manual oversight.

5. Conclusion

In conclusion, the DL-assisted uAI® Discover CoronaryCTA® solution facilitates a fully automated reconstruction of native coronary vessels, bypass grafts, stents, and origin anomalies, achieving both high precision and efficiency. Utilizing the DL model markedly reduces post-processing durations and enhances the CCTA post-processing workflow.

6. Image/Figure Courtesy

All images are the courtesy of three distinct hospital's comprising two tertiary - 1. Shanghai General Hospital, Shanghai, 2. Shanghai Jiao Tong University Affiliated Sixth

People's Hospital and one secondary institution - Shanghai General Hospital, Jiading Branch

7. References

1. Haase R, Schlattmann P, Gueret P et al (2019) Diagnosis of obstructive coronary artery disease using computed tomography angiography in patients with stable chest pain depending on clinical probability and in clinically important subgroups: meta-analysis of individual patient data. Bmj 365:l1945
2. Gulati M, Levy PD, Mukherjee D et al (2021) 2021 AHA/ACC/ASE/CHEST/SAEM/SCCT/SCMR Guideline for the Evaluation and Diagnosis of Chest Pain: A Report of the American College of Cardiology/American Heart Association Joint Committee on Clinical Practice Guidelines. Circulation 144:e368-e454
3. Knuuti J, Wijns W, Saraste A et al (2020) 2019 ESC Guidelines for the diagnosis and management of chronic coronary syndromes. Eur Heart J 41:407-477
4. Reeves RA, Halpern EJ, Rao VM (2021) Cardiac Imaging Trends from 2010 to 2019 in the Medicare Population. Radiol Cardiothorac Imaging 3:e210156
5. Einstein AJ, Hirschfeld C, Williams MC et al (2022) Worldwide Disparities in Recovery of Cardiac Testing 1 Year Into COVID-19. J Am Coll Cardiol 79:2001-2017
6. Liu K, Hsieh C, Zhuang N et al (2016) Current utilization of cardiac computed tomography in mainland China: A national survey. J Cardiovasc Comput Tomogr 10:76-81
7. Hilkewich MW (2014) Written Observations as a Part of Computed Tomography Angiography Post Processing by Medical Radiation Technologists: A Pilot Project. J Med Imaging Radiat Sci 45:31-36.e31
8. Zhou SK, Le HN, Luu K, V Nguyen H, Ayache N. Deep reinforcement learning in medical imaging: A literature review. Med Image Anal 2021;73:102193
9. Boudegga H, Elloumi Y, Akil M, Hedi Bedoui M, Kachouri R, Abdallah AB. Fast and efficient retinal blood vessel segmentation method based on deep learning network. Comput Med Imaging Graph 2021;90:101902.
10. Fu F, Wei J, Zhang M, et al. Rapid vessel segmentation and reconstruction of head and neck angiograms using 3D convolutional neural network. Nat Commun 2020;11(1):4829.
11. Wolterink JM, van Hamersvelt RW, Viergever MA, Leiner T, Išgum I. Coronary artery centerline extraction in cardiac CT angiography using a CNN-based orientation classifier. Med Image Anal 2019;51:46–60.
12. Zhang X, Zhang J, Ma L et al (2022). Progressive Deep Segmentation of Coronary Artery via Hierarchical Topology Learning. International Conference on Medical Image Computing and Computer-Assisted Intervention. Springer, Cham, 391-400.

Author Biography

Dr. Dijia Wu
Chief Technology Officer
United Imaging Intelligence,
Co. Ltd.
Shanghai, China

Dr. Wu is the Chief Technology Officer at United Imaging Intelligence, Co. Ltd., Shanghai. He received his Ph.D. from the Rensselaer Polytechnic Institute, Troy, NY. His research interests include machine learning and computer vision with applications to medical image analysis, especially involving computer-aided diagnosis of cardiovascular diseases. He has published dozens of peer-reviewed papers in top-tier conferences and journals and is also a recipient of numerous grants and prestigious awards.

Clinical Significance of Coronary Artery Calcium Score in Predicting Coronary Artery Disease: A CT Coronary Angiography Study

Anand H. K. [a], Ramachandra C. R. [a], Pooja B. P. [a], Arjun Raju[a], Akash Gandhamal[b], Dileep Kumar [b]
[a]Tenet Diagnostic Centre, Bengaluru, India
[b]Central Research Institute, Global Scientific Collaborations, United Imaging Healthcare

Abstract

Coronary Artery Disease (CAD) is a global health concern, contributing significantly to morbidity and mortality rates. The Coronary Artery Calcium Score (CACS) has emerged as a non-invasive predictive tool for coronary events. This study aimed to evaluate the clinical significance of CACS in predicting CAD in terms of coronary stenosis. A cohort of 153 subjects with varying CAD symptoms underwent Computed Tomography Coronary Angiography (CT-CAG) scans, and their CACS values were correlated with manual stenosis estimation. Sensitivity, specificity, accuracy, positive predictive value, and negative predictive value were assessed. The results indicated that CACS is a robust predictor of coronary stenosis, with a sensitivity of 96.04% and specificity of 90.38%. These findings highlight the potential of CT-CAG combined with CACS as an initial screening method for CAD in patients with mild to moderate symptoms, reducing the need for invasive diagnostic procedures.

1. Introduction

Coronary Artery Disease (CAD) is a leading cause of morbidity and mortality worldwide, imposing a significant burden on healthcare systems and society at large [1]. The profound impact it exerts on healthcare systems and society at large is a reminder of the urgent need for effective strategies in its management and prevention. Recognizing the importance of early detection and risk assessment as pivotal components of these strategies, the medical community has turned to innovative non-invasive approaches.

Among these approaches, the Coronary Artery Calcium Score (CACS) has emerged as a promising tool for evaluating CAD risk [2]. By quantifying the extent of calcium deposits within the coronary arteries, CACS furnishes clinicians with valuable insights into a patient's susceptibility to CAD [3]. This ability to offer a predictive glimpse into an individual's CAD risk profile is pivotal in enabling timely interventions and ultimately enhancing patient outcomes. However, the landscape of CAD assessment has evolved further with the widespread adoption of Computed Tomography Coronary Angiography (CT-CAG) in recent years [4]. This imaging modality has become the gold standard for assessing the degree of coronary artery stenosis, providing detailed anatomical information that enhances diagnostic precision. The logical progression in the field of CAD evaluation has led to the exploration of integrating CACS with CT-CAG to offer a more comprehensive and precise assessment of CAD risk [5] [6].

In this context, our study sets out to examine the clinical significance of CACS in predicting the presence or absence of coronary stenosis in patients presenting varying degrees of CAD symptoms. Our working hypothesis is that CACS can serve as an effective predictor of coronary stenosis, particularly in patients with mild to moderate symptoms. This, in turn, has the potential to substantially reduce the necessity for invasive diagnostic procedures, thus improving both patient comfort and healthcare resource allocation. In the pages that follow, we delve deeper into our research findings and their implications, ultimately validating the role of CACS in optimizing CAD risk stratification and diagnostic accuracy.

2. Materials and Methods

2.1 Study Population

A total of 153 subjects (mean age 57.19 ± 11.74 years, 63% male and 37% female) with a range of CAD symptoms, from none to severe, were enrolled in this study. All participants underwent the CT-CAG scans using the uCT 780 scanner (Mfg. - United Imaging Healthcare Co. Ltd, Shanghai). These individuals represented a diverse patient population with

varying levels of CAD risk.

2.2 CACS Calculation and Stenosis Estimation

CACS values were calculated using mass, volume, and Agatston Score estimation [7]. These approaches provide a comprehensive evaluation of calcium build-up within the coronary arteries, offering a nuanced understanding of a patient's coronary health. To complement this quantitative assessment, we engaged the expertise of a seasoned radiologist well-versed in cardiovascular imaging. This expert meticulously conducted manual stenosis estimations, a critical aspect of our study. Drawing upon his extensive experience and proficiency, the radiologist carefully evaluated the degree of coronary artery stenosis in each subject. Our classification of study participants was based on the results of these manual stenosis estimations. Specifically, we grouped individuals into two distinct categories: those with coronary artery disease (CAD) and those without CAD. The primary criterion for this classification was the presence or absence of non-zero stenosis, with the former serving as a clear indicator of CAD. In parallel to this manual assessment, we leveraged the CACS values obtained through our quantitative techniques to predict the likelihood of coronary stenosis. Notably, a CACS value greater than zero was indicative of the presence of coronary stenosis. This dual approach, combining expert radiological evaluation with quantitative CACS data, allowed us to comprehensively ascertain the CAD status of our study participants and form a robust foundation for our subsequent analyses. Few of the examples are shown in Figures 1 and 2 below differentiates the CAD and Non-CAD cases with zero and 2737 calcium scores respectively.

Figure 1 provides a notable observation: the CT-CAG under investigation by the radiologist displays an absence of any calcified structures within the arteries. This absence serves as a compelling indicator of the absence of CAD with Flow Limitations with zero CACS. Conversely, Figure 2 presents a markedly contrasting scenario. This image provides clear evidence of the presence of multiple eccentric calcified plaques, strongly suggestive of stenosis, particularly occlusions in the Left Anterior Descending Artery (LAD). Furthermore, the cumulative CACS, calculated as 2737, underscores the extent of calcification within the coronary arteries.

Figure 2 goes beyond merely pointing out the calcification in the LAD. It also reveals the presence of stenosis in multiple other arterial segments. Specifically, this image depicts 70-80% stenosis in the distal Right Coronary Artery (RCA), 60-70% stenosis in the distal LAD, 30-40% stenosis in the Left Circumflex Artery (LCX), 40-50% stenosis in the proximal RCA, and 20-30% stenosis in the Right Posterior Descending Artery (RPDA). These findings collectively contribute to a comprehensive assessment of the patient's coronary artery health and serve as crucial diagnostic information for clinical decision-making

2.3 Statistical Analysis

The quantitative evaluation of our study encompassed a meticulous analysis that involved an array of statistical parameters, each contributing to a comprehensive assessment of the effectiveness of the CACS as a predictive tool for coronary stenosis. These statistical metrics, including sensitivity, specificity, accuracy, positive predictive value (PPV), and negative predictive value (NPV), were harnessed to gauge the diagnostic performance of CACS.

Sensitivity, a crucial measure, quantified the ability of CACS to correctly identify individuals with coronary stenosis, thereby avoiding false negatives. It quantified the proportion of true positive predictions, highlighting the sensitivity of CACS in detecting coronary stenosis cases. Specificity, on the other hand, assessed the capacity of CACS to accurately identify individuals without coronary stenosis, minimizing false positives. It represented the proportion of true negative predictions, emphasizing the specificity of CACS in correctly ruling out coronary stenosis in non-CAD cases. Accuracy, as a fundamental metric, provided an overall measure of CACS's ability to correctly classify both positive and negative cases, offering insight into the overall diagnostic performance of this non-invasive tool. Positive Predictive Value (PPV) offered valuable insights into the likelihood of an individual with a positive CACS result truly having coronary stenosis. It highlighted the precision of CACS in identifying true CAD cases among those with positive test results. Conversely, Negative Predictive Value (NPV) evaluated the probability of an individual with a negative CACS result genuinely being free from coronary stenosis. NPV shed light on the capacity of CACS to effectively rule out coronary stenosis in those with negative test outcomes.

Together, these statistical parameters provided a comprehensive evaluation of CACS's diagnostic ability, with

its sensitivity, specificity, accuracy, and predictive values in finding the presence or absence of coronary stenosis. This thorough analysis is fundamental in determining the clinical utility of CACS as a screening tool for CAD and in informing medical decision-making for patients with varying degrees of CAD symptoms.

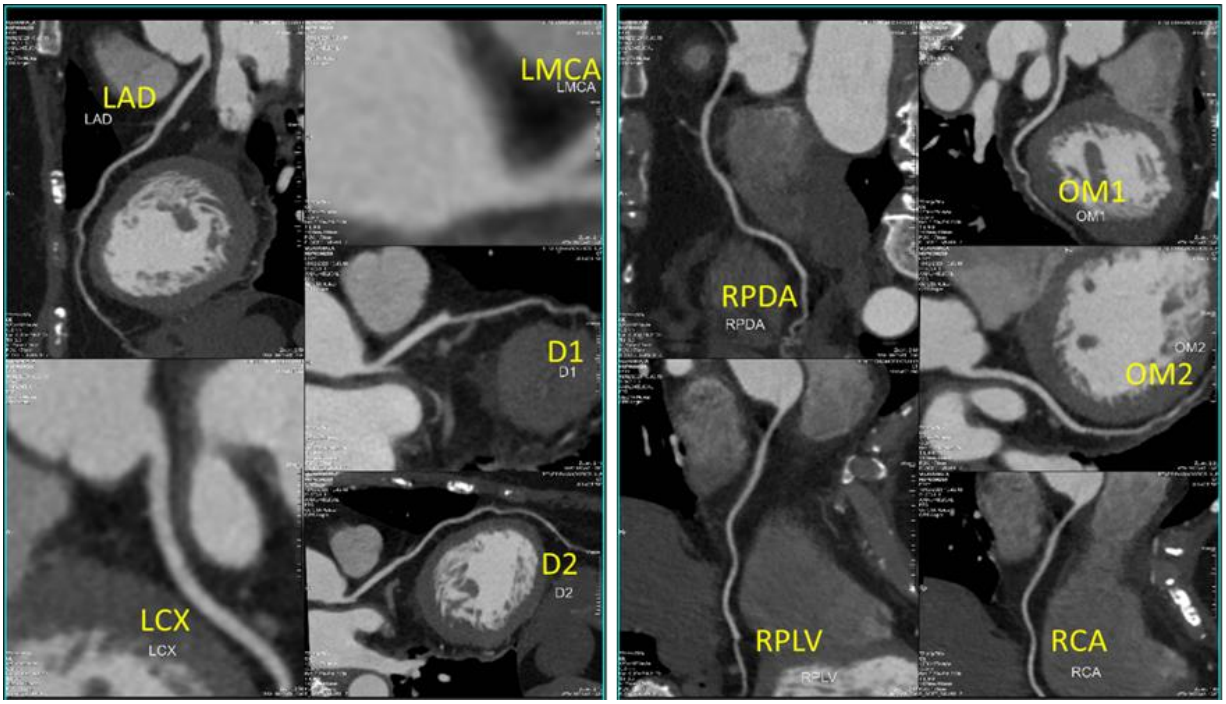

Figure 1. The progressive framework of the coronary segmentation model.

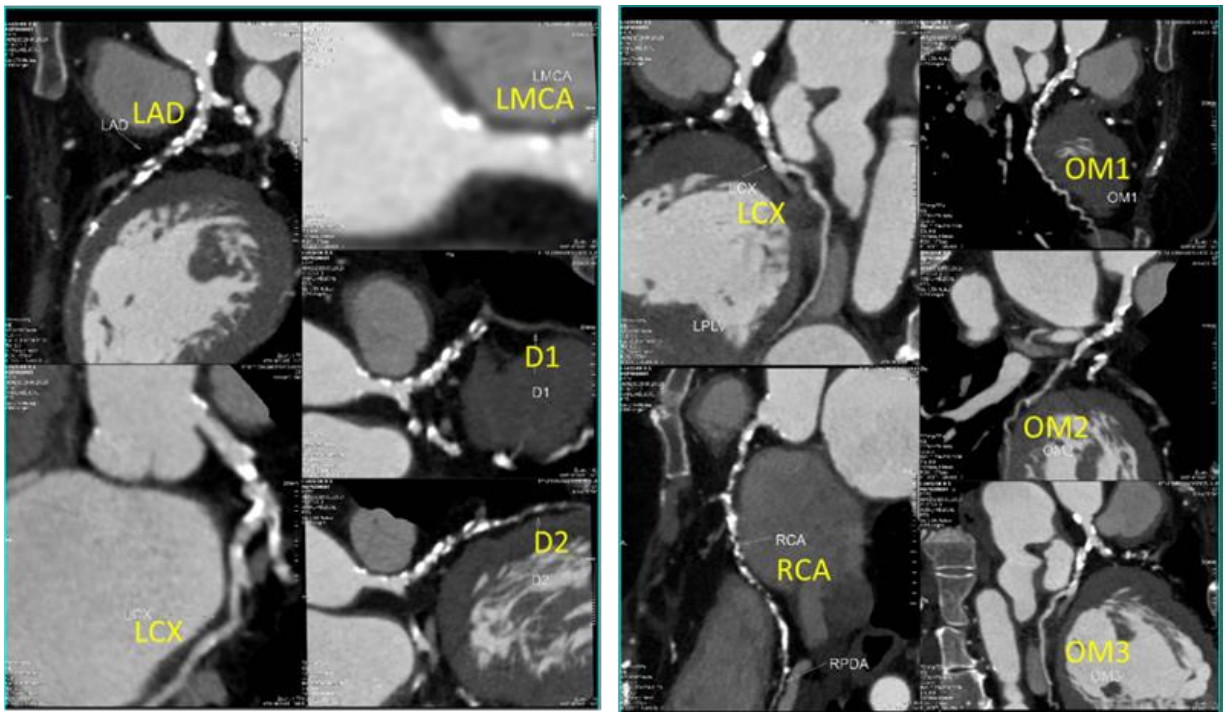

Figure 2. CT-CAG with the Calcium Score calculated as 2737 whereas, Diagnosis Impression reported by radiologists is the Occlusion of mid LAD with 70-80% stenosis of distal RCA, 60-70% stenosis of distal LAD, 30-40% stenosis of LCX and 40-50% stenosis on proximal RCA.

3. Results

Among the 153 patients included in our study, a substantial portion, 52 individuals (approximately 34%), displayed normal Computed Tomography Coronary Angiography (CT-CAG) results, indicating the absence of coronary stenosis. Notably, when we examined their CACS values, 51 of these patients were also classified as normal based on their CACS measurements. This congruence between CT-CAG and CACS findings reflected the high degree of agreement in identifying coronary health among these individuals. Impressively, 47 of these patients were correctly classified as having normal coronary arteries (True Positives), demonstrating the robustness of both CT-CAG and CACS in accurately identifying non-stenotic cases. However, four patients were misclassified as having coronary stenosis (False Negatives), emphasizing the importance of considering other clinical factors when making diagnostic decisions.

In contrast, 102 patients were classified as CAD-positive based on their non-zero CACS values, indicating the presence of coronary artery calcification. Among these individuals, 97 were correctly classified as having coronary stenosis (True Positives), highlighting the strong predictive capacity of CACS in identifying CAD cases. However, five patients were incorrectly classified as CAD-positive (False Positives) when compared to manual stenosis labelling. While this represented a small percentage of misclassified cases, it underscores the need for comprehensive evaluation in clinical practice. Figure 3 shows the comparative plot between the CACS and the Stenosis (%) showing the non-zero CACS values that indicates the presence of CAD. In addition, it can be validated from the plot that the zero CACS is indicative of no stenosis.

Our analysis of the data yielded compelling diagnostic statistics. The utilization of CACS as a predictor for coronary stenosis demonstrated an exceptional sensitivity of 96.04%, signifying its effectiveness in correctly identifying patients with coronary stenosis. Moreover, it exhibited a specificity of 90.38%, indicating its ability to accurately classify individuals without coronary stenosis. The overall accuracy of 94.12% reaffirmed the reliability of CACS as a diagnostic tool in CAD risk assessment through Table 1.

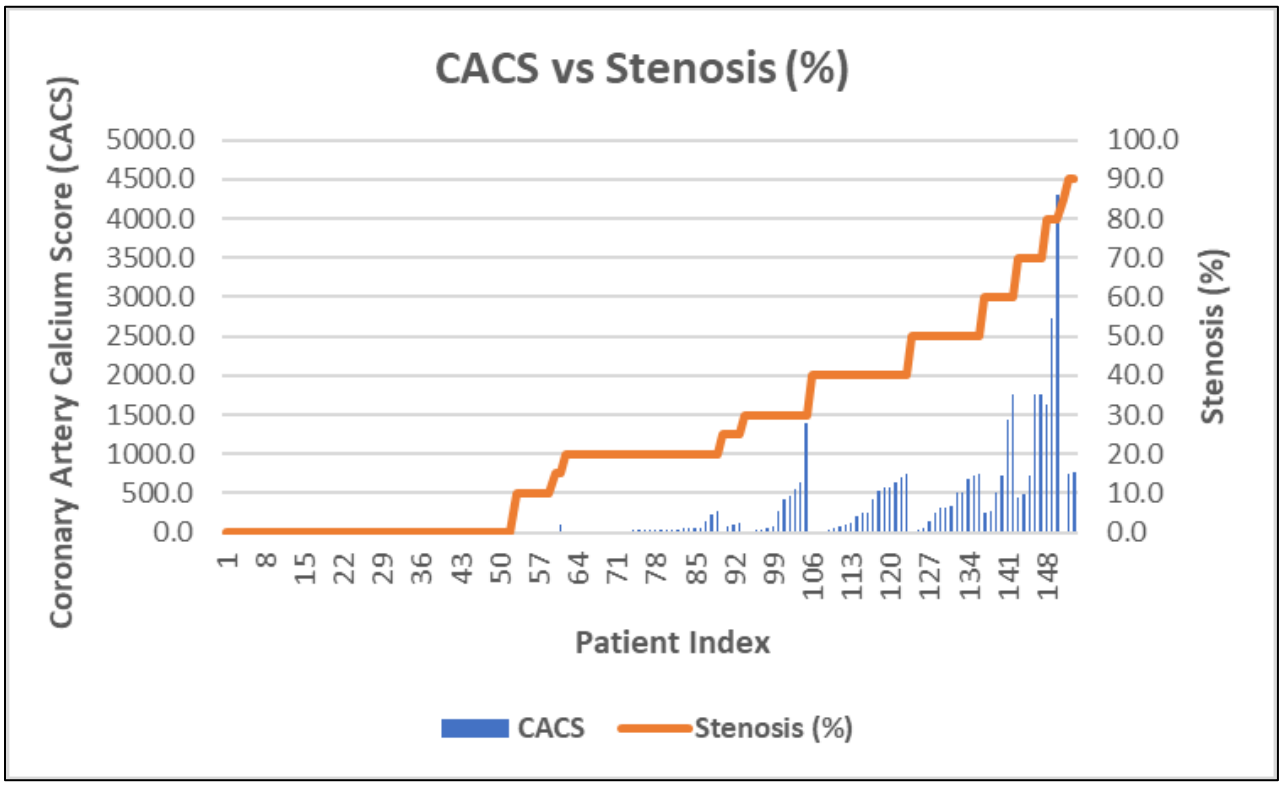

Figure 3. Comparative Plot CACS vs Stenosis (in %).

Table 1. Statistical Analysis CACS vs Stenosis.

	TP	FP	TN	FN	Sensitivity	Specificity	Accuracy	PPV	NPV
CACS > 0	97	5			**0.9604**	**0.9038**	**0.9412**	**0.951**	**0.9216**
CACS = 0			47	4					

TP: True Positive, FP: False Positives, TN: True Negatives, FN: False Negatives, PPV: Positive Predictive Value, NPV: Negative Predictive Value

The PPV of 95.10% highlighted the precision of CACS in identifying true CAD cases among those with positive test results. Simultaneously, the NPV of 92.16% underscored its ability to reliably exclude coronary stenosis in individuals with negative test results as shown in Table 1. These impressive results collectively underscore the robust predictive capability of CACS in effectively identifying coronary stenosis, demonstrating its clinical significance as a valuable tool in the realm of CAD diagnosis and risk assessment.

4. Conclusion

This extensive investigation demonstrated that the Coronary Artery Calcium Score (CACS) serves as a robust predictor of coronary stenosis across a diverse range of CAD symptoms. This highlights the versatility and clinical applicability of CACS, making it a valuable tool for identifying coronary stenosis in patients with varying CAD-related symptoms. Additionally, our study revealed the impressive accuracy of Computed Tomography Coronary Angiography (CT-CAG) in detecting coronary stenosis, with only a minimal 6% misclassification rate. These findings align with prior research, reinforcing the clinical significance of CACS in CAD risk assessment. Together, these results contribute to a better understanding of CAD diagnosis and emphasize the utility of CACS and CT-CAG for precise identification of coronary stenosis. Integrating these diagnostic approaches into clinical practice brings us closer to the goal of timely intervention, improved patient outcomes, and efficient healthcare resource allocation in CAD management.

5. Clinical Relevance

The combination of CT-CAG and CACS calculation holds clinical relevance as an initial screening method for detecting CAD in patients with mild to moderate symptoms. This approach offers several advantages, including its non-invasiveness, accuracy, and potential to reduce the need for invasive diagnostic procedures. Early identification of CAD risk through CACS can facilitate timely interventions and improve patient outcomes.

6. Limitations

It is essential to acknowledge certain limitations of this study. First, the study population was relatively small and heterogeneous. A larger and more diverse cohort may provide additional insights into the clinical utility of CACS. Additionally, the study did not assess the long-term outcomes of patients with varying levels of CAD risk. Further research is needed to determine the prognostic value of CACS in predicting cardiovascular events and mortality.

7. Image/Figure Courtesy

All images are courtesy of Tenet Diagnostic Centre, Bengaluru, India.

8. References

1. H Brown JC, Gerhardt TE, Kwon E. Risk Factors for Coronary Artery Disease. 2023 Jan 23. In: StatPearls [Internet]. Treasure Island (FL): StatPearls Publishing; 2023 Jan–. PMID: 32119297.

2. Yasuyuki Suzuki, Naoya Matsumoto, Shunichi Yoda, Yasuo Amano, Yasuo Okumura, Coronary artery calcium score: Current status of clinical application and how to handle the results, Journal of Cardiology, Volume 79, Issue 5, 2022, Pages 567-571, ISSN 0914-5087.

3. Liu W, Zhang Y, Yu CM, Ji QW, Cai M, Zhao YX, Zhou YJ. Current understanding of Coronary artery calcification. J Geriatr Cardiol. 2015 Nov;12(6):668-75. PMID: 26788045; PMCID: PMC4712374.

4. Sato A. Coronary plaque imaging by coronary computed tomography angiography. World J Radiol. 2014 May

28;6(5):148-59. doi: 10.4329/wjr.v6.i5.148. PMID: 24876919; PMCID: PMC4037541.

5. Divakaran S, Cheezum MK, Hulten EA, Bittencourt MS, Silverman MG, Nasir K, Blankstein R. Use of cardiac CT and calcium scoring for detecting coronary plaque: implications on prognosis and patient management. Br J Radiol. 2015 Feb;88(1046):20140594. doi: 10.1259/bjr.20140594. Epub 2014 Dec 12. PMID: 25494818; PMCID: PMC4614250.

6. Kiani R, Pouraliakbar H, Alemzadeh-Ansari MJ, Khademi A, Peighambari MM, Mohebbi B, Firouzi A, Zahedmehr A, Shakerian F, Hosseini Z, Rashidinejad A. The significance of coronary artery calcium score as a predictor of coronary artery stenosis in individuals referred for CT angiography. J Cardiovasc Thorac Res. 2020;12(3):203-208. doi: 10.34172/jcvtr.2020.34. Epub 2020 Sep 3. PMID: 33123326; PMCID: PMC7581835.

7. Neves PO, Andrade J, Monção H. Coronary artery calcium score: current status. Radiol Bras. 2017 May-Jun;50(3):182-189. doi: 10.1590/0100-3984.2015.0235. PMID: 28670030; PMCID: PMC5487233aase R, Schlattmann P, Gueret P et al (2019) Diagnosis of obstructive coronary artery disease using computed tomography angiography in patients with stable chest pain depending on clinical probability and in clinically important subgroups: meta-analysis of individual patient data. Bmj 365:l1945

Author Biography

Dr. Anand H. K.

Chief of Medical Services
and CEO,
Tenet Diagnostics,
Ex-President of Indian
Radiological and Imaging
Association (IRIA), Karnataka
Bengaluru, India

Dr. Anand H. K. is an experienced Radiology and Imaging expert with over 22 years in the field. He is the Chief of Medical Services and CEO at Tenet Diagnostics in Bengaluru. He completed his MBBS in 1996 and earned an MD in Radiology with a Gold Medal in 2000 from Kasturba Medical College, Manipal, India. Dr. Anand co-founded Clumax Diagnostics and has worked as a Consultant Radiologist at various healthcare institutions. He also served as an Assistant Professor at Kasturba Medical College and is an accomplished researcher in areas like Neuro Radiology, Body and Musculoskeletal Imaging, and Cardiac Imaging. He received multiple Radiologists Fellowships for CT Coronary Angiography and has presented and published research at national and international conferences. His contributions demonstrate his dedication to advancing the field of Radiology.

Clinical Evaluation of Advanced Algorithms for CCTA: A Focus on High BMI and Elevated Heart Rate Populations

John Osborne[a], Raju Kosuri[a], Nishant Surapaneni[b], Paul Murdock[c], Yongfeng Gao[d]
[a]State of the Heart Cardiology, Dallas, Texas, USA
[b]School of Medicine, Texas Christian University, Fort Worth, Texas, USA
[c]School of Medicine, Texas Christian University, Fort Worth, Texas, USA
[d]Global Scientific Collaborations, United Imaging Healthcare, Houston, USA

Abstract

The study aims to rigorously evaluate the performance of three advanced algorithms: Auto ALARA, CardioXPhase and CardioCapture, in enhancing the image quality and diagnostic accuracy of Coronary Computed Tomography Angiography (CCTA) in patients with high Body Mass Index (BMI) and elevated heart rates (HR). Eight patients characterized by high BMI (>30 kg/m^2) and HR (>75 bpm) were included in this retrospective study. The clarity and diagnostic quality of the images were analyzed by two experienced cardiologists using a segment-centric approach. Results showed that auto ALARA could optimize the radiation to subjects with large BMI, achieving good diagnostic image quality comparable to those with low BMI. Post-CardioXPhase, 88% (106 out of 120 segments) had diagnostic quality (average score 3.1 ± 0.37). After applying CardioCapture, all segments reached diagnostic quality with an average score of 3.6 ± 0.28. In conclusion, employing advanced algorithms, auto ALARA, CardioXPhase and CardioCapture significantly enhance diagnostic quality in CCTA images, especially for challenging patients with high BMIs and elevated heart rates.

1. Introduction

Coronary Computed Tomography Angiography (CCTA) has been established as an invaluable non-invasive diagnostic technique for the assessment of coronary artery disease (CAD). It empowers clinicians to procure intricate anatomical data without resorting to invasive measures, revolutionizing the diagnostic landscape [1]. Subsequent technological advancements in the field of CCTA have markedly enhanced both image quality and diagnostic precision, cementing its role as an indispensable instrument for evaluating patients with suspected or diagnosed CAD.

Despite these advancements, CCTA presents challenges when imaging patients with elevated Body Mass Index (BMI) and high heart rate (HR). High BMI can potentially lead to increased image noise, reduced spatial resolution, and diminished contrast-to-noise ratio, compromising the diagnostic efficacy of CCTA in this population. Additionally, patients with high HR present motion artifacts, blurring, and incomplete vessel opacification, further complicating accurate diagnosis.

To address these challenges inherent in imaging patients with elevated BMI and high HR, many technological innovations have been introduced. For instance, Electrocardiogram (ECG) triggering technology facilitates the synchronization of CT scans with a patient's cardiac cycle [2]. This capability significantly enhances the acquisition of high-quality images, even in instances of elevated heart rates. Similarly, wide-detector technology expedites scanning speed, thereby ameliorating the presence of motion artifacts and consequently improving overall image quality for patients with high HR [3].

Further technological advancements extend to algorithms designed to modulate radiation doses. These sophisticated algorithms are specifically calibrated to maintain a balance between achieving optimal image quality and minimizing radiation exposure, making them particularly beneficial for patients with high BMI. Among the more recent innovations is the introduction of a cutting-edge 320-row scanner with a rapid rotation time of 0.25 seconds (temporal resolution of 125 ms) [4]. This advanced scanner is equipped with an AI-driven dose-modulation algorithm called auto ALARA that automatically customizes the radiation dose, ensuring the least amount of radiation exposure while still preserving image integrity. CardioXphase empowers automatic selection of optimal reconstruction phase within a cardiac cycle, significantly streamlining tasks for technicians. Additionally, an AI-assisted motion correction algorithm

called CardioCapture enhances correction quality and computational efficiency. This algorithm is designed to be activated whenever residual motion artifacts are detected, thereby ensuring optimal image quality. Given these technological advancements, we hypothesized that the complexity inherent in the CCTA scanning workflow could be significantly streamlined. However, it's important to note that the performance of these innovations, particularly in populations with high BMI and elevated HR, has yet to be comprehensively evaluated.

This paper aims to conduct a rigorous evaluation of this wide-detector facility and its affiliated cutting-edge algorithms, specifically their impact on image quality, diagnostic accuracy, and clinical utility in high BMI and high HR patient cohorts undergoing CCTA.

2. Materials and Methods

2.1 Data Acquisition

This investigation is a retrospective cohort study conducted over a period spanning from September 2022 to January 2023. During this timeframe, a cohort of 135 subjects underwent CCTA examination. A subset of 96 subjects, characterized by a heart rate of less than 75 beats per minute (bpm), were systematically excluded from further analysis. Of the remaining 39 subjects, eight individuals were identified with a BMI exceeding 30. Within this subgroup, the mean BMI was 36.325 kg/m^2, and the average heart rate was 83.25 bpm. Gender distribution revealed that six out of the eight subjects were male. The mean age for this specific cohort was 58 years. Comprehensive demographic and clinical characteristics of the participant population are elaborated in Table 1.

All imaging procedures were conducted using the cutting-edge 320-row detector CT scanner (uCT® ATLAS, United Imaging Healthcare), integrated with prospective ECG triggering capable of capturing data within a single cardiac cycle. The data acquisition was intricately synchronized using a bolus-tracking technique, initiated precisely 6.0 seconds after the moment the attenuation values in the descending aorta surpassed 110 Hounsfield units. The acquisition window spanned from 30% to 55% of the R-R interval or 60% to 85% of the R-R interval which will be automatically determined by the scanner. During the CCTA, the scanning parameters were customized based on individual patient anatomy and needs. The z-coverage was selected from a range of 12 cm, 14 cm, or 16 cm, contingent on the patient's heart size. The reconstruction matrix was standardized at 512 × 512 pixels, with a voxel size of 0.5 mm. The gantry rotation time was set at an ultra-fast 0.25 seconds.

Table 1: Properties of subjects included in the study.

No.	Age	Sex	BMI (Kg/m^2)	Height (feet)	Weight (lb)	Heart Rate (bpm)
1	065Y	M	43.3	5'9"	293	79
2	057Y	F	38.7	5'7"	247	81
3	071Y	M	38.7	5'6"	240	81
4	062Y	M	36.5	5'8"	240	82
5	047Y	M	35.3	7'2"	260	108
6	050Y	M	34.2	5'	175	77
7	053Y	M	33.5	5'8"	220	78
8	056Y	F	30.4	5'2"	166	80

2.2 Advanced Algorithms

2.2.1 Auto ALARA

The "as low as reasonably achievable" (ALARA) principle is commonly employed in the fields of radiology and radiation safety to ensure that exposure to ionizing radiation is minimized to the lowest possible levels, given the constraints of economic and social factors. Auto ALARA is an advanced automatic exposure control algorithm. It automatically adjusts the X-ray tube voltage and current so that the subjects will get optimized image quality with minimum radiation dose. Tube voltage was automatically determined via the Auto-kV feature, offering options of 100 kV, 120 kV or 140 kV, while the tube current was optimized using dose modulation (DOM) techniques.

2.2.2 CardioXPhase

Employing CCTA at strategic temporal junctures when cardiac motion is minimized represents a robust strategy for ameliorating motion-induced artifacts. Conventionally, these moments occur during the systolic and diastolic phases, situated at approximately 45% and 75% of the cardiac cycle, respectively for an average heart rate patient. However, the best phase is not guaranteed in real-world scenarios, necessitating a manual intervention for phase selection.

The uCT ATLAS system is equipped with the automatic best

phase selection method known as CardioXPhase. This technique is built upon coronary quality evaluation [5]. Specifically, this algorithm consists of four steps. In the first step, a rapid multi-phase reconstruction is performed by employing a small Field of View (FOV) and a reduced matrix size including the coronary artery in its designated FOV. Subsequently, in the second step, the algorithm computes a motion map utilizing the Mean Absolute Difference (MAD) algorithm [6], pinpointing the phase characterized by minimal motion as the baseline phase. It then delineates an optimal phase range, centered around this reference phase. Although the MAD-determined phase may not precisely coincide with the coronary motion, it effectively defines a stable range for the cardiac cycles. Progressing to step 3, CardioXPhase extracts the coronary vessels within each phase across the optimal phase range from step 2, and then subjects them to a rigorous evaluation predicated on metrics such as circularity and sharpness. Lastly, in step 4, the phase exhibiting the highest score is deemed the optimal phase [7].

2.2.3 CardioCapture

In some cases, for example, irregular heartbeat (arrythmia), high heart rates, inability to sustain a breath hold, some motion artifacts may still show up. To mitigate the effects of motion artifacts effectively, the uCT ATLAS incorporates an innovative AI-driven motion correction feature called CardioCapture. The algorithm employs deep learning technology to segment coronary artery trees in adjacent temporal segments and derives motion vector models of coronary motion. It then performs motion correction based on those models to produce motion-free images of the heart.

One key of CardioCapture is to derive the motion vector between different time points in the imaging process. The algorithm first reconstructs the target phase (180° of acquisition data typically in the mid-diastole phase) as the weighted reference and then performs multi-temporal reconstruction with overlapping 180° acquisition data. The algorithm then uses deep learning technology to segment the multi-temporal coronary artery tree. Accurate segmentation of the multi-phase coronary artery tree is essential for the coronary artery motion vector calculation. A specialized V-Net architecture employing dilated convolutions is deployed for the segmentation of coronary arteries [8, 9]. Subsequent to this segmentation, an additional optimization algorithm is executed to derive a smoothed arterial centerline from the segmented mask of the coronary artery. Following this extraction, Coronary artery motion tracking is performed to obtain the coronary motion vector from the adjacent phase to the target phase.

By integrating CardioXPhase and CardioCapture, it becomes possible to conduct CCTA examinations with automatic optimized parameters for each patient. This amalgamation is anticipated to significantly augment both the efficiency and accuracy of these diagnostic tests.

2.3 Evaluation

All imaging data were subject to advanced reconstruction via a commercial hybrid iterative reconstruction algorithm (KARL3D, United-Imaging Healthcare), specifically set at level 3 to mitigate image noise. The optimal cardiac phase was automatically determined by the CardioXPhase function, followed by an additional layer of refinement through the CardioCapture algorithm. Two distinct sets of image series, one originating from an automatically selected cardiac phase and another incorporating supplemental motion correction strategies, were generated for subsequent evaluation.

Importantly, all these computational reconstructions were achieved without requiring manual oversight from a radiologist or cardiologist. To evaluate the performance of this automatic reconstruction method, the image quality is evaluated in this retrospective study. A nuanced four-point Likert scale was deployed to rigorously assess the image quality across each coronary artery segment. This assessment was meticulously performed by two experienced cardiologists and conformed to the rigorous 18-segment coronary artery model. The ensuing analysis was executed on a segment-by-segment basis, ensuring a granular level of scrutiny. The procedure of the evaluation is shown in Figure 1.

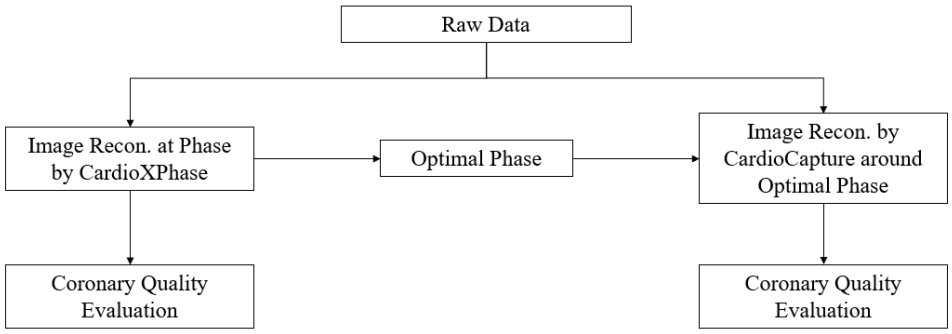

Figure 1. Flowchart Illustrating the Evaluation Procedure. Recon. denotes the image reconstruction.

2.4 Statistical analysis

All statistical investigations were executed utilizing SPSS software (version 22.0; SPSS, Chicago, Ill). Quantitative variables are depicted as mean values accompanied by their standard deviations. The McNemar test was performed to gauge the statistical significance of disparities between paired proportions, where a p-value of less than 0.05 suggests that there is a statistically significant difference between the paired proportions or groups being compared. The agreement between the two cardiologists on the subjective image quality score was assessed using the Cohen kappa test, interpreted as follows: kappa values below 0.20 signified poor agreement; values between 0.21 and 0.40 indicated fair agreement; a range of 0.41 to 0.60 denoted moderate agreement; values within the 0.61 to 0.80 span suggested good agreement; and values from 0.81 to 1.00 manifested excellent agreement.

3. Results

3.1 Evaluation on the auto ALARA

Figure 2 demonstrates auto ALARA-acquired images from two male subjects with different BMIs: one at 43.3 kg/m^2 and the other at 28.8 kg/m^2, both having a heart rate of 79 bpm. For the subject with a BMI of 43.3, auto ALARA fine-tuned the parameters to 140 kV and 660 mA, whereas for the subject with a BMI of 28.8, the optimized settings were 100 kV and 606 mA. Upon visual inspection, both sets of images exhibit comparable image quality, particularly with respect to texture clarity and noise levels.

The radiation dose delivered to patients is influenced by various factors, among which X-ray tube voltage and current are particularly significant. Elevated level current is directly proportional to increased radiation exposure. Voltage is not proportional but positively correlated to radiation exposure. Figure 3 shows the scatter plot of the relationship between BMI and the product of tube voltage (kV) and current (mA) of the subjects in this study. It shows a positive correlation. Overall tendency shows that the higher BMI subject will have higher voltage and current product. This implies the efficacy of the DOM strategy in tailoring imaging parameters to accommodate variations in BMI.

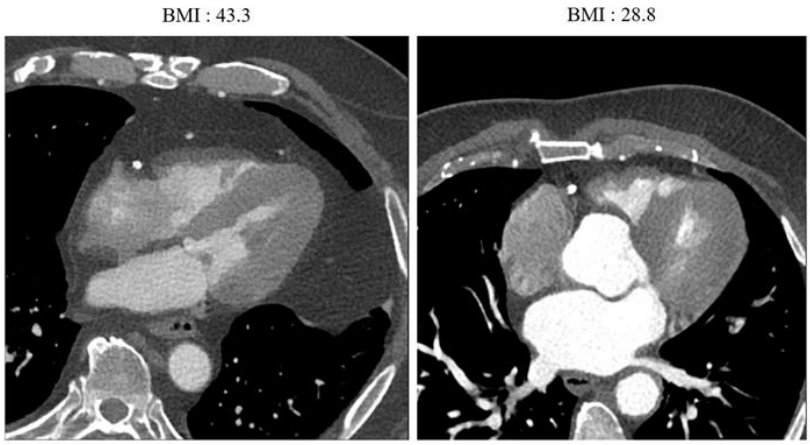

Figure 2. Comparative Imaging Acquired via Auto ALARA for Two Male Subjects with Identical Heart Rates of 79 bpm, Displayed Using a Window Level (WL) of 100 and a Window Width (WW) of 700. All the following CT images used the same display window and will not be emphasized.

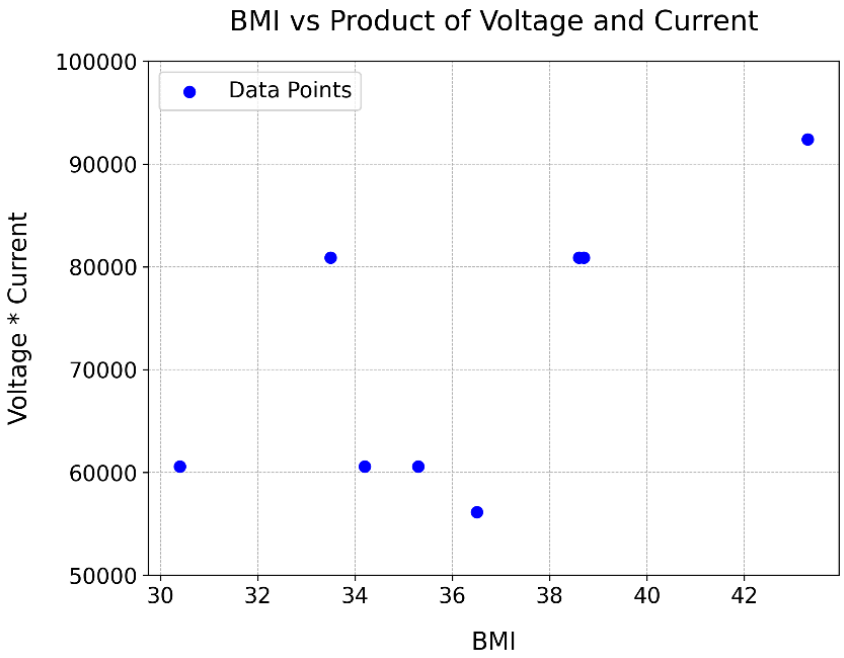

Figure 3. The correlation between BMI and the multiplicative interaction of tube voltage and current within the study cohort.

3.2 Evaluation on the CardioXphase and CardioCapture

3.2.1 Qualitative Evaluation

Adhering to the evaluation procedure presented in Figure 1, two experienced cardiologists assessed the quality of the coronary. Figure 4 shows images generated using CardioXPhase for phase selection and CardioCapture for motion correction. The subject, a male with a BMI of 35.3 kg/m², exhibited a heart rate of 108 bpm. The images demonstrate that CardioXPhase effectively identifies the optimal reconstruction phase for this individual, even with his extremely elevated heart rate. The image quality is already diagnostically reliable, with only minimal motion artifacts present. Subsequent application of CardioCapture further enhances the sharpness of the coronary structures.

Figure 4. 47-year-old man with heart rate 108 bpm. Left panel: the image after CardioXpahse. Right panel: the image after CardioCapture.

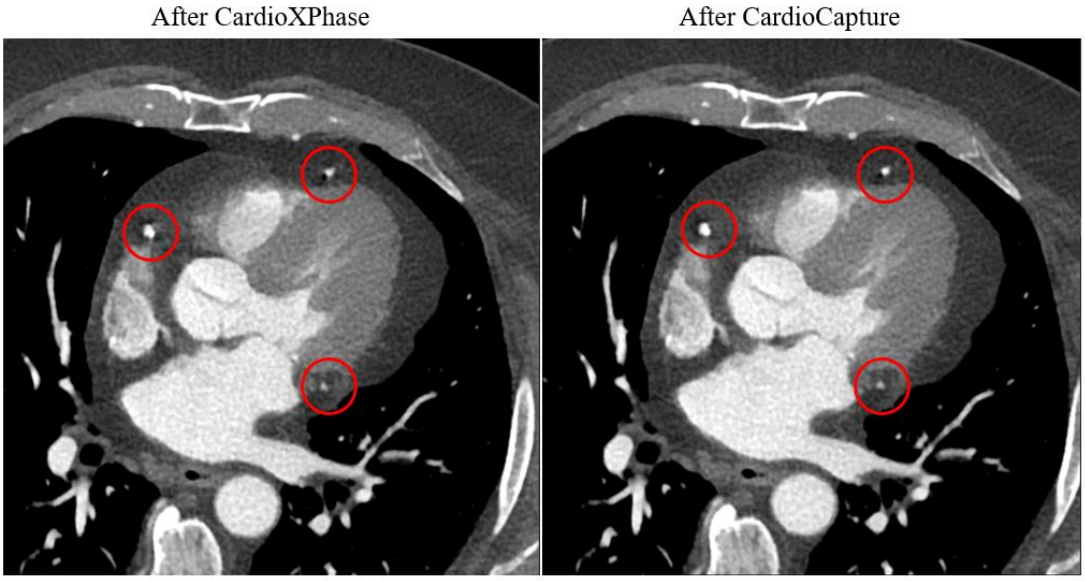

Figure 5. 71-year-old man with heart rate 81 bpm. Left panel: the image after CardioXpahse. Right panel: the image after CardioCapture.

Table 2: Score statistics of four major vessels after CardioXpahse and CardioCapture.

	RCA	LM	LAD	LCX
Mean score after CardioXPhase	2.9	3.3	3.3	2.9
Mean score after CardioCapture	3.7	3.5	3.6	3.6
Mean difference	0.8	0.2	0.3	0.7
p	<0.05	0.21	0.16	<0.05

Figure 5 presents an illustrative example featuring a male subject with a BMI of 38.7 kg/m² and a heart rate of 81 bpm. The images visibly demonstrate the presence of motion artifacts even after the application of the CardioXPhase algorithm. However, these artifacts are significantly reduced upon the subsequent utilization of the CardioCapture algorithm. For easier reference, the coronary arteries of interest have been distinctly highlighted within red circles.

3.2.2 Quantitative Evaluation

A total 124 out of the 144 segments were identified for evaluation in 8 patients with 20 (13.8%) segments being excluded (diameters < 1.5 mm). The subjective consistency of image scoring between two cardiologists was in excellent agreement. After CardioXPhase reconstruction, among the 124 segments, 106 segments (88%) were rated as having diagnostic image quality (scores 2–4) and the average score for all vessels was 3.1 ± 0.37 (Table 2). When CardioCapture was applied, diagnostic segments number became 124 (100%) and the average score is 3.6 ± 0.28.

In four major vessels (RCA, LM, LAD, LCX), CardioCapture results are shown in Table 2. The RCA and LCX depicted significant improvements post-CardioCapture, with mean scores surging from 2.9 to 3.7 and from 2.9 to 3.6, respectively, both reflecting statistical significance with p values less than 0.05. Meanwhile, the LM and LAD, despite showcasing enhancements from 3.3 to 3.5 and 3.3 to 3.6 respectively, did not achieve statistical significance with p-values of 0.21 and 0.16. Notably, the scores for LM and LAD after using CardioXphase had already achieved 3.3, indicating strong diagnostic image quality leaving minimal motion artifacts left for CardioCapture to address.

4. Discussion and Conclusion

In populations characterized by elevated heart rates and high BMIs, this study illuminated the transformative potential of advanced algorithms in enhancing CCTA diagnostic outcomes. The auto ALARA algorithm showcased its adaptability and precision by ensuring consistent image quality across subjects with varying BMIs, reaffirming its utility in such specialized cohorts. The CardioXPhase algorithm was effective in these challenging populations to select the optimal reconstruction phase. CardioCapture proved to be effective to address the motion correction left after CardioXPhase, particularly in boosting image quality for the RCA and LCX vessels. Collectively, these findings emphasize the significance and potential of tailoring advanced algorithms for CCTA to address the unique challenges posed by patients with high heart rates and elevated BMIs. The complexity inherent in the CCTA scanning workflow could be significantly streamlined given these advanced algorithms.

While our study engaged a limited group of eight participants, it's essential to note that we assessed a substantial 144 segments of the coronary arteries. This granularity offers a broader context than the participant count might suggest. Given our specific focus on extreme cases, such as those with rapid heart rates and elevated BMIs, the findings hold significant value. Expanding this evaluation to a larger population would be one of our future interests.

5. Image/Figure Courtesy

All images are the courtesy of Carrollton Regional Medical Center, Dallas, Texas.

6. References

1. Yan, C., Zhou, G., Yang, X., Lu, X., Zeng, M. and Ji, M., 2021. Image quality of automatic coronary CT angiography reconstruction for patients with HR≥ 75 bpm using an AI-assisted 16-cm z-coverage CT scanner. BMC Medical Imaging, 21(1), pp.1-8.
2. Yang, L., Zhou, T., Zhang, R., Xu, L., Peng, Z., Ding, J., Wang, S., Li, M. and Sun, G., 2014. Meta-analysis: diagnostic accuracy of coronary CT angiography with prospective ECG gating based on step-and-shoot, Flash and volume modes for detection of coronary artery disease. European radiology, 24, pp.2345-2352.
3. Al-Mallah, M.H., Aljizeeri, A., Villines, T.C., Srichai, M.B. and Alsaileek, A., 2015. Cardiac computed tomography in current cardiology guidelines. Journal of cardiovascular computed tomography, 9(6), pp.514-523.
4. Yan, C., Zhou, G., Yang, X., Lu, X., Zeng, M. and Ji, M., 2021. Image quality of automatic coronary CT angiography reconstruction for patients with HR≥ 75 bpm using an AI-assisted 16-cm z-coverage CT scanner. BMC Medical Imaging, 21(1), pp.1-8.
5. Wang, Y., Wu, X. and Quan, G., 2019, March. An automatic dynamic optimal phase reconstruction for coronary CT. In Medical Imaging 2019: Physics of Medical Imaging (Vol. 10948, pp. 686-691). SPIE.
6. Manzke, R., Köhler, T., Nielsen, T., Hawkes, D. and Grass, M., 2004. Automatic phase determination for retrospectively gated cardiac CT: Automatic phase determination for retrospectively gated cardiac CT. Medical physics, 31(12), pp.3345-3362.
7. Stassi, D., Dutta, S., Ma, H., Soderman, A., Pazzani, D., Gros, E., Okerlund, D. and Schmidt, T.G., 2016. Automated selection of the optimal cardiac phase for single - beat coronary CT angiography reconstruction. Medical physics, 43(1), pp.324-335.
8. Milletari, F., Navab, N. and Ahmadi, S.A., 2016, October. V-net: Fully convolutional neural networks for volumetric medical image segmentation. In 2016 fourth international conference on 3D vision (3DV) (pp. 565-571). Ieee.
9. Chen, L.C., Papandreou, G., Schroff, F. and Adam, H., 2017. Rethinking atrous convolution for semantic image segmentation. arXiv preprint arXiv:1706.05587.

Authors Biography

Dr. John A. Osborne.

MD, PhD, FACC, FNLA
Founder and Director
State of the Heart Cardiology
Metroplex Cardiology

Dr. Osborne obtained his BS with honors from Penn State University, his MD magna cum laude from Jefferson Medical College, and his Ph.D. in cardiovascular physiology from Thomas Jefferson University. After graduation, he continued his postdoctoral studies at Harvard Medical School and Brigham and Women's Hospital in Boston, Massachusetts where he completed his Internship, Residency and Research Residency in Internal Medicine and a Fellowship in Cardiovascular Disease.

He is the founder and director of State of the Heart Cardiology in Southlake, Texas and is the Director of Cardiovascular CT at the Carrollton Regional Medical Center. He is the Director of Medicine and Clinical Innovation at Market Dynamics, an IQVIA company, which focuses on life sciences consultancy services and has a nationwide U.S. presence, as well as presence in Canada and the Caribbean, to support in-office and in-home testing, drug initiation, and monitoring services.

Nishant Surapaneni

Medical Student,
School of Medicine,
Northeast Ohio Medical University,
Rootstown, Ohio, USA

Nishant Surapaneni is a third-year medical student at NEOMED with a vibrant background in biology and biotechnology from the University of Southern California. As a co-founder and board member of Inhale on Motorola, Nishant has demonstrated his entrepreneurial acumen by co-developing a product that monitors air quality for patients with respiratory distress. His success in fundraising and strategic partnership cultivation has positioned the venture at the forefront of technological innovation in healthcare.

Beyond his start-up endeavors, Nishant's expertise extends to healthcare mergers and acquisitions with Oracle USA, and as a financial analyst for SANA Healthcare, he has deepened his understanding of the financial facets of healthcare delivery. His professional journey reflects a commitment to enhancing patient care through technological advancements, pursuing a blend of medical knowledge and technological innovation.

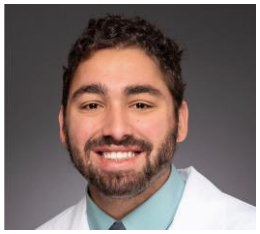

Paul Murdock.

Medical Student,
School of Medicine
Texas Christian University
Fort Worth, TX,

Paul Murdock is currently a medical student at the TCU School of Medicine in Fort Worth, TX. He has a Master of Science from The Johns Hopkins University School of Medicine in Applied Health Sciences Informatics. He is a graduate of the University of Cincinnati, where he received a Bachelor of Science in Medical Sciences and a minor in Psychology. Paul plans to use his degrees to become a physician scientist. He also strives to become a well-rounded learner, researcher, and citizen while in medical school.

Myocardial Perfusion Imaging by PET with Myocardial Blood Flow is Proving to be the Gatekeeper for Identifying Physiologic Severity of CAD by Guiding Treatment with Invasive Procedures and Revascularization – So Why is Adoption Limited?

Amanda Roby, MBA, PET, CNMT, RT(N)

1. Introduction

Positron emission tomography (PET) myocardial perfusion imaging (MPI) with quantitative myocardial blood flow (MBF) has become the scientific standard for assessing coronary artery disease (CAD) severity, including diffuse and microvascular disease. It guides surgical intervention and ensures the safety of lifestyle-medical treatment. There are definitive scientific reports supporting the reliance on the modality, but many limitations on implementation persist. The wide acceptance of PET MPI MBF is hindered by factors such as the need for capital investment by hospitals and clinics, hardware and software limitations that scanner manufacturers have not addressed, gaps in technologist and physician education, and inconsistencies in MBF software.

The nuclear medicine stress test has been instrumental in helping cardiologists evaluate and monitor patient symptoms to identify which patients could benefit from invasive evaluation and therapy since the mid-70s. Thallium-201 (Tl-201) was the first myocardial perfusion tracer used for stress, rest, and viability in a single injection. However, its low gamma emission results in lower image quality and higher radiation exposure compared to the Tc-99m or PET tracers that followed. It also requires a scan time of 4 to 24 hours. Hibernating myocardium is still identified with Tl-201 today but is not commercially available in the United States. Cardiac MRI, PET, or dobutamine ECHO are the alternatives for assessing for hibernating myocardium, which have variable availability.

The Tc-99m perfusion tracers came to market in the 90s with a higher gamma peak and a shorter half-life than Tl-201allowing for the injection of a dose which is 10 times higher. This increases the target-to-background ratio improving image quality while reducing acquisition time. Unfortunately, the Tc-99m tracers lock into the mitochondria and do not redistribute like the sodium-potassium analog Tl-201 removing the ability to define hibernating myocardium. The introduction of Stress-first Tc-99m SPECT MPI improved efficiency by identifying normal patients quickly. However, without the ability to redistribute like Tl-201, patients with a stress perfusion defect require 12 to 24 hours complete the diagnosis of scar verses reversible perfusion defect. SPECT only boasts 65% sensitivity and 70% specificity. Diaphragmatic and breast attenuation defects also result in equivocal studies adding referrals to other modalities and increasing time to diagnosis, cost, radiation exposure, and risk of invasive procedures leading to unnecessary revascularization.

2. Early PET Advances

The development of PET MPI with MBF occurred alongside SPECT, but PET lagged in acceptance due to limitations in computing technology, cost, and tracer accessibility. The commercial availability of Rb-82 generators in the early 2000s facilitated the expansion of cardiac PET MPI beyond academic facilities with cyclotrons, enabling the routine clinical acquisition of PET MBF. The 2000s also saw the conversion from PET with rotating rod sources to hybrid PET/CT systems. The replacement of rotating rods with CT reduced acquisition time, improved the quality of attenuation correction, and added information like coronary calcium burden, but it also brought additional struggles for PET MPI. Attenuation correction images acquired with rotating rod sources occur over minutes and account for the contraction and respiratory translation of the heart. CT for attenuation correction is captured over seconds and may lead misregistration with the PET emission. This misregistration causes artifacts in the PET data increasing the likelihood of false-positive findings.

Advances in software and hardware have addressed these issues, but PET MPI acquisition, reconstruction, and processing are still complicated. Physicians and technologists need a deeper understanding of PET physics, scanner correction structure, and coronary physiology to acquire, process, and report PET MPI MBF. 3D PET scanners are optimized to scan lower doses of 18-F for oncologic-focused exams or "hot spot" imaging, but cardiac imaging bases its principles on "cold spot" imaging. Cardiac PET utilizes "cold spot" imaging that requires accurate count recovery. Accuracy is degraded by inability or sub-optimal scatter, prompt gamma, and random corrections and deadtime and crystal saturation data loss. 3D PET scanners are more susceptible to these problems than 2D systems, especially with high-count, short half-life tracers like the most commonly used Rb-82. 3D systems, when acquired accurately, have higher sensitivity and improved image quality over 2D PET with lower radiation exposure. 2D PET systems are being phased out of production, so this discussion focuses on 3D PET. Scanner manufacturers should test the limitations of each iteration of the model they produce with the common commercial cardiac tracers like Rb-82, O-15, and N-13. Unfortunately, only F-18 and long-lived isotopes like Ge-68 in phantoms are used for validation. Many factors can affect scanner limitations, such as detector material composition, electronic hardware, and computing power for corrections. Because of the range of configurations, it has been difficult for third-party MBF software providers to recommend protocol standards, delaying confidence in reporting MBF and creating confusion. Collectively, these limitations have delayed widespread adoption of cardiac PET MPI with MBF.

Over the past 15 years, cardiac PET has seen a boom in the market, with the volume of outpatient clinics tripling from 2010-2019. Increases in reimbursement in the US have aided this growth, rising from $2250.50 to $2750.50 just in 2022 to 2023 alone. Cardiac PET with Rb-82 allows for rest and stress to be completed in less than 30 minutes, improving the volume efficiency of the nuclear stress lab and offsetting the cost of PET operations. A generator also provides on-demand radionuclide for fast throughput of chest pain units, emergency departments, and hospitals. With few contraindications, cardiac PET can accommodate patients weighing up to 250kg with heart rate or rhythm abnormalities like atrial fibrillation, implanted devices, severe coronary calcium burden, or impaired renal function. More importantly, the sensitivity and specificity of PET MPI are much higher than other modalities, with a sensitivity of 95%, specificity of 90% with high positive and negative predictive values comparable to cardiac catheterization, and an exam failure rate of less than 2%. However, cardiac PET is technically demanding and requires a high level of quality and physiologically informed interpretation to achieve similar precision.

3. A Focus on Quality and Education

3.1 Scanner Hardware and Software

Quality cardiac PET imaging requires multiple components, including scanner design, data acquisition protocol, PET and attenuation correction alignment, and validated MBF software. Each PET scanner has unique limitations when imaging the high-count, short half-life tracers used for MBF. Optimizing protocol structure is the first step to ensure quantitative data accuracy and account for these limitations. The 3D PET list mode acquisition and correction applications are the drivers for the protocol structure and reconstruction timing. High count rate tracers and rapidly changing location dynamics of first-pass arterial activity imaging require corrections of the raw data to occur every 5 seconds or less for scatter, dead time, randoms, and prompt gamma.

The United Imaging 3D solid-state PET/CT Scanner corrects the PET data independently of the acquisition timing every 5 seconds to produce accurate quantification for any reconstruction timing protocol, whether static, dynamic, or gated. This decoupling the list mode data from the acquisition is a novel approach in list mode data correction. Other conventional PET/CT scanners apply raw data corrections based on acquisition timing structure and require careful reconstruction to ensure accurate quantification. Accurate quantification of Rb-82, for scanners with connected acquisitions and corrections, requires dynamic reconstruction of 5 seconds per frame or less for the arterial input phase (~2 minutes) and 10-30 seconds per frame for the uptake phase (~5 minutes). Moreover, it’s crucial to understand the limitations of the crystals, electronics, and correction algorithms with high-count images. Each PET system requires specific testing and protocol evaluation with the tracer planned for patient use and high-count activity to assess its limitations and adapt protocols and dosing accordingly.

3.2 Technologist Education

Nuclear Medicine technologists perform flow on many body parts using a p-scope to assist in positioning with immediate visual display. Positioning the left ventricle can be challenging without this visual tool. Transitioning to PET/CT requires a greater knowledge of cross-sectional anatomy to position the heart with CT rather than a p-scope. PET/CT FOV ranges from 16-24cm in width. 16cm FOV scanners allow coverage for most hearts but can be difficult in patients with large cardiomyopathies. The preferred FOV for cardiac PET is 20-24cm. As reviewed above, using CT for cardiac attenuation correction incurs a high risk for misalignment. Co-registration of PET and CT is also not a skill taught in general nuclear medicine. With long-lived tracers, patient motion is typically corrected by reimaging. Mediation of the motion caused by heart contracting and breathing is not realistically possible. This inherent cardiac and respiratory motion, combined with the 75-second half-life of Rb-82, requires technologists to coach their patients to remain still during acquisition phases. Manual or automated co-registration software is available across all manufactures of modern PET/CT scanners. Registration should allow for translation in the x, y, and z-axis. United Imaging takes this further by adding a rotational shift to its alignment software [1, 2]. Every PET cardiac image must be assessed and corrected for misalignment with the attenuation map, even on systems with automated registration techniques. Any relative perfusion defect not supported by patient history, symptoms, or other findings requires technologists and physicians to scrutinize the images a second time for misalignment. Alignment of PET and attenuation maps for cardiac PET is a specialized technologist skill, not comparable to any other exam processing in nuclear medicine. Hence technologist experience and training play a large role in image quality. Cardiac PET images typically require at least two iterations of reconstruction. The first is the initial unaligned images, then repeating all reconstructions with an aligned attenuation correction. These steps are not automated within the acquisition protocols provided by any manufacture and require additional expertise and time compared to oncologic PET/CT.

Some technologist processing skills are transferable from nuclear medicine cardiac imaging, including angulation and apex, base, and contouring limits to exclude extracardiac activity and ejection fraction calculation. Performing these tasks accurately and reliably is paramount for comparing artery-specific perfusion changes from rest to stress and day to day for comparisons. Processing MBF comprises new theory, processing skills, and critical thinking outside the skill set of an entry level technologist. Many MBF software platforms are available for purchase but vary greatly in concept and accuracy. Johnson's 2021 editorial summarizes how buyers should compare each software vendor to a comprehensive list of validation criteria [3]. The list includes validation in animal models, normal volunteers to ischemic and infarcted patients, precision established by test-retest, customizable arterial input, and documented for clinical utility by use in a clinical outcome review, economic benefit, and randomized trial.

Once an institution decides on a flow package, technologists must be trained to process the data for visualization, flow, and assessment for quality. Unfortunately, current nuclear medicine training programs have neither the clinical sites nor time required to train students in cardiac PET. Cardiac PET is a specialty rotation, allowing a maximum of 4 to 5 weeks of instruction. Our institution's experience in cross-training nuclear medicine technologists in cardiac PET suggests a minimum training period of 3 to 6 months to gain competency. The time to train a technologist depends on the complexity of the PET/CT system they are using and their base knowledge of Rb-82 imaging. To address the workforce education gap, the University of Texas Medical School – Houston has created a Cardiac PET Workforce Training program. Post-graduate nuclear medicine technologists spend six months gaining a comprehensive education in cardiac PET/CT exams, including stress testing, viability, and inflammation imaging as well as certification on two different brands of PET/CT systems, the Cardiogen Rb-82 infusion system, and HeartSee quantitative perfusion software.

Adding flow acquisition and processing to a facility that is currently acquiring Rb-82 presents a smaller learning curve than creating a new service line of cardiac PET with MBF. Cardiac software packages attempt many tasks automatically for the technologist, which creates efficiency for experienced technologists but can degrade quality for inexperienced technologists. Without proper training, technologists will lack the ability to connect patient history, stress results, and image findings to assess accuracy.

Time-activity curve (TAC) modeled software has automated alignment that assists with alignment of the PET flow phase

(24+ frames) and uptake (10+ frames) within segmental cardiac boundaries but is not routinely complete. Misalignment causes substantial errors in quantitative perfusion and technologists must check, correct when necessary, and recognize when those boundaries, though aligned, cannot accurately define the TAC modeled MBF due to the rigid segmentation [4].These tasks are typically considered physician-level duties, but unfortunately, physicians are also not trained to process PET MBF in radiology or cardiology fellowship programs to address this issue, the UT Cardiology fellowship program has recently added a one-month rotation in cardiac PET.

Frame alignment is unnecessary for compartmental model packages that do not use segmental boundaries for the flow and myocardium. Removing segmental boundaries also improves accuracy as averaged segmental flow values in a 17-segment model that arbitrarily overlap arterial distributions are not reported. The overlap causes confusion, routinely under-representing severity, when comparing PET MBF to IAC-FFR. PET's high resolution allows for pixel-level expression of severity, substantially increasing accuracy of an artery-specific diagnosis over the aged 17-segment model carried over from nuclear medicine SPECT [5]. Furthermore, third-party cardiac software often only allows for visualization of the final MBF processing, not the console reconstruction and alignment. Additionally, Radiology Business magazine recently reported that "41% of radiologists surveyed expressed doubt in their skills processing cardiac images," along with 28% doubting their ability in nuclear medicine, despite documented competence [6]. The cardiac PET technologist plays an integral role by applying their knowledge of nuclear physics, instrumentation, coronary physiology, and each patient's unique history to present the most accurate data to the physician for interpretation while working in high-throughput clinics.

3.3 Clinical Gatekeeper

The Supporting Science: Over extensive literature publication for the past 40 years, the University of Texas cardiac PET Center has established the physiologic basis, technological requirements, and clinical application of PET using HeartSee perfusion software. Coronary Flow Capacity (CFC) maps by HeartSee offer particular value to invasive cardiology not provided by any other invasive or non-invasive technology [7]. Coronary angiographic anatomy measurement of percent stenosis fails to adequately stratify CAD risk severity because risk is derived from coronary blood flow and it depends on the arterial lumen radius raised to the 4th power. Therefore, the angiogram's limited resolution cannot accurately measure small changes in stenosis dimension that may cause life threatening changes. The arteriogram is commonly considered the “gold standard” of CAD, but extensive literature proves otherwise. Every randomized trial of coronary stents or bypass surgery guided by angiographic severity has failed to reduce mortality.

Invasive simulated fractional flow reserve (IAC-FFR) based on intra-coronary pressure during maximal coronary blood flow has advanced beyond the angiogram for assessing coronary stenosis. However, it remains inferior to CFC by PET for two reasons. Randomized trials of FFR guided revascularization have failed to demonstrate a reduction in mortality since IAC-FFR also fails to account for coronary blood flow or myocardial perfusion. Cardiac PET does so accurately and quantifies mortality risk and its predicted improvement after revascularization.

PET CFC identifies patients with high mortality that reduces by 54% after PET guided revascularization compared to no-revascularization for comparable PET severity in large non-randomized cohorts of 7000 patients followed for 14 years for major adverse coronary events (MACE) [8-13]. Figure 1 summarizes the transformation of a single observation in a single artery to not only quantifying perfusion per pixel, but the impact of revascularization related to flow by PET taken from the Gould et al publication in 2022. The PET guided survival benefit has now been confirmed by the randomized CENTURY trial being reported at the European Society of Cardiology (ESC) congress in August 2023. The recently completed randomized CENTURY trial also indicates that clinical management and interventions guided by PET HeartSee perfusion software reduced death, myocardial infarction, late revascularization and major adverse coronary events (MACE) compared to standard community care without PET. The HeartSee CFC display condenses the complexity of PET perfusion and MBF giving physicians and patients reassurance to safely pursue lifestyle-medical management and reserving invasive interventions only for objectively severe, high-risk, perfusion abnormalities.

PACIFIC and ReASSESS trials show that PET MBF has the highest accuracy rate (86%) compared to intraarterial cardiac catheterization fractional flow reserve (IAC-FFR), verses SPECT or FFRCT accuracy rates of 68-76% and 70%,

respectively. PET also accommodates patients with atrial fibrillation, metal implants, high BMI, and dense coronary calcium, unlike FFRCT and cardiac MRI (cMRI). And although technically difficult, PET MPI with MBF reports a much lower exam failure rate of 2% compared to FFRCT of 13%[14-16] If the goal is patient-centered care, we must choose the exam that provides the patient with the most accurate and comprehensive result.

A recent case represents the limited scope of anatomical imaging. A 66-year-old female presented to the ER with chest and arm pain radiating to shoulder and back accompanied with vomiting. The day prior she was found to have COVID after feeling generalized malaise and unwell for a week. She had a past history of CAD and PCI to LAD in 2019, anomalous origin of the RCA from the left coronary sinus with course between the aorta and pulmonary artery, as well as hypertension, hyperlipidemia, diabetes, and obesity. Her high-sensitivity troponins peaked at ~1800 and downtrended, anterolateral T-wave inversion without ST-segment elevation. The outlying hospital diagnosed NSTEMI and transferred her for possible intervention of the anomalous RCA.

The patient underwent a left heart catheterization (LHC) which showed a patent stent to the LAD, no stenosis of the left circumflex, but unable to engage the RCA. Cardiac CTA confirmed anomalous origin of a right dominant system from the left coronary cusp, with an intramural course and mild to moderate stenosis with calcified atherosclerotic plaque. Two days later, the patient underwent a second LHC which successfully engaged a patent RCA. The care team considered RCA unroofing verses single vessel CABG but ordered quantitative rest-stress PET perfusion imaging to confirm RCA as source of angina. Dipyridamole stress replicated her angina and caused significant ST depression despite PET MPI showing no resting or stress induced perfusion defect and good CFC with normal regional and global rest-stress flows of 1.76 and 2.23 cc/min/g respectively. Relative tomographic images revealed reduced subendocardial to subepicardial perfusion ratio due to left ventricular hypertrophy and diffuse non-obstructive epicardial coronary atherosclerosis during high coronary flow.

Figure 2 displays this patient's course of events that finally achieved an answer for her angina and a plan for her care. The PET report recommended vigorous blood pressure and heart rate control (201/80 mmHg and 81 bpm at baseline) to decrease the myocardial demand causing reduced hyperemic coronary pressure and subendocardial ischemia. Slowing the heart rate also provides longer diastolic perfusion time for better perfusion through a thickened LV wall. Prior to PET, the invasive and non-invasive anatomical imaging failed to identify the cause of this patient's chest pain after 9 days of in-patient care, accumulating 2215 mGy of radiation exposure and administering 330 ml of contrast media. The PET MPI with MBF provided the care team and the patient confidence to cancel the planned surgery on the anomalous RCA in favor of medical management.

3.4 Summary

While substantial capital investment is required to initiate a PET MPI with MBF program, its downstream efficiency compensates by reducing expenses throughout the care system from less accurate modalities and their associated costs and lost time. It is accepted that accurately quantified cardiac PET is the most robust tool for assessing the severity and directing clinical management of the CAD patient. Adopting such imaging protocol confidently requires investing personnel time and resources to understand the PET/CT system, quantitative perfusion software, coronary pathophysiology and its clinical application. Achieving the best patient care at an efficient cost necessitates collaboration between physicians and technologists unmatched by any other invasive or non-invasive technology.

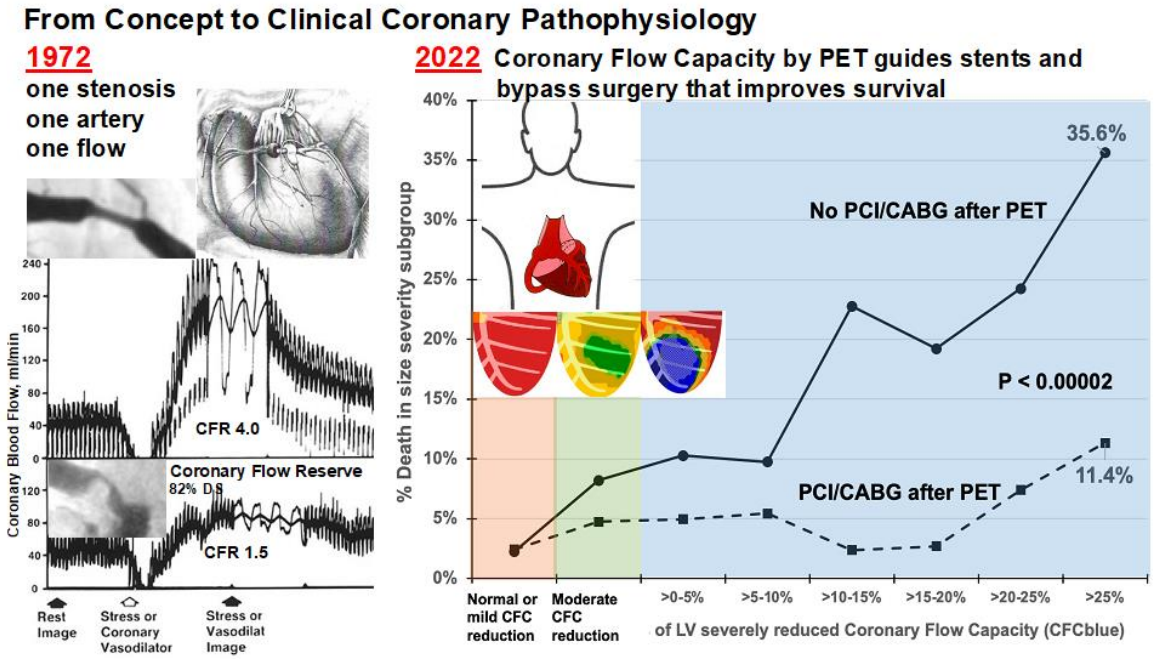

Figure 1 Quantifying perfusion per pixel, and the impact of revascularization related to flow by PET

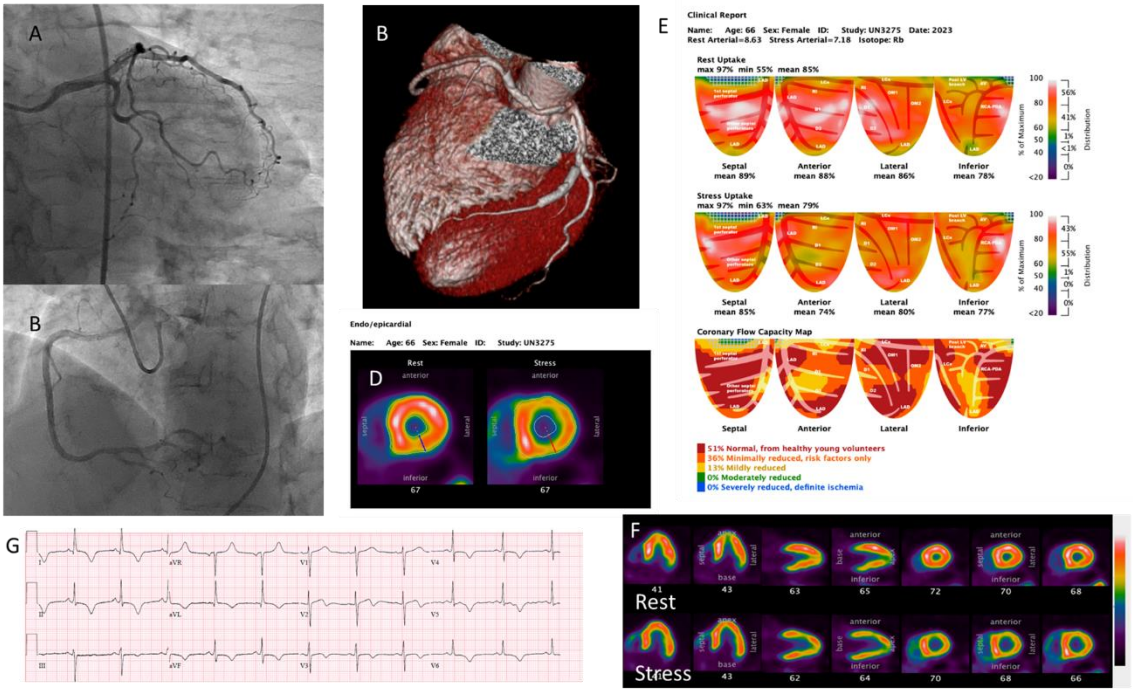

Figure 2: Case study of 66-year-old female presenting with chest pain and complex coronary angiogram for which planned bypass surgery was avoided by quantitative rest-stress PET perfusion imaging (see text for details). (A) LHC patent LAD, no stenosis of LCx, unable to engage the RCA. (B) Cardiac CTA suggesting moderate narrowing of the RCA. (C) repeat LHC found RCA to have mild to moderate stenosis. (D) Reduced stress relative subendo/subepicardial ratio by HeartSee software. (E) HeartSee PET rest-stress relative perfusion and CFC maps. (F) Tomographic PET images. (G) ECG at admission with T-wave inversion.

4. References

1. Loghin C, Sdringola S, Gould KL. Common artifacts in PET myocardial perfusion images due to attenuation-emission misregistration: clinical significance, causes, and solutions. J Nucl Med. 2004 Jun;45(6):1029-39. PMID: 15181138.

2. Slomka P, Diaz-Zamudio M, Dey D, Motwani M, Brodov Y, Choi D, Hayes S, Thomson L, Friedman J, Germano G, Berman D. Automatic registration of misaligned CT attenuation correction maps in Rb-82 PET/CT improves detection of angiographically significant coronary artery disease. doi:10.1007/s12350-014-0060-9

3. Johnson NP, Gould KL. How shall we judge a PET flow model? J Nucl Cardiol. 2022 Oct;29(5):2551-2554. doi: 10.1007/s12350-021-02805-5. Epub 2021 Sep 24. PMID: 34561847

4. Koenders SS, van Dijk JD, Jager PL, Ottervanger JP, Slump CH, van Dalen JA. How to detect and correct myocardial creep in myocardial perfusion imaging using Rubidium-82 PET? J Nucl Cardiol. 2019 Jun;26(3):729-734. doi: 10.1007/s12350-019-01650-x. Epub 2019 Feb 20. PMID: 30788759; PMCID: PMC6517341.

5. Johnson NP, Gould KL Retention models: 'tis the gift to be simple. J Nucl Cardiol 2022; 5:2595-2598.

6. Radiologists read across an average of 5 subspecialties but aren't always confident doing so. June 22, 2023. https://radiologybusiness.com/topics/healthcare-management/medical-practice-management/radiologists-read-across-average-5-subspecialties-arent-always-confident-doing-so. Accessed July 20, 2023.

7. Johnson NP, Gould KL. Physiologic basis for angina and ST change: PET-verified thresholds of quantitative stress myocardial perfusion and coronary flow reserve. J Am Coll Cardiol: Cardiovascular Imaging 2011;4:990-998. Awarded the 2011 Young Author Achievement Award by the Journal of the American College of Cardiology Cardiovascular Imaging.

8. Gould KL, Nguyen T, Kirkeeide RL, Roby AE, Bui L, Kitkungvan D, Patel MB, Madjid M, Haynie MP, Lai D, Li R, Narula J. Subendocardial and Transmural Myocardial Ischemia: Clinical Characteristics, Prevalence and Outcomes With and Without Revascularization. J Am Col Cardiol CV Imaging 2023;16:78-94.

9. Gould KL, Kitkungvan D, Johnson NP, et al. Mortality Prediction By Quantitative PET Perfusion Expressed As Coronary Flow Capacity With and Without Revascularization. J Am Coll Cardiol CV Imaging 2021;14:1020-34.

10. Gould KL, Nguyen TT, Kirkeeide R, Johnson NP. Atlas of Nuclear Cardiology, Chapter 6 Clinical Coronary Physiology and Quantitative Myocardial Perfusion, Fifth Edition, Editors Dilsizian and Narula, 2021, Springer Nature Switzerland.

11. Gould KL, Johnson NP, Roby AE, et al. Regional artery specific thresholds of quantitative myocardial perfusion by pet associated with reduced mi and death after revascularization in stable coronary artery disease. J Nucl Med 2019;60:410-417.

12. Gould KL, Johnson NP, Bateman TM, et al. Anatomic versus Physiologic Assessment of Coronary Artery Disease: Role of CFR, FFR, and PET Imaging in Revascularization Decision-Making. J Am Coll Cardiol 2013;62:1639–53.

13. Gould K, Johnson NP. Coronary physiology: Beyond CFR in microvascular angina. J Am Coll Cardiol 2018;72:2642-62 (Selected for Highlights of the year 2018 in J Am Coll Cardiol 2019;73:849).

14. Driessen RS, Danad I, Stuijfzand WJ, Raijmakers PG, Schumacher SP, van Diemen PA, Leipsic JA, Knuuti J, Underwood SR, van de Ven PM, van Rossum AC, Taylor CA, Knaapen P. Comparison of Coronary Computed Tomography Angiography, Fractional Flow Reserve, and Perfusion Imaging for Ischemia Diagnosis. J Am Coll Cardiol. 2019 Jan 22;73(2):161-173. doi: 10.1016/j.jacc.2018.10.056. PMID: 30654888.

15. Sand NPR, Veien KT, Nielsen SS, Nørgaard BL, Larsen P, Johansen A, Hess S, Deibjerg L, Husain M, Junker A, Thomsen KK, Rohold A, Jensen LO. Prospective Comparison of FFR Derived From Coronary CT Angiography With SPECT Perfusion Imaging in Stable Coronary Artery Disease: The ReASSESS Study. JACC Cardiovasc Imaging. 2018 Nov;11(11):1640-1650. doi: 10.1016/j.jcmg.2018.05.004. Epub 2018 Jun 13. PMID: 29909103.

16.Johnson NP, Gould KL. Coronary physiology – Simulations can't beat the real thing. J Am Coll Cardiol CV Imaging 2020 (In press on line, https://doi.org/10.1016/j.jcmg.2020.02.014)

Author Biography

Amanda E Roby, PET, CMNT, RT(N), MBA
Weatherhead PET Imaging Center
Assistant Director PET Technical Operations

Amanda Roby is a graduate of the University of Oklahoma Nuclear Medicine program with 18 years of experience predominately in cardiac PET, and Assistant Director of Technical Operations at the University of Texas Weatherhead PET/CT Imaging Center. The Weatherhead PET Center is located in the heart of the Texas Medical Center. She worked with the team to invent and validate HeartSee, a myocardial perfusion and quantitative coronary flow software, and the measurement of Coronary Flow Capacity. She has contributed many publications on the subject to their extensive databas of over 12000 PETs and 15 years of patient follow up data.

Role of Cardiac T1, T2 Mapping and Extracellular Volume in the Diagnosis of Clinical Cardiomyopathies

Kamal Aggarwal[a], Dharmesh Singh[b], Anjali Anand[b], Dileep Kumar[b]
[a]Department of Radiology, SSB Faridabad, India
[b]Central Research Institute, Global Scientific Collaborations, United Imaging Healthcare, Shanghai, China

1. Introduction

Cardiomyopathy refers to diseases of the heart muscle that affect the heart's ability to pump blood effectively. There are different types of cardiomyopathies, with dilated cardiomyopathy (DCM) and ischemic cardiomyopathy (ICM) being two major clinical forms [1] [2]. Cardiac magnetic resonance (CMR) imaging is commonly used in a variety of cardiovascular diseases [3]. The primary advantage of CMR is its ability to examine and characterize myocardial tissues. T1 and T2 mapping sequences have been incorporated into standard CMR imaging techniques and are rapidly establishing as gold standard [4].

The conventional sequences are primarily focused on magnetic characteristic, such as T1 relaxation for the purpose of scar imaging, commonly referred to as late gadolinium enhancement (LGE), and T2 relaxation for visualizing edema. T1 relaxation time characterizes each tissue precisely since it depends on the molecular environment of the water molecules in the tissue [5]. Another tissue-specific time measure, T2 relaxation time is utilized to distinguish between normal and abnormal cardiac tissues as well as myocardial edema [6]. However, T2-weighted sequences are particularly susceptible to artifacts. The inability to differentiate global cardiac diseases such as pan-inflammation or prominent fibrosis is a significant shortcoming of these conventional sequences.

Advances approaches such as T1 and T2 mappings were developed and evolved significantly in recent years [4]. A single breath-hold method (mainly performed in short-axis views) is used to generate T1 and T2 maps of the myocardium [7]. These use colored pixel maps to represent T1 or T2 values. In contrast to T2 mapping, T1 mapping can be performed without contrast agent administration, referred to as native T1 mapping. Additionally, T1 mapping can also be performed after the administration of a contrast agent, known as post-contrast T1 mapping. Native T1 values are higher in cardiac diseases such as fibrosis, edema which causing an increase in the extracellular compartment compared to healthy volunteers [8][9]. Renal clearance, gadolinium dose, acquisition time post-bolus injection, hematocrit level, and body composition affect post-contrast T1 mapping values. Extracellular volume fraction (ECV) has been shown to provide a more precise measure of tissue perfusion by subtracting pre- and post-contrast maps with hematocrit correction at adequate equilibrium, which typically occurs 15 minutes after bolus injection [10]. ECV is determined using a formula that integrates hematocrit value, native T1, and post contrast T1. Increased ECV is an indicator of cardiac degeneration that is most caused by excessive collagen deposition (in the absence of amyloid or edema) [10]. T2 mapping identifies myocardial edema in acute infarction and inflammatory disease [11].

Kellman and Hansen [12] reported myocardial ECV in healthy volunteers to be similar at field strengths of 1.5T (0.25) and 3 T (0.26). Giri et al. reported normal myocardial T2 values acquired using steady-state free precession (SSFP) MR imaging [13]. The incremental utility of image-based cardiovascular diagnosis using ML for various types of significant diseases, such as coronary artery disease (CAD) and heart failure, has already been demonstrated in previous studies [14],[15].

In summary, native T1, ECV and T2 values have proved to be promising parameters in the field of cardiac imaging. Machine learning based analysis has not been thoroughly evaluated for the diagnostic classification of active cardiomyopathy conditions using T1, ECV and T2 together. The objective of this study was to examine the additional efficacy of T1 mapping, T2 mapping, and ECV in the diagnosis of cardiomyopathies in a clinical setting.

2. Materials and Methods

2.1 MRI data

This prospective study used an MRI dataset of 32 subjects (age: 45 ± 15 years) who had abnormal left ventricle (LV) ejection fraction and were suspected of having cardiac diseases, specifically DCM and ICM with approval from the Institutional Review Board. Scanning was performed on a 1.5T MR scanner (uMR 580, United Imaging Healthcare Co., Ltd., Shanghai, China) at SSB Hospital, Faridabad using a dedicated cardiac coil from January 2023 to May 2023. The CMR protocol comprised gated fast spin echo (FSE) T1, FSE T2, and cine in axial, long axis, and short axis planes with SSFP sequences aligned to 2 chamber view, 4 chamber views well as T1 and T2 mapping. Intravenous gadolinium-based contrast agent with a dose of 0.15 mmol/kg was injected, and post-contrast T1 mapping was performed 10 minutes after contrast media injection (this approach was used for ECV measurements).

T1 mapping were obtained from three short-axis images (basal, center, apical) of the LV using Modified Look-Locker Imaging (MOLLI) technique. T2 mapping was carried out using a conventional T2-prepared single shot SSFP sequence. Table 1 presents the protocol parameters.

Table 1: Mapping protocols

Mapping	TR/TE (ms)	Slice thickness (mm)	Field of view (mm^2)	Acquisition matrix	No of slices
T1	3.44/1.58	8	320 × 360	342 × 384	5
T2	3.44/1.58	8	320 × 360	342 × 384	5

2.2 Data processing

MRI data in DICOM format were transferred to a workstation and processed using MATLAB (v. 2018; MathWorks, Natick, MA, USA).

2.2.1 Measurement of T1, T2 and ECV

Following image acquisition, T1 and T2 maps were generated from the MR workstation (uWS-MR, United Imaging Healthcare Co., Ltd., Shanghai, China). T1 times were measured from myocardium and blood pool region of interest (ROI) before and after contrast agent administration. Myocardial ROIs were used to measure T2 times. The estimation of ECV requires the assessment of myocardial and blood T1 values both before and after the administration of contrast agents, in addition to the patient's hematocrit level. The ECV formula is as follows:

$$ECV = (1 - hematocrit) \times (\Delta R1 myocardium / \Delta R1 blood),$$

where R1 = 1/T1

Figure 1 demonstrates the basal short-axis native T1, post-contrast T1, ECV, and T2 maps of a 25-year-old male without active cardiomyopathy. Figure 2 depicts the native T1, post-contrast T1 map, ECV map, and T2 map of a 55-year-old male diagnosed with dilated cardiomyopathy at the basal short-axis level. In comparison, figure 3 illustrates the same maps for a 79-year-old patient with ischemic cardiomyopathy. Standardized global and focal T1, T2 mapping, and ECV measurements were carried out in each of the case studies that were reported.

2.2.2 Diagnostic performance of the T1, T2 and ECV

Machine learning methods such as linear support-vector machine (SVM), Gaussian SVM, and linear discriminant analysis (LDA) were employed to evaluate the efficacy of T1, T2, and ECV in the clinical diagnosis of cardiomyopathies. The proposed framework presents a classification approach for differentiating between individuals without active cardiomyopathy (n=16) and those with active cardiomyopathy (n=16). Here, DCM and ICM were both considered the forms of active cardiomyopathy.

2.2.3 Statistical analysis

The diagnostic accuracy of the proposed classification was validated using 5-fold cross-validation. The sensitivity, specificity, accuracy, and area under the receiver-operating characteristic curve (AUC) were measured to evaluate the performance of classification. The paired *t*-test and boxplots were used to compare the T1, T2, and ECV values of the two groups.

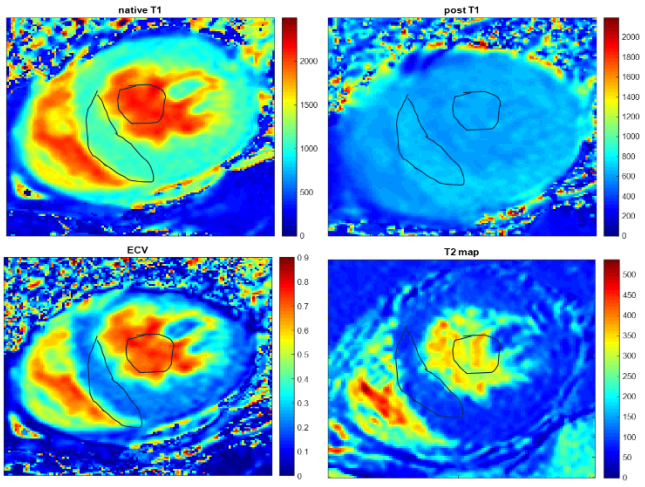

Figure 1: Representative images of native T1, postcontrast T1, extracellular volume fraction (ECV) map and T2 map of a 25-year-old without active cardiomyopathy subject. Region of interests for myocardium and blood pool regions are also shown. His left ventricle was normal (LV end-diastolic dimension=4.9 cm, volume=148 mL) and showed LV ejection fraction was 54

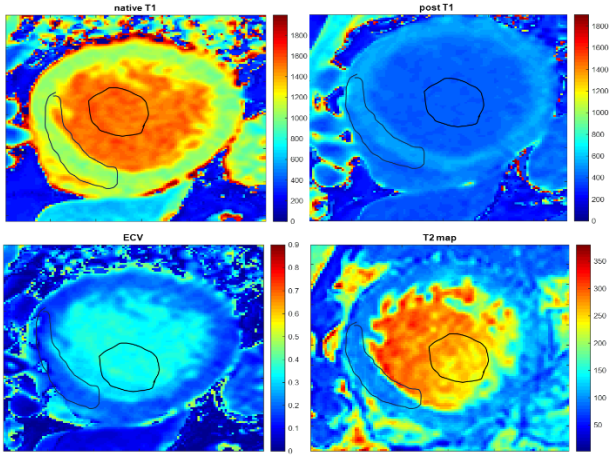

Figure 2: Representative images of native T1, postcontrast T1, extracellular volume fraction (ECV) map and T2 map of a 55-year-old with active dilated cardiomyopathy patient. Region of interests for myocardium and blood pool regions are also shown. His left ventricle was dilated (LV end-diastolic dimension = 7.06 cm, volume = 361 mL) and showed low LV ejection fraction (11.30%).

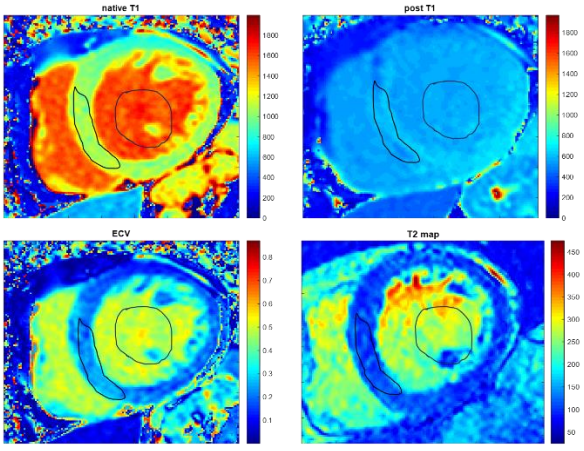

***Figure 3*:** Representative images of native T1, postcontrast T1, extracellular volume fraction (ECV) map and T2 map of a 79-year-old with chronic ischemic cardiomyopathy patient. Region of interests for myocardium and blood pool regions are also shown. His left ventricle end-diastolic dimension = 5.70 cm, volume = 360 mL) and showed low LV ejection fraction (24%).

3. Results

3.1 T1, T2 and ECV values

The mean native T1, T2 and ECV of myocardial regions in patients with active cardiomyopathy were 1315.45 ± 65 ms, 62.34 ± 7.26 ms and 32.72 ± 3.20% respectively, while patients without active cardiomyopathy had mean values of 1184.60 ± 67 ms, 53.12 ± 9.10 ms and 24.06 ± 3.52%. Patients Table 2 demonstrates the results of two class classification (without vs. with active cardiomyopathy) using three different maps and combinations of these maps. The combination of T1 and T2 achieved the sensitivity of 76.47 ± 1.23 %, specificity of 90.90 ± 1.59%, accuracy of 82.00 ± 2.05% and AUC of 0.78 using 5-fold cross-validation. The classification performance using ECV alone and for a combination of T1, T2 diagnosed with active cardiomyopathy had considerably ($p < 0.05$) greater native T1, T2 and substantially increased ECV values when compared to participants who did not have active cardiomyopathy. Boxplots comparing the T1, T2, and ECV values of the two groups are depicted in Figure 4.

3.2 Diagnostic performance using machine learning methods

and ECV was also evaluated. The linear SVM classifier achieved the highest performance with sensitivity of 92.30 ± 2.60 %, specificity of 86.67 ± 1.76 %, accuracy of 89.30 ± 1.95%, and AUC of 0.92 in two-class classification using a combination of T1, T2 and ECV. Figure 5 shows the ROC graphs for the two-class classifications using three different maps and combinations of these maps

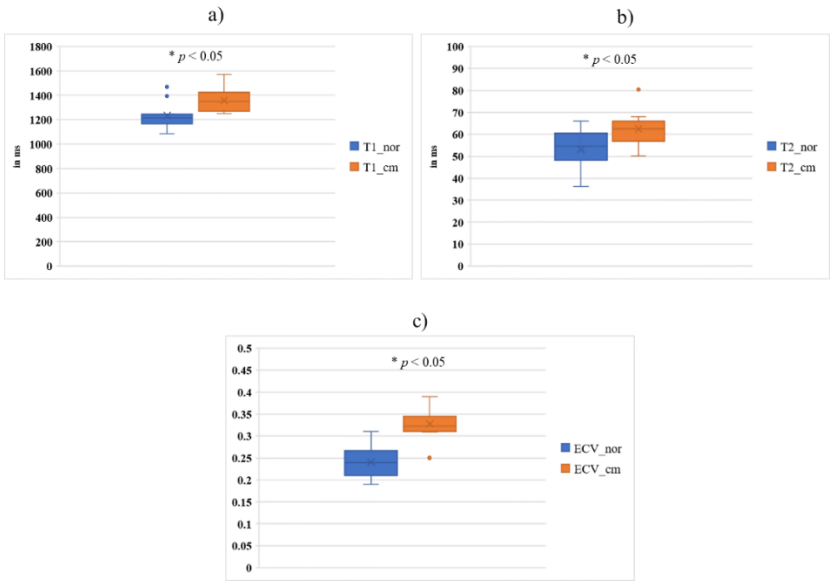

Figure 4: Boxplots for the comparison of T1, T2 and ECV blues between two groups. nor = Patients without active cardiomyopathy and cm = Patients without active cardiomyopathy.

Table 2: Classification performance of the proposed model for two class classification using 5-fold cross-validation.

Maps	Accuracy (%)	Sensitivity (%)	Specificity (%)	AUC
T1	75.00 ± 2.50	72.23 ± 1.45	80.00 ± 1.90	0.80
T2	67.90 ± 1.15	63.63 ± 1.50	58.50 ± 2.12	0.68
ECV	71.40 ± 1.20	72.00 ± 2.50	72.00 ± 1.90	0.84
T1+T2	82.00 ± 2.05	76.47 ± 1.23	90.90 ± 1.59	0.78

T1+T2+ECV	89.30 ± 1.95	92.30 ± 2.60	86.67 ± 1.76	0.92

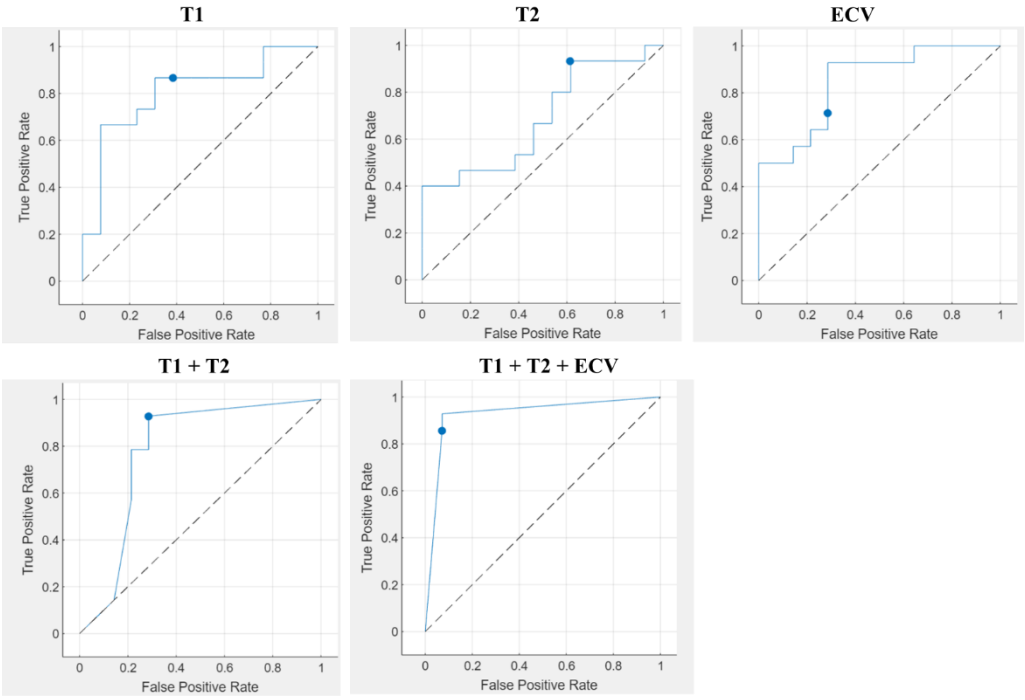

Figure 5: ROC graphs for the two-class classification using T1, T2 and ECV alone and the combination of these maps

4. Discussion

In this work, the role of T1 mapping, T2 mapping and ECV has been demonstrated in the diagnosis of cardiomyopathies (both dilated and acute ischemic cardiomyopathies) in a clinical setting.

These sequences are becoming increasingly available and are being utilized more frequently in clinical routine settings. Many studies in the recent literature demonstrated that mapping is an effective approach in the detection and measurement of global or diffuse cardiac processes without the necessity for endomyocardial biopsy [16]. According to Roller et al. (2015) [17], the application of mapping and ECV techniques exhibits significant promise in the assessment of prognostic indicators for various cardiac conditions. Furthermore, these measures can potentially serve as endpoints in clinical trials or aid in the monitoring of therapeutic interventions.

The T1, T2 mapping, and ECV have showed distinct advantages over alternative imaging techniques and sequences in the identification of early stages of several cardiomyopathies. This is primarily attributed to their ability to quantify T1 and T2 values at a voxel level, enabling the visualization of both local and global cardiac processes [17]. It has been found that native T1, T2 and ECV showed additional improvements in the diagnosis of cardiac diseases [18]. Nevertheless, it has still to be determined if the combination of mappings will play a significant role in the diagnosis of myocardial inflammation, offering enhanced diagnostic accuracy, rather than only being an additional feature in CMR settings.

The current study reported that patients diagnosed with active cardiomyopathy have higher levels of native T1 (1315.45 ± 65 ms vs. 1184.60 ± 67 ms), increased T2 (62.34 ± 7.26 vs. 53.12 ± 9.10 ms, $p < 0.05$), and significantly higher ECV expansion (32.72 ± 3.20% vs. 24.06 ± 3.52%) in comparison to patients who do not have active cardiomyopathy. The performance of the classification of active cardiomyopathy and no cardiomyopathy subjects was assessed by the T1, T2 mapping, and ECV individually, as well as in combination with T1, T2, and T1, T2, ECV. The classifier results showed that the incorporation of ECV together with T1 and T2 contributed to

a significant improvement (p<0.05) in the classification accuracy (89.30% vs. 82%).

Furthermore, the combination of T1, T2 mapping and ECV may serve as a prognostic tool or provide additional diagnostic advantages. Additionally, it might contribute to a deeper understanding of the underlying pathophysiology. However, there are some limitations of the study. One primary limitation of the study is the small sample size. The small sample size only offers initial indications regarding the diagnostic efficacy of mapping techniques; a large cohort and multicentre study can provide stronger evidence for larger clinical application. Furthermore, a direct comparison between native T1, T2, and ECV measurements and histological findings was not conducted due to the limited number of patients who had endomyocardial biopsy.

5. Conclusion

The integration of T1, T2, and ECV mapping techniques has showed encouraging outcomes in diagnosing of clinical cardiomyopathies, with an accuracy of 76% and AUC of 0.78. Furthermore, the implementation of these mapping techniques has the potential to consistently enhance the diagnosis of cardiomyopathies, which needs to be further evaluated with larger sample size.

6. Image/Figure Courtesy

All images are the courtesy of SSB Hospital, Faridabad, India.

7. References

1. Griffin BP, editor. Manual of Cardiovascular Medicine (4th Ed.). Philadelphia, PA: Lippincott Will José Marín-García,

2. Alimadadi A, Manandhar I, Aryal S, et al. Machine learning-based classification and diagnosis of clinical cardiomyopathies. Physiol Genomics. 2020;52: 391–400.

3. Yoon YE, Hong YJ, Kim HK, et al. 2014 Korean guidelines for appropriate utilization of cardiovascular magnetic resonance imaging: a joint report of the Korean Society of Cardiology and the Korean Society of Radiology. Korean J Radiol. 2014;15:659–688

4. Piechnik SK, Ferreira VM, Lewandowski AJ, et al. Normal variation of magnetic resonance T1 relaxation times in the human population at 1.5 T using ShMOLLI. J Cardiovasc Magn Reson. 2013;15:13

5. Burt JR, Zimmerman SL, Kamel IR, et al. Myocardial T1 mapping: techniques and potential applications. Radiographics 2014;34:377–395.

6. Kim PK, Hong YJ, Im DJ, et al. Myocardial T1 and T2 mapping: techniques and clinical applications. Korean J Radiol 2017;18:113–13

7. Piechnik SK, Ferreira VM, Dall'Armellina E, et al. Shortened Modified Look-Locker Inversion recovery (ShMOLLI) for clinical myocardial T1-mapping at 1.5 and 3 T within a 9 heartbeat breathhold. J Cardiovasc Magn Reson. 2010;12:69.

8. Dass S, Suttie JJ, Piechnik SK et al. Myocardial tissue characterization using magnetic resonance non contrast T1 mapping in hypertrophic and dilated cardiomyopathy. Circ Cardiovasc Imaging, 2012; 6: 726– 733

9. Ferreira VM, Piechnik SK, Dall'Armellina E et al. Non contrast T1 mapping detects acute myocardial edema with high diagnostic accuracy: a comparison to T2-weighted cardiovascular magnetic resonance. J Cardiovasc Magn Reason, 2012; 14: 42

10. Banypersad SM, Sado DM, Flett AS, et al. Quantification of myocardial extracellular volume fraction in systemic AL amyloidosis: an equilibrium contrast cardiovascular magnetic resonance study. Circ Cardiovasc Imaging 2013;6:34–39.

11. Thavendiranathan P, Walls M, Giri S et al. Improved detection of myocardial involvement in acute inflammatory cardiomyopathies using T2 Mapping. Circ Cardiovasc Imaging 2012; 5: 102–110

12. Kellman P, Hansen MS. T1-mapping in the heart: accuracy and precision. J Cardiovasc Magn Reson 2014;16:2.

13. Giri S, Shah S, Xue H, et al. Myocardial T2 mapping with respiratory navigator and automatic nonrigid motion correction. Magn Reson Med. 2012;68:1570–1578

14. Leiner T, Rueckert D, Suinesiaputra A, et al. Machine learning in cardiovascular magnetic resonance: basic

concepts and applications. J Cardiovasc Magn Resonan. 2019; 21:61.

15. Martin-Isla C, Campello VM, Izquierdo C, et al. Image-Based Cardiac Diagnosis with Machine Learning: A Review. Front Cardiovasc Med. 2020;7:1.

16. P. Lurz, I. Eitel, J. Adam, et al. Diagnostic performance of CMR imaging compared with EMB in patients with suspected myocarditis. J Am Coll Cardiol Img, (2012); 5: 513-524

17. Roller FC, Harth S, Schneider C, et al. T1, T2 Mapping and Extracellular Volume Fraction (ECV): Application, Value and Further Perspectives in Myocardial Inflammation and Cardiomyopathies. Rofo. 2015;187(9):760-770.

18. Ntusi NA, Piechnik SK, Francis JM et al. Subclinical myocardial inflammation and diffuse fibrosis are common in systemic sclerosis--a clinical study using myocardial T1-mapping and extracellular volume quantification. J Cardiovasc Magn Reson. 2014;16:21..

Author Biography

Dr. Kamal Aggarwal

Director & Senior Consultant

Radiology Department,

SSB Hospital, Faridabad, Haryana, India

Dr. Kamal Aggarwal graduated with his MBBS from the University of Delhi in Delhi in 1993. He received his MD in 1998 in Radio Diagnosis/Radiology from the University of Delhi. He has 23 years of experience in the radiology field. Dr. Kamal Aggarwal practices at SSB Multispecialty Hospital in Sector 20A, Faridabad, India.

A Vision for Magnetic Resonance Imaging to Assess Cardiotoxicity

Mary P. Watkins[1], Anne H. Atteberry[1], Arun Innanje[2], Shanhui Sun[2], Xiao Chen[2], Terence Chen[2], Qamer Syed[1], Joshua D. Mitchell[1], Morgan Wang[3], Gregory M. Lanza[1]
[1] Division of Cardiology, Washington University Medical School, St. Louis, MO, USA
[2] United Imaging Intelligence, Cambridge, MA, USA
[3] United Imaging Healthcare America, Houston, TX, USA

1. Introduction

A cancer survivor, as defined by the NCI, encompasses individuals from diagnosis throughout life. In the U.S., there were 18.1 million survivors in 2022, projected to be 26 million by 2040, with 60% surviving past 5 years and 40% past 10 years [1]. Having survived cancer, they face ongoing risks of treatment-related toxicities and comorbidities that could compromise their hard-earned quality of life [2]. Cardiovascular toxicity is a major cause of morbidity and mortality during or after cancer therapy [3,4]. It is very challenging to evaluate cardiotoxicity with cardiac imaging and circulating biomarkers findings, so clinical heart failure may serve as sole reliable evidence of toxicity [3,4,5]. Once heart failure occurs, near normal cardiac recovery is unlikely, and even with guideline-directed medical therapy (GDMT), there continues to be an elevated long-term risk for cardiovascular issues. Cardiotoxicity may present as tissue inflammation, fibrosis, edema associated with cancer therapies or toxicities relating to infiltration into the myocardial interstitium by various substances like proteinaceous amyloid fibrils, immune and inflammatory cells, iron-related deposits, and liposaccharides.

Cardiac MRI (cMRI) is a well-recognized "gold-standard" quantitative imaging reference. However, cMRI's benefits outside of academic centers are limited by barriers. To implement cMRI effectively, experienced technologists who understand cardiac anatomy and function are needed for precise imaging such as obtaining appropriate scout scans, accurate slice placement and precise magnetic focusing (shimming). Post-processing approaches of cMRI require time, expertise and dedicated software which are not typically available in nonacademic institutions, such as global and regional strain analyses, T1 and T2 mapping, extracellular volumes (ECV), and late gadolinium enhancement (LGE; so-called "scar imaging").

To make advanced cMRI accessible to all patients, future MRI scanners should simplify and speed up the entire process. Automation and AI-enhanced systems will assist technologists in producing reproducible imaging data and analyses in less time (Figure 1). This benefits older or sicker patients and allows for more efficient use of MRI scanners, improving diagnostic quality and patient management.

2. Scout Scans

cMRI begins with scout scans with breath-holds to obtain the four standard views (Figure 1). UIH EasyScan™, previously reported (1), is a new technique enabling a single acquisition of transverse images in one breath-hold that are quickly AI-processed into the four standard views for slice placement (Figure 2). EasyScan™ allows accurate slice planning with minimal effort and high reproducibility, esp. for less-experienced technologists. Experienced cMRI technologists may stick to traditional approach to "tweak" plane positioning, but when patient movement requires redoing scout scans, EasyScan™ is the quick and preferred solution.

Magnetic Shimming: To accurately evaluate cardiac anatomy and functions qualitatively and quantitatively, cMRI sequences require "magnetic field focusing", typically achieved by adjusting the B0 field. UIH AIshim™ optimizes the B0 field for the entire cardiac image in one go, delivering faster better images and improved quantification (Figure 3) [1].

3. Structural and Functional Metrics

Since 2020, the UIH MR scanner has automatically used AI to quantify LV and RV size, volume, mass and function. After initial acquisition of short axis slices (SAX), the MR technologist verifies or tweaks the segmentation map. The adjustments propagate through the slices and a table of key quantitative LV and RV data is generated. Because that segmentation map was not transferable to other processes in the previous version, a new AI approach that segments the

LV and RV images and computes the structural and functional data is being developed and currently under final testing. In the current version, the segmentation maps are available for other pipeline processes including: 1) feature tracking estimates of global and regional longitudinal, circumferential and radial strains; 2) conversion of T1 and T2 (T2*) relaxation time maps into maps of abnormal T1 and T2 myocardium estimates and processing of ECV; and 3) mapping and quantitating LV LGE for tissue viability estimates ("scar imaging") (Figure 1).

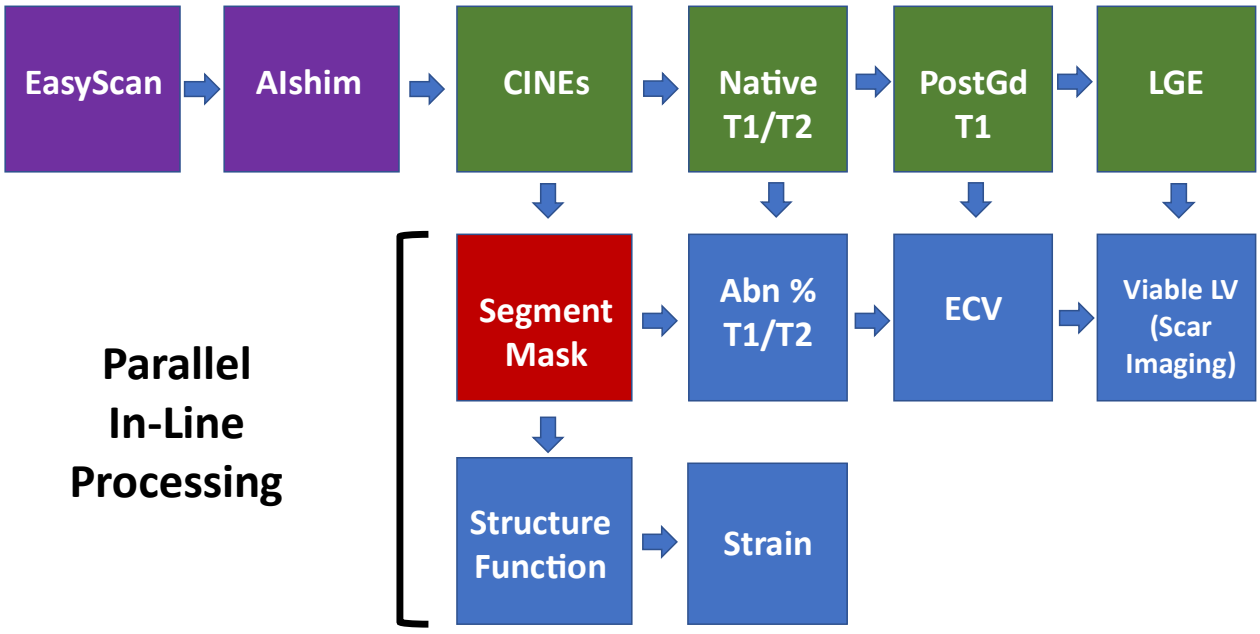

Figure 1. Schematic of the automated workflow pipeline with parallel in-line image processing. Purple boxes reflect new, AI-enabled and simplified scout scan acquisition and shimming. Green boxes represent current standard cMR imaging data obtained in typical non-ischemic cardiomyopathy evaluation which further processed for complete evaluation. The Red box reflects image segmentation performed on CINE images. Blue are image post-processing results generated automatically with AI and reported to the reader with the images for final interpretation.

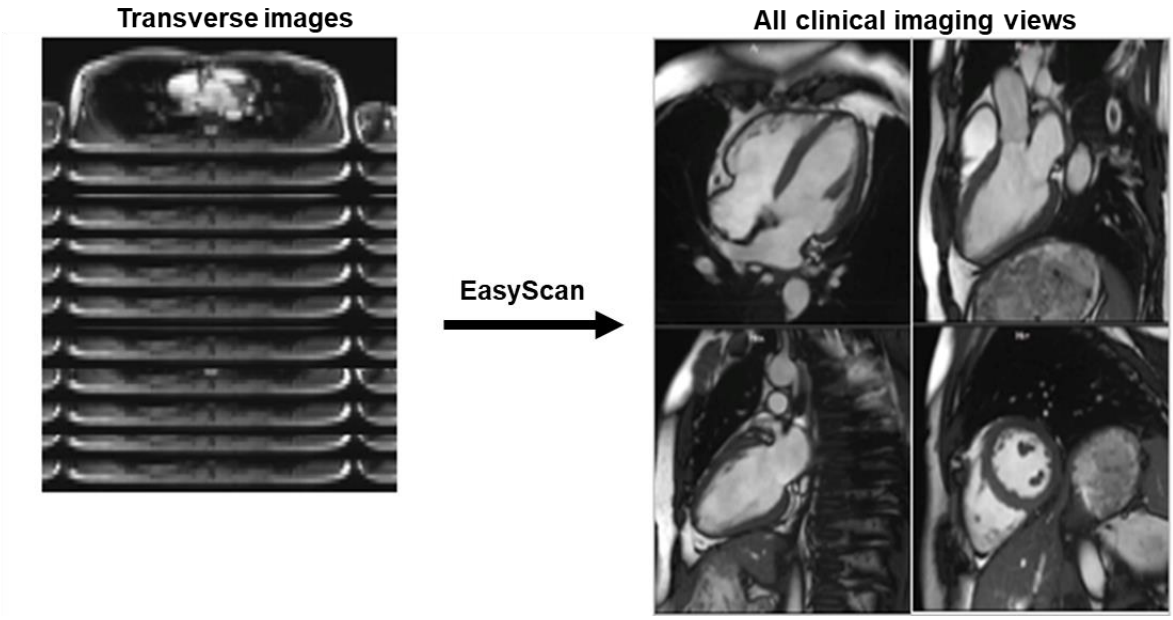

Figure 2.UIH EasyScan™ automatically acquires transverse images and uses AI/Deep learning to generate clinical views with 1 breath hold (Ref 1).

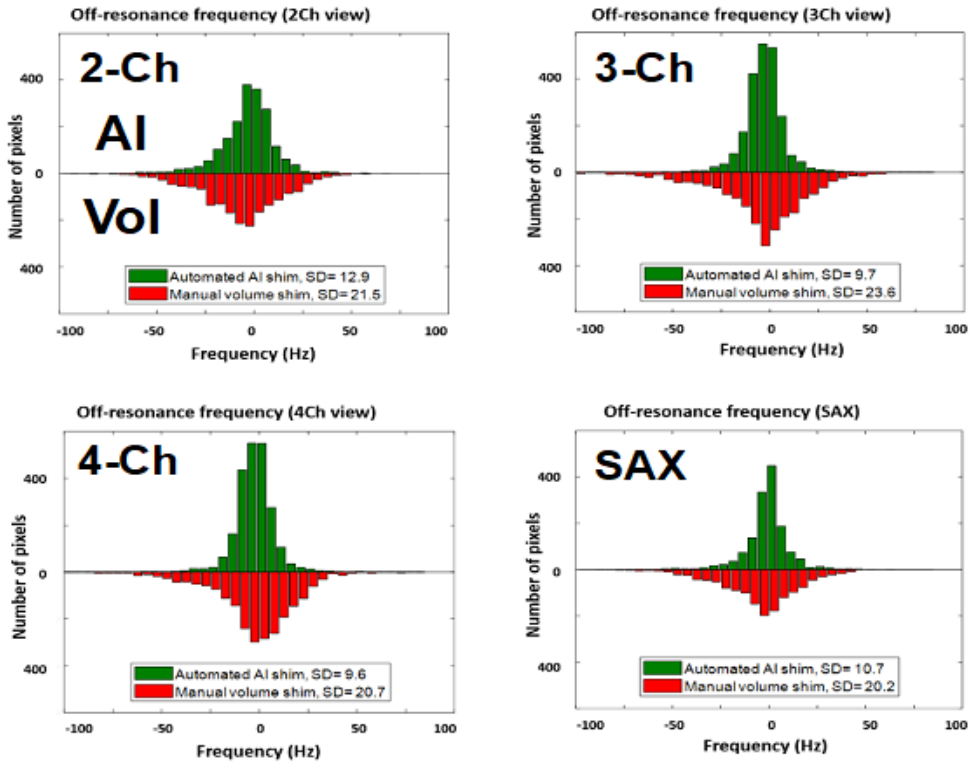

Figure 3. Four standard views illustrating improved on-frequency image distribution with UIH AIshim. AIshim (Green) vs Volume shim (Red) yields crisper images, higher SNR, and improved quantitative results (Ref 1).

4. Myocardial Strain

Global myocardial deformation, i.e., strain imaging, with AI enhanced speckle is now integrated into cardiology management guidelines. Strain estimates in MRI have been studied for many years using tagging approaches including DENSE (University of Virginia, Charlottesville, VA) and SENC (MyoScan; Myocardial Solutions, Inc.; Morrisville, NC). SENC images are acquired rapidly (6 sec/plane). AI off-line processing of the images yields a complete report in several minutes. Alternative non-tagging and AI feature tracking (FT) methodology are similarly used for off-line post-processing by CIRCLE Cardiovascular Imaging (Calgary, Canada) and by UIH. UIH scanners have a built-in data processing approach, where CINE images are transferred to a powerful multi-GPU workstation and processed automatically to generate the report. AI FT methods reprocess the balanced steady state free precession (bSSFP) CINE images used for structure and function assessments to obtain strain analyses. This in-line AI approach saves time by processing the data while the scanner operating system acquires additional study images.

5. Myocardial Characterization

The Washington University in Saint Louis -UIH approach to myocardial characterization enhances the utility of the T1/T2 maps by covering the entire heart (up to 9 slices). Voxels that deviate 2 or 3 standard deviations above or below expected nominal myocardial T1 or T2 relaxation times are color-coded yellow or red, respectively. We retain abnormal myocardium voxels that are contiguous with two or more such voxels, eliminating the remaining isolated abnormal and normal voxels. The resultant color map is superimposed on a grayscale image slice, offering an easily-interpretable quantitative abnormal map of each slice. The percent volume of abnormal myocardium (high and low) is calculated for each slice and the entire heart. We empirically categorize the percent volume into ranges of normal, mild, moderate, high, and very high, and such sensitive, quantitative metrics can aid cardiomyopathy diagnoses and support longitudinal progression determinations (Figure 4). Moreover, while T1/T2 maps typically require a short breath-hold per slice, free breathing sequences for acquiring T1/T2 maps under

investigation show potential to improve patient comfort without compromising accuracy of mapping.

T1 maps pre- and post-gadolinium are acquired, segmented, and aligned to estimate ECV normalized for hematocrit for each slice and the entire heart. ECV, structural/function metrics, global longitudinal strain and T1/T2 indexes of abnormal myocardium form a comprehensive dataset for characterizing cardiotoxicity associated with myositis, myocardial edema, and differentiating cardiac fibrosis from amyloid infiltration (Figures 5, 6). Renal dysfunction can preclude the use of gadolinium for ECV estimates. In our experience, cardiac amyloidosis shows a long insidious progression associated with increasing abnormal T1 myocardium and expanding ECV. In the late phase, it is associated decreased LV contractility, increased EDV, increasing wall thickness and diminishing GLS. In contrast to cardiac amyloid infiltration, diffuse fibrosis is associated with reduced GLS earlier in its progression, often followed by declining cardiac function, changes EDV, ESV or wall thickness. Regardless, these diagnoses require confirmation with biochemical tests, biopsy, or Tc-99m pyrophosphate scan.

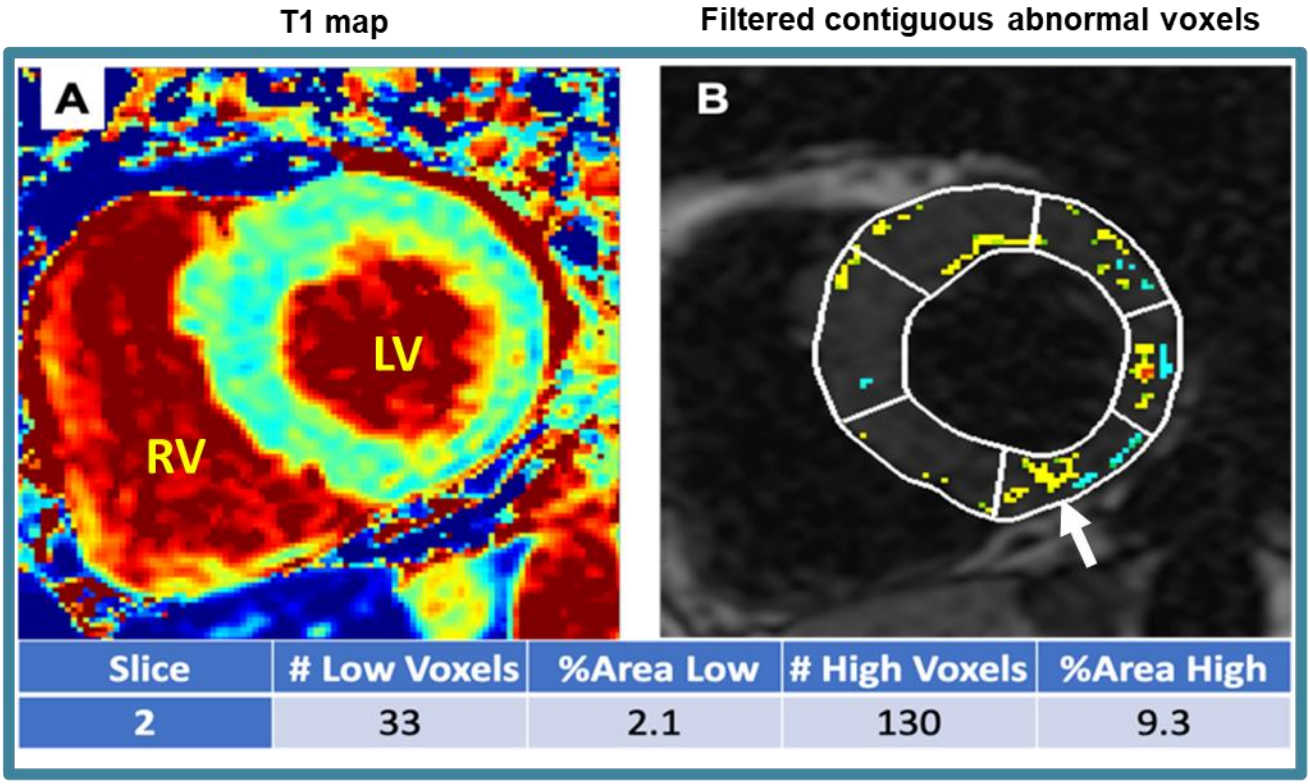

Fig 4. Conversion of colorized T1 or T2 relaxation maps into abnormal myocardium displaying only the abnormal voxels 2 std dev above or below nominal values for myocardium superimposed on grayscale slice image. (A) Typical T1 parameter map of color coded T1 value. (B) Filtered contiguous abnormal T1 voxels on an MR image. Percent abnormal myocardium is determined for each slice and the entire heart. Current Grading: Normal, <20%; Mild, 20 to 35%; Moderate, 35 to 50%; High 50 to 75%; Very High, 75+ %.

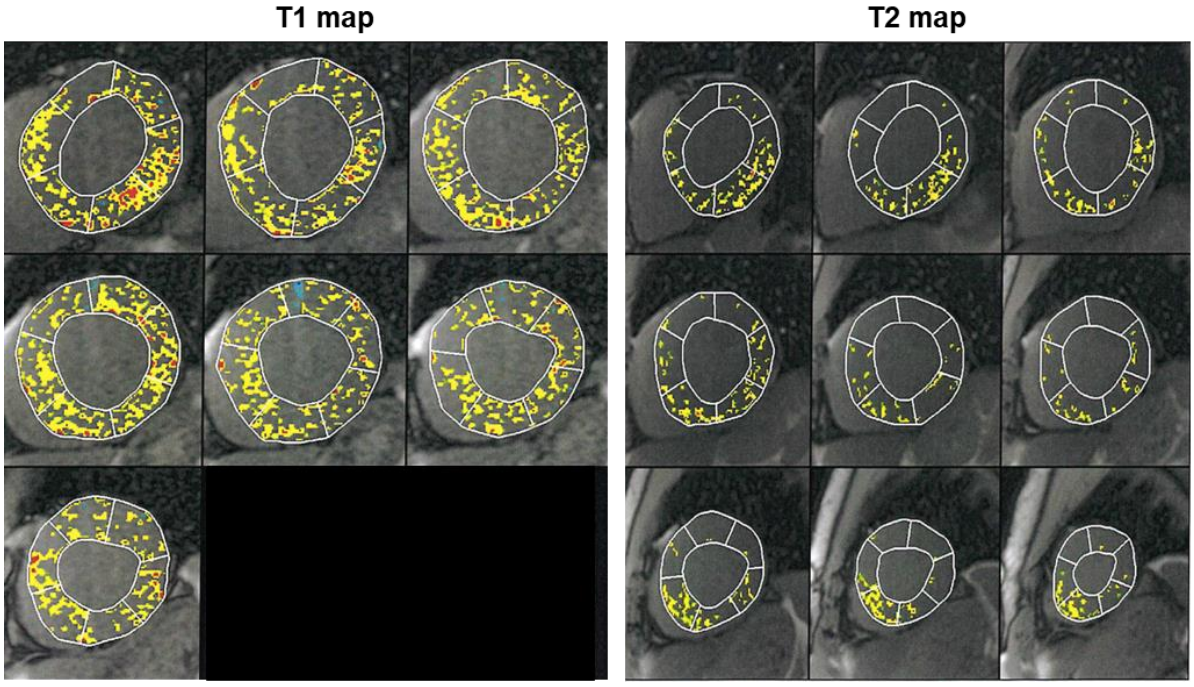

Fig. 5. A patient with hypertension and cocaine use and interventricular septum diastole at 1.5 cm is referred to rule out amyloidosis due to declining ejection fraction and increased septal thickening by echocardiography. The patients is diagnosed with dilated cardiomyopathy with moderately reduced ejection fraction, severely decreased global longitudinal strain of left ventricle, normal extracellular volume, and mildly increased T1 abnormal myocardium consistent with fibrosis.

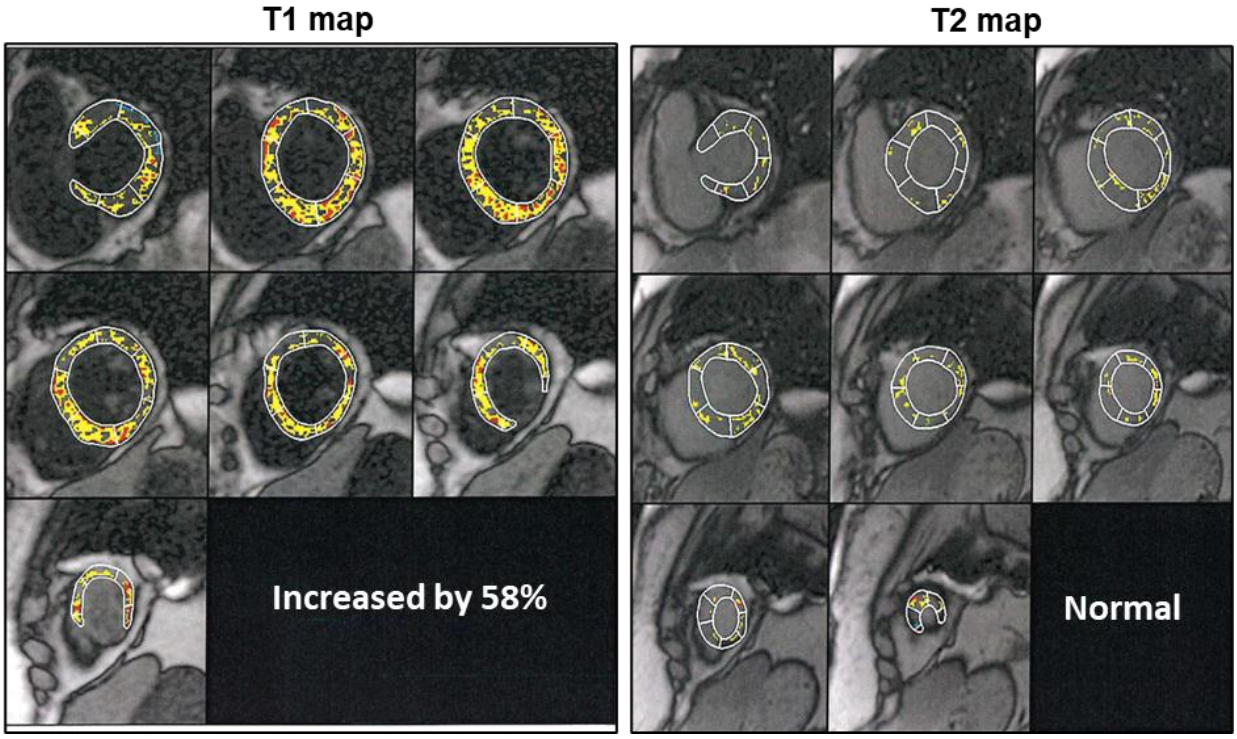

Fig. 6. A patient with carpal tunnel syndrome is referred to rule out amyloidosis. The patients is diagnosed with normal LV end diastolic volume and function with normal LV and RV global longitudinal strains. T1 abnormal myocardium (%) is highly increased associated with a marked extracellular volume increase (>3 std dev). The findings are consistent with amyloidosis.

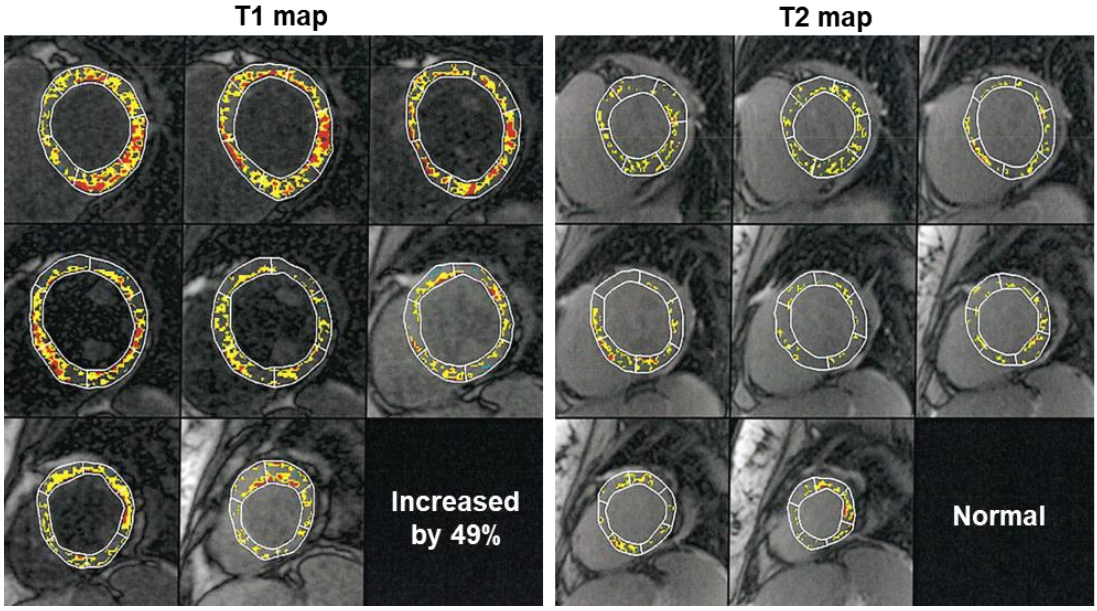

Fig 7A. A 77-year-old patient with cardiomyopathy is referred to rule out cardiac amyloidosis. Note, the LV dilates to preserve cardiac output (or EF). Increased abnormal myocardium associated with amyloid can be differentiated from diffuse fibrosis by changes in ECV and strain. In our lab, increased ECV > 3 standard deviations above nominal (i.e., ≥ 36%) is associated with amyloid infiltration. Strain decreased at higher levels fibril infiltration as noted by higher percentages T1 abnormal myocardium. The patient is diagnosed with mildly dilated LV with minimally decreased systolic function and moderately decreased LV global longitudinal strain. T1 abnormal myocardium (%) is moderately increased associated with moderately high extracellular volume increase (>3 std dev). The findings are consistent with amyloidosis.

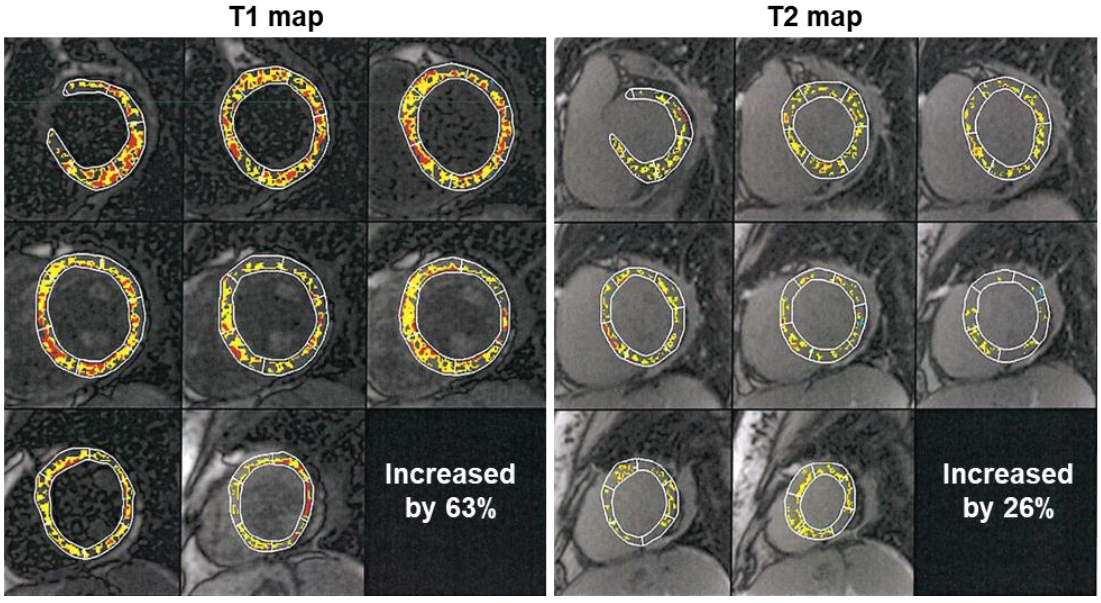

Fig 7B. A patient was followed up at 6 months after the diagnosis of cardiomyopathy to assess cardiac function and amyloid progression. While progressive amyloid infiltration can be monitored by its impact on ECV, IV access was not obtained in this patient. Direct assessment of percent T1 abnormal myocardium demonstrated considerable progression of infiltrative disease, while cardiac structure, function, and strain metrics improved with guideline directed medical management (GDMT). Using percent T1 abnormal myocardium to assess progression rather than ECV, reduced patient study time (20-30 min), and eliminated: 1) the need for recent hematocrit and serum creatinine assays, 2) placement of IV access, 3) the use of gadolinium, and 4) physician supervision. The patients was diagnosed with normal LV EDV with minimally decreased systolic function and mildly decreased LV global longitudinal strain. T1 abnormal myocardium (%) is highly increased. T2 abnormal myocardium (%) is mildly increased reflecting tissue edema. Amyloid tissue infiltration progressed (T1 abnormal myocardium: 49% to 63%) while cardiac structure, function and strain improved.

As illustrated in Fig 7 A and B, following the diagnosis of cardiac amyloid, disease progression can be monitored using ECV to assess the interstitium expansion effects of fibril infiltration. Alternatively, serial changes in native T1 map of abnormal myocardium directly reflect fibril accumulation. This metric eliminates the need for gadolinium contrast, IV access, recent hematocrit and serum creatinine levels, and physician supervision. It also shortens patient study time by

20 to 30 minutes.

6. Conclusion

Cardiac MRI offers a wide range of advanced imaging techniques and quantitative metrics to diagnose or differentiate various cardiomyopathy, ischemic disease, and myocarditis disease. It is crucial to understand that no single measurement can capture the entire picture. Our collective vision is to achieve “Equal Healthcare for All”, making strengths of cMRI accessible to all patients, regardless of hospital size, location and availability of image post-processing resources. Cardio-oncology patients will benefit from robust serial cMRI studies conducted over months to years, facilitated by an automatic workflow that minimizes personnel requirements, reduces resource demands, and enhances longitudinal quality control.

7. Image/Figure Courtesy

All images are the courtesy of Division of Cardiology, Washington University Medical School, St. Louis, MO, USA

8. References

1. Edalati M, Zheng Y, Watkins MP et al. Implementation and prospective clinical validation of AI-based planning and shimming techniques in cardiac MRI. Med Phys 2022;49:129-143.
2. Bluethmann SM, Mariotto AB, Rowland JH. Anticipating the "Silver Tsunami": Prevalence Trajectories and Comorbidity Burden among Older Cancer Survivors in the United States. Cancer Epidemiol Biomarkers Prev 2016;25:1029-36.
3. Sturgeon KM, Deng L, Bluethmann SM et al. A population-based study of cardiovascular disease mortality risk in US cancer patients. Eur Heart J 2019;40:3889-3897.
4. Strongman H, Gadd S, Matthews A et al. Medium and long-term risks of specific cardiovascular diseases in survivors of 20 adult cancers: a population-based cohort study using multiple linked UK electronic health records databases. Lancet 2019;394:1041-1054.
5. Von Hoff DD, Layard MW, Basa P et al. Risk factors for doxorubicin-induced congestive heart failure. Ann Intern Med 1979;91:710-7. 21..

Author Biography

Dr. Gregory Lanza

Professor of Medicine,
Biomedical Engineering,
and Biology and Biomedical Sciences
Washington University
School of Medicine
St Louis, MO, USA

Dr. Gregory Lanza is a Cardiologist and Professor of Medicine, Biomedical Engineering, Biology and Biomedical Sciences at the Washington University School of Medicine in St Louis. His clinical areas of interest include echocardiography and cardiac magnetic resonance imaging, with specific research interests in the development of novel nanotechnologies for biomedical molecular imaging and targeted drug delivery in cardiovascular, neurological, inflammatory, and oncological disease.

He obtained his Doctor of Philosophy from University of Georgia, Athens and his Doctor of Medicine from Northwestern University Medical School, Chicago; he did his residency at Washington University School of Medicine in St Louis. He is also a recipient of numerous grants and prestigious awards.

Free-Breathing Simultaneous Cardiac Multi-Parametric Mapping: Technical Developments and Initial Clinical Experience

Haikun Qi[a,b], Zhenfeng Lyu[a,b]
[a] School of Biomedical Engineering, ShanghaiTech University, Shanghai, China
[b] Shanghai Clinical Research and Trial Center, Shanghai, China

1. Introduction

Cardiac magnetic resonance (CMR) parametric mapping has emerged as a promising non-invasive tool for diagnosing various cardiovascular diseases [1]. The commonly used T1 and T2 mapping approaches provide valuable diagnostic information by assessing alterations of myocardial relaxation times [2]. Edema, acute ischemia and necrosis contribute to an elevation of both T1 and T2; while scar and fibrosis result in an increase specifically in T1 values [1, 3-5]. Decrease of T1 is rare, with known causes of Fabry disease and the deposition of iron or fat [3, 6, 7]. In contrast, T1ρ mapping employs a spin-lock radiofrequency pulse with a low frequency of several hundred Hertz to measure the longitudinal relaxation in a rotating frame. This distinctive methodology endows T1ρ mapping with sensitivity to variations in macromolecular content [8]. Several studies have demonstrated that T1ρ is a promising endogenous contrast for detection of focal and diffuse myocardial fibrosis [9, 10]. Compared with native T1, the increase of which is not specifically attributed to fibrosis, T1ρ may serve as a better biomarker for myocardial fibrosis. However, T1ρ CMR is challenging, especially for high field scanners, as the conventional T1ρ preparation module with rectangular tip-down, spin-lock and tip-up pulses is sensitive to B0 and B1 inhomogeneities. We have designed and optimized T1ρ preparation pulses including the adiabatically excited continuous continuous-wave spin-lock and composite spin-lock [11-13], which are robust to field inhomogeneities, making T1ρ CMR ready for clinical application.

The combination of multiple parameters holds the potential to improve the diagnostic sensitivity and bolster diagnostic confidence for suspected cardiomyopathy, as these parameters offer complementary insights into the myocardium [2, 14]. For example, by analyzing T2 and T1ρ together, the myocardial fibrosis index (mFI) [15] can be derived as the difference of the two parameters, which has been shown to be a better indicator for myocardial fibrosis than T1ρ in hypertrophic cardiomyopathy [16]. However, conventional mapping techniques measure myocardial parameters individually in separate breath-hold acquisitions and requires dummy cardiac cycles to allow for longitudinal magnetization recovery [17-19]. This practice may result in nonregistered parameter maps, prolonged scanning duration, patient discomfort, and heart rate dependency of parameter estimation.

Simultaneous multi-parametric mapping is an active research area, and numerous techniques have been proposed to improve the efficiency of data acquisition and generate co-registered parameter maps. Most simultaneous multi-parameter mapping techniques focus on cardiac T1 and T2 mapping. Among these methods, magnetic resonance fingerprinting (MRF) stands out by employing transient imaging to generate different signal evolutions for tissues with different parameter combinations and then matching the acquired signal to a simulated dictionary for parameter quantification [20-25]. Although promising, cardiac MRF relies on highly undersampled non-Cartesian trajectories due to ECG-triggering and limited breath-hold duration, which requires complex reconstruction to reduce the influence of aliasing artifacts on dictionary matching. The complex post-processing of cardiac MRF may preclude its wide clinical application. Recently, Henningsson demonstrates the feasibility of single-shot Cartesian acquisition and dictionary matching for simultaneous myocardial T1 and T2 mapping [26]. It only acquires ten time-points along the magnetization evolution and involves simplified post-processing with conventional Cartesian acquisition, and is therefore readier for clinical translation. However, the Cartesian dictionary matching based technique still requires breath-hold. A free-breathing multi-parameter mapping technique is warranted when the patients cannot

hold their breath or the acquisition time exceeds the limit of breath-hold duration.

This article introduces the techniques we recently developed for free-breathing simultaneous myocardial multi-parametric mapping and their initial clinical applications. The joint T2 and T1ρ mapping technique was based on the conventional exponential model fitting but has been optimized regarding the order of preparation pulses [27]. Following this technique, a more efficient multi-parametric technique based on single-shot Cartesian acquisition and dictionary matching was developed and validated for free-breathing simultaneous T1, T2 and T1ρ mapping with inhomogeneous B1 correction. To enable free-breathing acquisition, the diaphragm navigator (dNAV) was utilized for real-time slice tracking to correct the through-plane motion during acquisition, while the group-wise multi-contrast registration [29] was adopted to correct in-plane motion after acquisition.

2. Free-breathing joint myocardial T2 and T1ρ mapping

2.1 Technical developments

The difference between myocardial T2 and T1ρ, termed as myocardial fibrosis index, has shown to outperform other native parameters in correlating with late gadolinium enhancement in hypertrophic cardiomyopathy [15, 16]. The aim of the joint T2 and T1ρ mapping technique is to provide co-registered T2 and T1ρ maps to facilitate the calculation of mFI. The sequence diagram and post-processing steps are presented in Fig. 1. This method comprises seven electrocardiogram-triggered single-shot acquisitions, involving T2 preparation (T2-prep) with three echo times (TE) and T1ρ preparation (T1ρ-prep) with four spin-lock durations (TSL) to introduce T2 and T1ρ sensitization. Furthermore, three dummy heartbeats were interposed between two single-shot acquisitions for signal recovery, resulting in a total acquisition time of 25 cardiac cycles. The parameters for the preparation modules were: T2-prep TEs = [0, 30, 55] ms, T1ρ-prep TSLs = [2, 16, 30, 50] ms, and the spin-lock frequency was set to 350 Hz. To minimize the impact of incomplete longitudinal relaxation recovery on parameter quantification, the modules with shorter TE or TSL were acquired first. The interleaved acquisition of T2-prep and T1ρ-prep images also has benefit of reducing misalignment between the T2 and T1ρ parameter maps.

To correct respiratory motion and enable free-breathing acquisition, real-time adjustments of the imaging plane were performed utilizing a cross-pair dNAV with an empirical tracking factor of 0.6 [30, 31]. The dNAV was applied before the T2 and T1ρ preparation to avoid any influence of preparation pulses on the dNAV signal. The slice-tracking with dNAV effectively eliminates through-plane motion during the acquisition, and after acquisition, a group-wise registration approach was employed to correct any in-plane motion and align the multi-contrast images [29]. The T2 and T1ρ parameter maps were derived by fitting the images to the two-parameter exponential decay model [32, 33], and mFI was calculated as the difference between T1ρ and T2.

2.2 Clinical applications

All MR exams were performed on the 3T uMR 890 scanner (United Imaging Healthcare Shanghai, China). Figure 2 shows the parametric maps and slice-matched Late Gadolinium Enhancement (LGE) images of two patients: a 71-year-old female patient with myocardial hypertrophy; a 40-year-old male patient with hypertensive cardiomyopathy. For Patient #1, there is LGE in the inferoseptal segment, accompanied by an elevation in T2 values, thereby implying the potential manifestation of edema. Furthermore, the anterior and anterolateral segments also exhibit LGE, where the T1ρ and mFI are increased, thereby indicating the possible presence of fibrosis. For Patient #2, no LGE is found, while conspicuous increase of T1ρ and mFI values can be observed across the myocardium, suggesting there may be diffuse myocardial fibrosis in this patient.

3. Free-breathing simultaneous myocardial T1, T2 and T1ρ mapping

3.1 Technical developments

The joint T2 and T1ρ mapping technique lacks the quantification of the important parameter of T1 and requires empty cardiac cycle for signal recovery which features low acquisition efficiency. Following the two-parameter mapping technique, we developed a more efficient free-breathing multi-parametric mapping technique (FB-MultiMap) to achieve simultaneous T1, T2 and T1ρ quantification with inhomogeneous B1 correction in a single acquisition. The framework of the proposed FB-MultiMap is shown in Fig. 3,

which includes the multi-contrast image acquisition with the optimized sequence, multi-contrast image registration, dictionary generation with Bloch simulations and parameter mapping with dictionary matching. FB-MultiMap adopts single-shot Cartesian acquisition with a 2D bSSFP readout. The inversion recovery (IR), T2-prep and T1ρ-prep pulses are introduced in FB-MultiMap for sensitizing T1, T2 and T1ρ, respectively.

The precision and accuracy of parameter measurements can be influenced by the configuration of the preparatory pulses [26]. Several candidate sequences were empirically designed and compared in simulations, phantom and in vivo experiments regarding estimation accuracy and precision. The optimized FB-MultiMap sequence is demonstrated in Fig. 3, where the IR pulses are played at the first and the ninth cardiac cycles; T2-preps are played in the fifth to eighth cardiac cycles with durations = [35, 45, 55, 65] ms; T1ρ-prep with TSLs = [16, 30, 40, 50] ms are played in the 13th to 16th cardiac cycles.

The inhomogeneity of B1, particularly in high-field scanners, if not accounted for, will impact the accuracy of dictionary-based parameter estimations. Hence, besides estimating T1, T2, and T1ρ, we also measure the B1 factor for correcting the nominal flip angle. Furthermore, a variable flip angle strategy was proposed and optimized to improve sensitization of the B1 factor. Following the optimization of angle combinations, the sequence alters the flip angle after two IR pulses, the initial T2-prep pulse and the initial T1ρ-prep pulse, and the optimized four flip angles are 45°/35°/70°/50°.

Similar to the free-breathing joint T2 and T1ρ mapping technique, FB-MultiMap achieved prospective respiratory motion correction by employing dNAV to adjust the imaging plane in real-time [30, 31]. To minimize the influence of the non-selective IR on the signal of the dNAV, a slice-selective IR pulse was incorporated into the sequence, aligning with the imaging position of the dNAV. Moreover, the dNAV was played before the T2-prep and T1ρ-prep modules to avoid their interference. Subsequently, a group-wise registration method was performed to align all the multi-contrast images [29].

Parametric mapping was performed with dictionary matching, where the subject-specific dictionary was simulated with Bloch equation and the recorded R-wave intervals and trigger delays for ranges of T1, T2, T1ρ and B1. In contrast to MRF, where magnetization is modeled for each readout, the Cartesian sampling approach acquired a single image per cardiac cycle, with the primary contrast determined by the central region of k-space. As a result, the construction of the dictionary solely relied on the simulated transverse magnetization corresponding to the center of k-space.

3.2 Clinical applications

The proposed FB-MultiMap has been evaluated in phantoms [28], healthy subjects and several patients with different cardiac diseases. All MR images were acquired on the 3T uMR 890 scanner (United Imaging Healthcare Shanghai, China). Example T1, T2 and T1ρ maps at three short-axis slices of a representative healthy subject are provided in Fig. 4, where good mapping quality can be observed for FB-MultiMap with no discernable motion artifacts compared with conventional mapping methods and the multi-parametric mapping performed under breath-hold (BH-MultiMap), which is possible in healthy subjects.

Fig. 5 shows the parameter maps of four patients: a 66-year-old male patient with hypertensive cardiomyopathy; a 76-year-old female patient with myocardial hypertrophy; a 31-year-old male patient with Fabry disease; a 62-year-old male patient with chronic renal disease. Except for the patient with renal disease where the administration of gadolinium contrast agent is not applicable, the LGE images were acquired for the three mentioned patients to detect any focal enhancement. For Patient #3, the left ventricle has patchy LGE regions, where increased T1 and T1ρ values can be observed. For Patient #4, enhancement can be observed in the lateral myocardium, and the lateral T2 and T1ρ values are higher than the septal region. The T1 values are overall increased as can be observed in both MOLLI and FB-MultiMap, albeit that there is less motion blurring in FB-MultiMap compared with MOLLI. Patient #5 has been diagnosed with Fabry disease, the T1 values of whom is around 100 ms lower than the healthy subjects, while the T2 and T1ρ values are not obviously differed. Patient #6 has higher myocardial T1 and T1ρ values compared with healthy subjects, while the T2 values are not elevated.

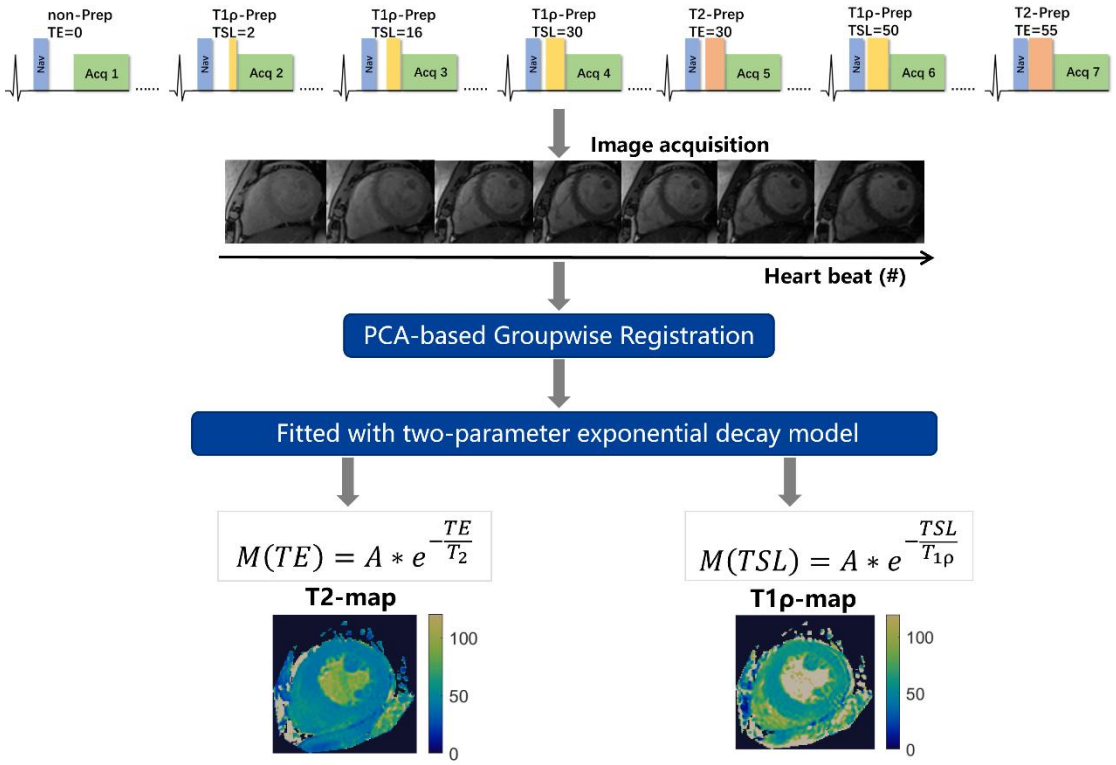

Figure 1. Sequence diagram and post-processing steps of the proposed free-breathing joint myocardial T2 and T1ρ mapping technique. This sequence has seven ECG-triggered single-shot acquisitions, with three dummy cardiac cycles inserted between two acquisitions for signal recovery, resulting in a total of 25 cardiac cycles. The T2 and T1ρ prepared images are acquired alternately. dNAV is employed for real-time prospective respiratory motion correction, followed by retrospective in-plane motion correction with group-wise image registration. Subsequently, the acquired images are fitted to the exponential decay model to derive T2 and T1ρ parameter maps.

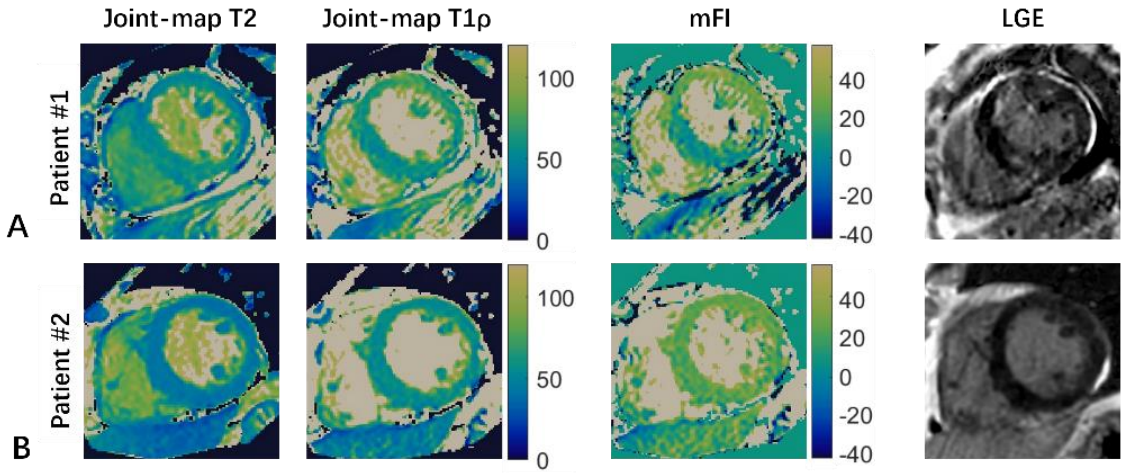

Figure 2. Parameter maps obtained with the joint T2 and T1ρ mapping method along with the LGE images for two patients. (A) a 71-year-old female patient with myocardial hypertrophy and intramural LGE in the inferoseptal, anterior and anterolateral segments; (B) a 40-year-old male patient with hypertensive cardiomyopathy without focal LGE.

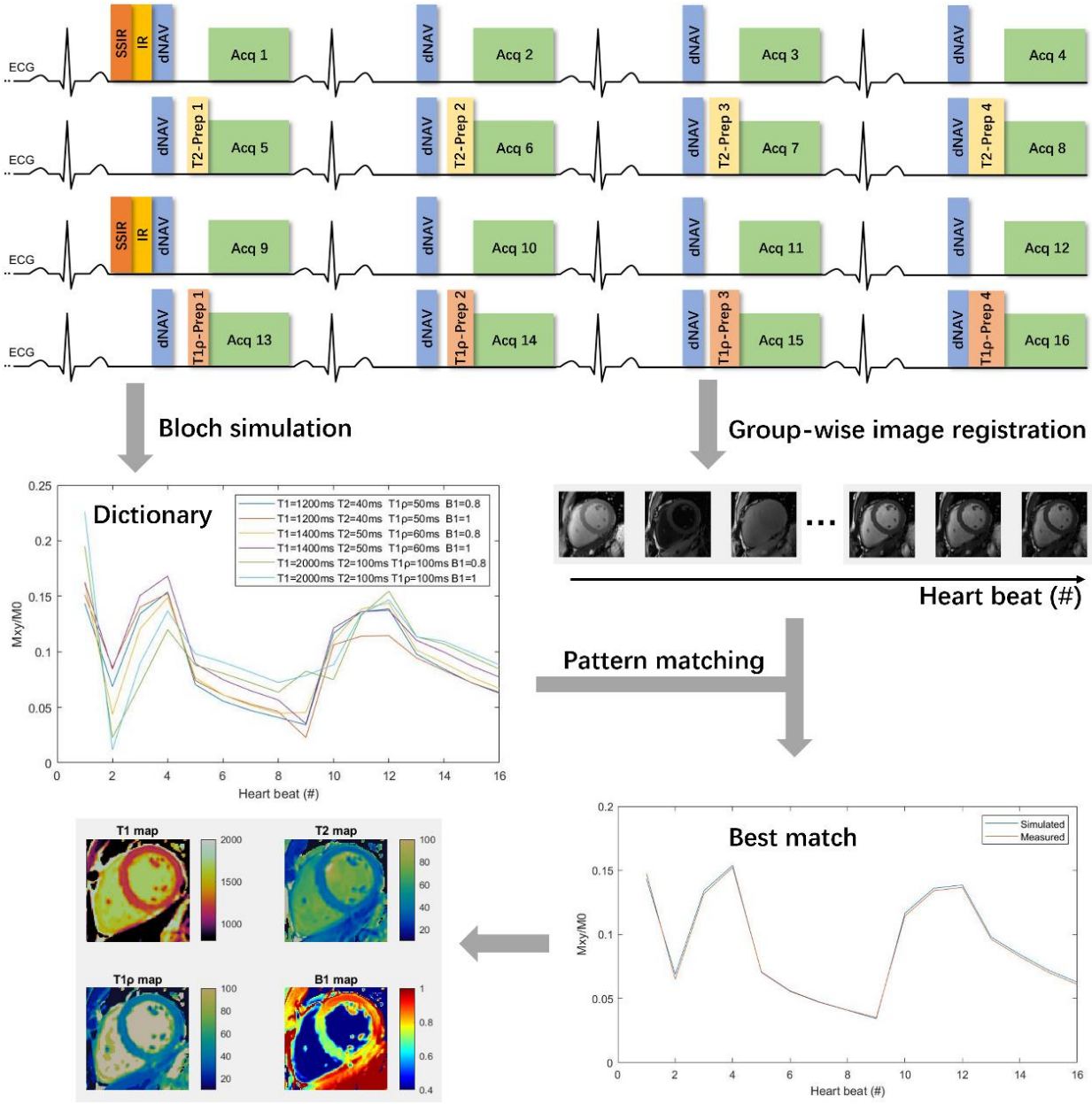

Figure 3. Sequence diagram and post-processing steps for the proposed free-breathing simultaneous myocardial T1, T2 and T1ρ mapping technique. The sequence involves the ECG-trigged diastolic acquisition of sixteen cardiac cycles using inversion recovery (IR), T2-prep, and T1ρ-prep pulses to introduce T1, T2, and T1ρ sensitization. Real-time updates of the imaging plane are performed using dNAV for prospective respiratory motion correction. The slice-selective IR (SSIR) is applied to restore the diaphragm signal. Following image acquisition, retrospective correction of in-plane motion is achieved through group-wise image registration. Subsequently, dictionary matching is performed to find the dictionary entry that best matches the acquired signal at each pixel for T1, T2, T1ρ and B1 mapping.

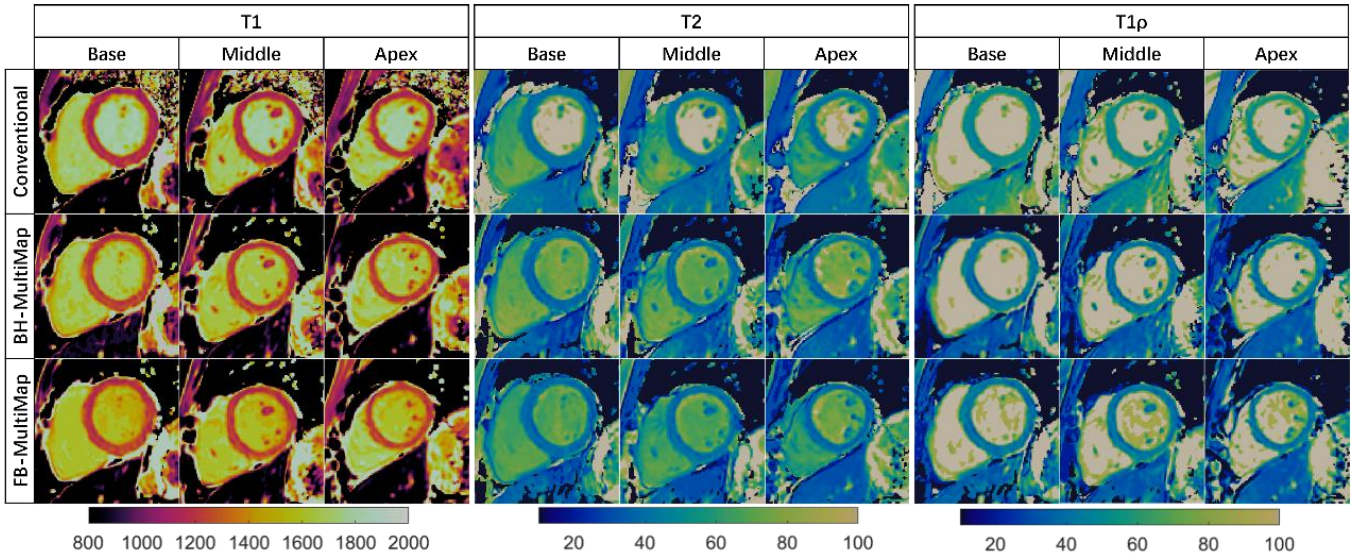

Figure 4. T1, T2, and T1ρ maps measured at three short-axis slices of a typical healthy subject using separate breath-hold mapping techniques including MOLLI, T2-prep, and T1ρ-prep bSSFP, and the proposed multi-parametric mapping technique performed under breath-hold (BH-MultiMap) and free-breathing (FB-MultiMap).

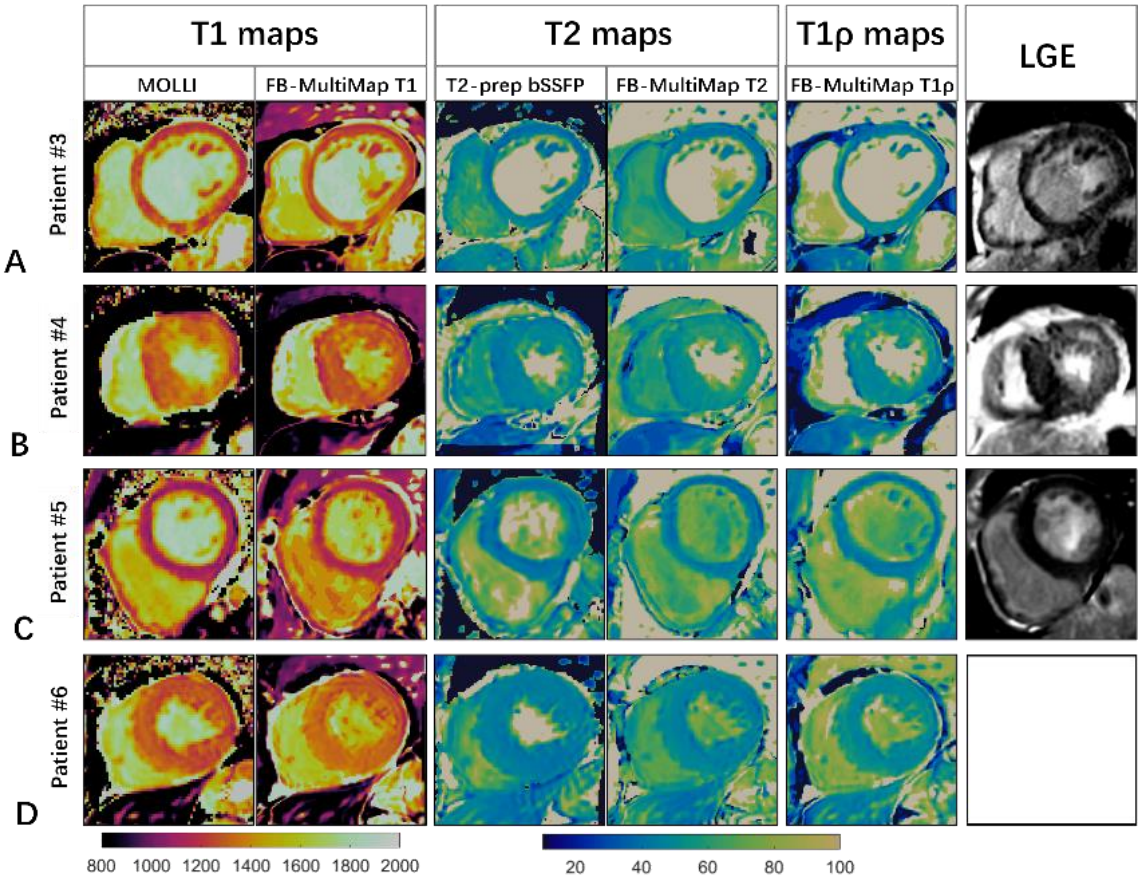

Figure 5. Parameter maps obtained with FB-MultiMap and traditional techniques of MOLLI and T2-prep bSSFP of four patients. LGE images were acquired and shown for three patients with normal renal function. (A) a 66-year-old male with hypertensive cardiomyopathy and patchy LGE; (B) a 76-year-old female patient with myocardial hypertrophy and lateral myocardial enhancement; (C) a 31-year-pld male patient with Fabry disease and no obvious LGE; (D) a 62-year-old male patient with chronic renal failure.

4. Discussion and Conclusion

Cardiac MRI has unique capability of characterizing myocardial tissue non-invasively and quantitatively compared with other imaging modalities. The myocardial parameters, including T1, T2 and T1ρ can reflect different pathological changes, and can be analyzed together to help diagnose complex cardiomyopathies. The clinical value of multi-parametric CMR has been increasing recognized. However, for estimation of multiple parameters, conventional techniques either measure the parameters individually with separate breath-hold acquisitions, which may result in unregistered parameter maps, or estimate multiple parameters in a prolonged breath-hold acquisition, which may be intolerable to patients. To overcome these limitations, we have been developing free-breathing cardiac multi-parametric mapping techniques. Notably, the proposed FB-MultiMap can generate B1-corrected T1, T2 and T1ρ maps in single efficient free-breathing acquisition of 16 heartbeats. The pathological alterations detected by FB-MultiMap agree with the conventional separate breath-hold measurements and also exhibit promising correspondence with LGE, which suggests the potential of FB-MultiMap in comprehensive myocardial tissue characterization without contrast agents.

For free-breathing multi-parametric mapping, the most challenging part would be to correct the respiratory motion and mitigate mapping errors caused by motion. As the two techniques introduced in this article, the dNAV was utilized for prospective motion correction by tracking the imaging slice in real time, followed by multi-contrast image registration for retrospective motion correction. The two-step motion correction strategy works well in healthy subjects and the preliminary patients. However, there is still room for improvement. Firstly, a fixed slice-tracking factor was adopted for the dNAV based through-plane motion correction. Adopting a patient- and slice-specific motion model trained in a calibration scan to characterize the heart motion relative to dNAV may help to further improve motion correction. Secondly, registering images with abrupt contrast changes is challenging. The model-based registration method [10, 34] which plug the physical model into the registration process to avoid the registration of different contrasts is worth exploring to improve the retrospective motion correction. Finally, the introduced techniques are for 2D imaging with limited resolution along the slice direction. The 3D high-resolution free-breathing cardiac multi-parametric mapping techniques are under development.

5. Image/Figure Courtesy

All images are the courtesy of School of Biomedical Engineering, ShanghaiTech University, Shanghai, China.

6. References

1. Messroghli DR, Moon JC, Ferreira VM, Grosse-Wortmann L, He T, Kellman P, et al. Clinical recommendations for cardiovascular magnetic resonance mapping of T1, T2, T2* and extracellular volume: A consensus statement by the Society for Cardiovascular Magnetic Resonance (SCMR) endorsed by the European Association for Cardiovascular Imaging (EACVI). J Cardiovasc Magn Reson. 2017;19(1):75.
2. Warnica W, Al-Arnawoot A, Stanimirovic A, Thavendiranathan P, Wald RM, Pakkal M, et al. Clinical Impact of Cardiac MRI T1 and T2 Parametric Mapping in Patients with Suspected Cardiomyopathy. Radiology. 2022;305(2):319-26.
3. Captur G, Manisty C, Moon JC. Cardiac MRI evaluation of myocardial disease. Heart. 2016;102(18):1429-35.
4. Ugander M, Bagi PS, Oki AJ, Chen B, Hsu L-Y, Aletras AH, et al. Myocardial edema as detected by pre-contrast T1 and T2 CMR delineates area at risk associated with acute myocardial infarction. JACC: Cardiovascular Imaging. 2012;5(6):596-603.
5. Hinojar R, Foote L, Ucar EA, Dabir D, Schnackenburg B, Higgins DM, et al. Myocardial T2 mapping for improved detection of inflammatory myocardial involvement in acute and chronic myocarditis. Journal of Cardiovascular Magnetic Resonance. 2014;16(1):1-2.
6. Kali A, Tang RL, Kumar A, Min JK, Dharmakumar R. Detection of acute reperfusion myocardial hemorrhage with cardiac MR imaging: T2 versus T2*. Radiology. 2013;269(2):387-95.
7. Pica S, Sado DM, Maestrini V, Fontana M, White SK, Treibel T, et al. Reproducibility of native myocardial T1 mapping in the assessment of Fabry disease and its role in early detection of cardiac involvement by cardiovascular

magnetic resonance. Journal of Cardiovascular Magnetic Resonance. 2014;16:1-9.

8. Muthupillai R, Flamm SD, Wilson JM, Pettigrew RI, Dixon WT. Acute myocardial infarction: tissue characterization with T1ρ-weighted MR imaging--initial experience. Radiology. 2004;232(2):606-10.

9. Thompson EW, Kamesh Iyer S, Solomon MP, Li Z, Zhang Q, Piechnik S, et al. Endogenous T1ρ cardiovascular magnetic resonance in hypertrophic cardiomyopathy. J Cardiovasc Magn Reson. 2021;23(1):120.

10. Bustin A, Toupin S, Sridi S, Yerly J, Bernus O, Labrousse L, et al. Endogenous assessment of myocardial injury with single-shot model-based non-rigid motion-corrected T1ρ mapping. J Cardiovasc Magn Reson. 2021;23(1):119.

11. Qi H, Bustin A, Kuestner T, Hajhosseiny R, Cruz G, Kunze K, et al. Respiratory motion-compensated high-resolution 3D whole-heart T1ρ mapping. J Cardiovasc Magn Reson. 2020;22(1):12.

12. Qi H, Lv Z, Xu J, Hu P. Optimization of spin-lock preparation pulses for B1 and B0 insensitive cardiac T1ρ mapping. Toronto: ISMRM; 2023. p. 4003.

13. Qi H, Lv Z, Hu J, Xu J, Botnar R, Prieto C, et al. Accelerated 3D free-breathing high-resolution myocardial T1ρ mapping at 3 Tesla. Magn Reson Med. 2022;88(6):2520-31.

14. Sanchez Tijmes F, Thavendiranathan P, Udell JA, Seidman MA, Hanneman K. Cardiac MRI Assessment of Nonischemic Myocardial Inflammation: State of the Art Review and Update on Myocarditis Associated with COVID-19 Vaccination. Radiol Cardiothorac Imaging. 2021;3(6):e210252.

15. Zhang Y, Zeng W, Chen W, Chen Y, Zhu T, Sun J, et al. MR extracellular volume mapping and non-contrast T1ρ mapping allow early detection of myocardial fibrosis in diabetic monkeys. European radiology. 2019;29:3006-16.

16. Wang K, Zhang W, Li S, Jin H, Jin Y, Wang L, et al. Noncontrast T1ρ dispersion imaging is sensitive to diffuse fibrosis: A cardiovascular magnetic resonance study at 3T in hypertrophic cardiomyopathy. Magnetic Resonance Imaging. 2022;91:1-8.

17. Baessler B, Schaarschmidt F, Stehning C, Schnackenburg B, Maintz D, Bunck AC. Cardiac T2-mapping using a fast gradient echo spin echo sequence - first in vitro and in vivo experience. J Cardiovasc Magn Reson. 2015;17(1):67.

18. Sprinkart AM, Luetkens JA, Traber F, Doerner J, Gieseke J, Schnackenburg B, et al. Gradient Spin Echo (GraSE) imaging for fast myocardial T2 mapping. J Cardiovasc Magn Reson. 2015;17(1):12.

19. Messroghli DR, Radjenovic A, Kozerke S, Higgins DM, Sivananthan MU, Ridgway JP. Modified Look-Locker inversion recovery (MOLLI) for high-resolution T1 mapping of the heart. Magn Reson Med. 2004;52(1):141-6.

20. Liu Y, Hamilton J, Rajagopalan S, Seiberlich N. Cardiac Magnetic Resonance Fingerprinting: Technical Overview and Initial Results. JACC Cardiovasc Imaging. 2018;11(12):1837-53.

21. Cruz G, Jaubert O, Qi H, Bustin A, Milotta G, Schneider T, et al. 3D free-breathing cardiac magnetic resonance fingerprinting. NMR Biomed. 2020;33(10):e4370.

22. Qi H, Bustin A, Cruz G, Jaubert O, Chen H, Botnar RM, et al. Free-running simultaneous myocardial T1/T2 mapping and cine imaging with 3D whole-heart coverage and isotropic spatial resolution. Magn Reson Imaging. 2019;63:159-69.

23. Phair A, Cruz G, Qi H, Botnar RM, Prieto C. Free-running 3D whole-heart T1 and T2 mapping and cine MRI using low-rank reconstruction with non-rigid cardiac motion correction. Magn Reson Med. 2023;89(1):217-32.

24. Hamilton JI, Jiang Y, Chen Y, Ma D, Lo WC, Griswold M, et al. MR fingerprinting for rapid quantification of myocardial T1, T2, and proton spin density. Magn Reson Med. 2017;77(4):1446-58.

25. Milotta G, Bustin A, Jaubert O, Neji R, Prieto C, Botnar RM. 3D whole-heart isotropic-resolution motion-compensated joint T1/T2 mapping and water/fat imaging. Magn Reson Med. 2020;84(6):3009-26.

26. Henningsson M. Cartesian dictionary-based native T1 and T2 mapping of the myocardium. Magn Reson Med. 2022;87(5):2347-62.

27. Miao Q, Lv Z, Hua S, Zhang Z, Xu J, Hu P, et al. Free-breathing simultaneous myocardial T2 and T1ρ mapping for non-contrast assessment of uremic cardiomyopathy. Toronto: ISMRM; 2023. p. 1433.

28. Lv Z, Hua S, Guo R, Shi B, Hu P, Qi H. Free-Breathing Simultaneous Native Myocardial T1, T2, and T1ρ Mapping with Cartesian Acquisition and Dictionary Matching. Toronto: ISMRM; 2023. p. 0179.

29. Tao Q, van der Tol P, Berendsen FF, Paiman EHM, Lamb HJ, van der Geest RJ. Robust motion correction for myocardial T1 and extracellular volume mapping by principle component analysis-based groupwise image registration. J Magn Reson Imaging. 2018;47(5):1397-405.

30. Guo R, Cai X, Kucukseymen S, Rodriguez J, Paskavitz A, Pierce P, et al. Free-breathing simultaneous myocardial T1 and T2 mapping with whole left ventricle coverage. Magn Reson Med. 2021;85(3):1308-21.

31. Giri S, Shah S, Xue H, Chung YC, Pennell ML, Guehring J, et al. Myocardial T2 mapping with respiratory navigator and automatic nonrigid motion correction. Magn Reson Med. 2012;68(5):1570-8.

32. Stoffers RH, Madden M, Shahid M, Contijoch F, Solomon J, Pilla JJ, et al. Assessment of myocardial injury after reperfused infarction by T1ρ cardiovascular magnetic resonance. J Cardiovasc Magn Reson. 2017;19(1):17.

33. Akcakaya M, Basha TA, Weingartner S, Roujol S, Berg S, Nezafat R. Improved quantitative myocardial T2 mapping: Impact of the fitting model. Magn Reson Med. 2015;74(1):93-105.

34. Xue H, Shah S, Greiser A, Guetter C, Littmann A, Jolly MP, et al. Motion correction for myocardial T1 mapping using image registration with synthetic image estimation. Magn Reson Med. 2012;67(6):1644-55.10. Abedi V, Goyal N, Tsivgoulis G, Hosseinichimeh N, Hontecillas R, Bassaganya-Riera J, Elijovich L, Metter JE, Alexandrov AW, Liebeskind DS, Alexandrov AV, Zand R. Novel Screening Tool for Stroke Using Artificial Neural Network. Stroke. 2017 Jun;48(6):1678-1681. doi: 10.1161/STROKEAHA.117.017033. Epub 2017 Apr 24. PMID: 28438906.

Author Biography

Dr. Haikun Qi

Professor
School of Biomedical Engineering, ShanghaiTech University, Shanghai, China
Shanghai Clinical Research and Trial Center, Shanghai, China

Dr. HaiKun Qi is a tenure-track Assistant Professor at the School of Biomedical Engineering, ShanghaiTech University. She obtained her Ph.D. in Biomedical Engineering in 2018 from Tsinghua University, China and worked as a postdoctoral fellow at King's College London, UK from 2018 to 2021. Her research interest lies in developing fast and/or quantitative MRI techniques for cardiovascular diseases. She has published more than 35 papers in the field of MRI and served as reviewer for several high-quality journals and conferences of medical imaging. She is also the principal investigator of several projects and grants, including a grant from the National Natural Science Foundation of China.

Expert Interview: Cardiac Imaging, Inc. Interview with Jens Huettges

Jens Huettges [a]
[a] Chief Technology Officer at Cardiac Imaging, Inc.

Interviewer: Joshua Wiley (JW)

JW: Tell me about your business and why there is a need for mobile Cardiac PET imaging?

JH: "There is a need for mobile Cardiac PET (Positron Emission Tomography) imaging services, particularly in areas with low population density and limited access to advanced medical facilities. There are challenges faced by smaller towns and rural areas where the availability of high-end medical equipment and specialized services like Cardiac PET is scarce. These challenges are due to financial constraints, lack of patient volume, and difficulties in acquiring necessary isotopes."

CII, in collaboration with United Imaging has addressed these challenges with mobile Cardiac PET imaging. CII brings expertise, equipment quality, isotopes, and knowledge to make the Cardiac PET service successful. A specialized trailer was designed with the required equipment to overcome hurdles like power availability at remote sites. The company also utilizes fast internet connectivity for data processing and quality control off-site. By providing their own staff, they offer a comprehensive service that doesn't burden the local facilities.

Jens also discussed the advantage of Cardiac PET imaging for patients in low-density areas, particularly older patients, where access to high-quality cardiac diagnostics can significantly impact patient care. He explains that their use of updated technology, such as CFR (Coronary Flow Reserve) measurements, leads to improved accuracy, image quality, and better patient outcomes compared to older systems that may still be in use in some locations.

JW: What types of patients benefit from your cardiac PET service?

JH: "The importance of higher sensitivity and specificity provided by their exams, which allow for more accurate characterization of patients' conditions. This leads to better treatment decisions, ensuring that patients receive the appropriate treatment when needed and avoiding unnecessary treatments when they're not required."

Jens highlights the significance of quantification software and research in the PET field, which allows for predictive diagnosis, patient management, and care optimization.

Looking to the future, CII aims to provide solutions for a wide range of cardiac needs. They offer both mobile and fixed-site services, and they're actively involved in supporting physicians and facilities. He expresses the vision of making cardiac PET scans more accessible to patients, replacing older modalities with state-of-the-art technology.

JW: What are the attributes of cardiac PET perfusion that contribute to the high quality of cardiac PET perfusion images?

JH: Jens discusses several factors that contribute to the quality of cardiac PET images:

1. Understanding the Workflow: A deep understanding of the workflow is crucial in nuclear medicine. This involves knowing how the process works and handling various elements effectively.

2. Patient Preparation: Patient cooperation is essential for minimizing movement during scans. The patients should be instructed not to move much, as patient motion can affect image quality significantly.

3. Quality of Scanner: While the scanner is a key factor, it's not the sole contributor. Having a high-quality scanner is important, but it's only one part of the equation.

4. High Sensitivity: High sensitivity in producing quality images. Higher sensitivity leads to more counts for image reconstruction, resulting in clearer images.

5. Image Reconstruction: Image reconstruction with higher counts improves the clarity of the images, enhancing the overall quality.

6. Quantification: The importance of quantification, which

is a significant aspect of nuclear medicine. Precise and reliable quantification is challenging but crucial for accurate functional assessments.

7. Functionality vs. Resolution: While nuclear medicine might not always focus on achieving high-resolution images, functional assessment is critical. This is particularly relevant in cardiac PET perfusion imaging.

JW: Why do you think that cardiac PET myocardial perfusion imaging is not more widely utilized?

JH: "There are several advantages of cardiac PET imaging over other methods, such as lower radiation doses, faster scans, and the absence of residual radioactivity after the procedure."

Despite these benefits, he outlines the challenges that hinder widespread adoption:

1. Reimbursement Variability: Reimbursement for cardiac PET varies across different regions in the US, making it less accessible in some areas due to financial considerations.

2. Provider Willingness: Not all healthcare providers are willing to invest in or pay for cardiac PET scans, which could impact the technology's penetration in the market.

3. Coexistence with SPECT: Jens suggests that while cardiac PET is advancing, SPECT (Single Photon Emission Computed Tomography) will likely still be around in the next decade as certain medical communities continue to work on it.

4. Isotope Costs: The cost of isotopes used in cardiac PET is a significant factor. These isotopes have a constant cost, regardless of patient volume, and this can affect the financial feasibility of adopting the technology.

5. Geographical Density: The viability of adopting cardiac PET also depends on the population density of a given area. In more densely populated regions, there's a higher likelihood of accumulating enough patients to make the technology financially sustainable.

JW: Where do you see the use of Cardiac PET in the next few years?

JH: 1. Expansion and Attractiveness of Business Model: Jens mentions that their business is expanding, and they have plans to introduce their cardiac PET services in more states. The rate that CII is growing indicates that there's a demand for this technology among healthcare providers. The attractiveness of their business model suggests that physicians and healthcare facilities see value in offering cardiac PET services to their patients.

2. Interest and Education in PET Technology: There is a growing interest in cardiac PET technology, seminars and conferences are focused on discussing PET technology and its applications. This interest implies that the medical community is recognizing the potential benefits and advancements that cardiac PET can bring to patient care and disease management.

3. Higher Sensitivity and Specificity: Cardiac PET is known for its higher sensitivity and specificity compared to SPECT (Single Photon Emission Computed Tomography). This means that cardiac PET can provide more accurate and detailed information about the physiological and functional aspects of the heart. This improved accuracy can lead to better disease detection, diagnosis, and treatment planning.

4. Disease Prevention and Early Detection: Cardiac PET can play a significant role in disease prevention and early detection. By providing accurate and detailed images of the heart's function and blood flow, it can help identify cardiac issues at earlier stages. Early detection allows for timely intervention and treatment, potentially preventing the progression of diseases and improving patient outcomes.

5. Cost Savings and Efficient Resource Allocation: The higher accuracy of cardiac PET can lead to more targeted and effective treatment plans. This, in turn, can result in better patient outcomes and potentially reduce the need for costly interventions and hospitalizations that might have otherwise been necessary with less accurate imaging methods.

6. Patient Experience and Safety: Cardiac PET offers benefits like lower radiation doses and faster scan times compared to certain alternatives. This improved patient experience can lead to greater patient satisfaction and reduced stress during diagnostic procedures. Moreover, the absence of residual radioactivity after the procedure eliminates the need for patients to wait before returning home.

7. Challenges and Market Penetration: Despite the advantages of cardiac PET, Jens acknowledges that challenges exist in terms of reimbursement variability, provider willingness to invest in the technology, and the need for sufficient patient volume in some areas. Overcoming these challenges is crucial to making cardiac PET more

accessible across different regions and healthcare settings.

Cardiac PET holds promise in disease prevention, accurate diagnostics, patient experience improvement, and potential cost savings for the healthcare system. While challenges exist, the growing interest, expanding business, and higher accuracy of cardiac PET suggest that it is an important technology for the future of medical imaging and patient care.

Expert's Biography

Jens Huettges
Chief Technology Officer,
Cardiac Imaging, Inc.

Jens Huettges joined Cardiac Imaging Inc in 2020 as the Chief Technology Officer (CTO) with now 2 decades of nuclear medicine experience. As CTO, Jens is responsible for acquiring, maintaining, servicing and improving all Cardiac Imaging Inc equipment including: PET and PET/CT scanners, mobile imaging trailers, digital infrastructure.

Cardiac Imaging, Inc. (CII) is a leading provider of PET cardiology imaging services in the United States performing Rubidium-82 PET myocardial perfusion imaging (MPI) exams. CII offers the latest cardiac technology including the uMI® 550 mobile digital PET/CT system. CII's mission is to bring the latest cardiac technology to cardiologists and their patients. We had an opportunity to talk to Jens Huettges, Chief Technology Officer about PET MPI imaging.

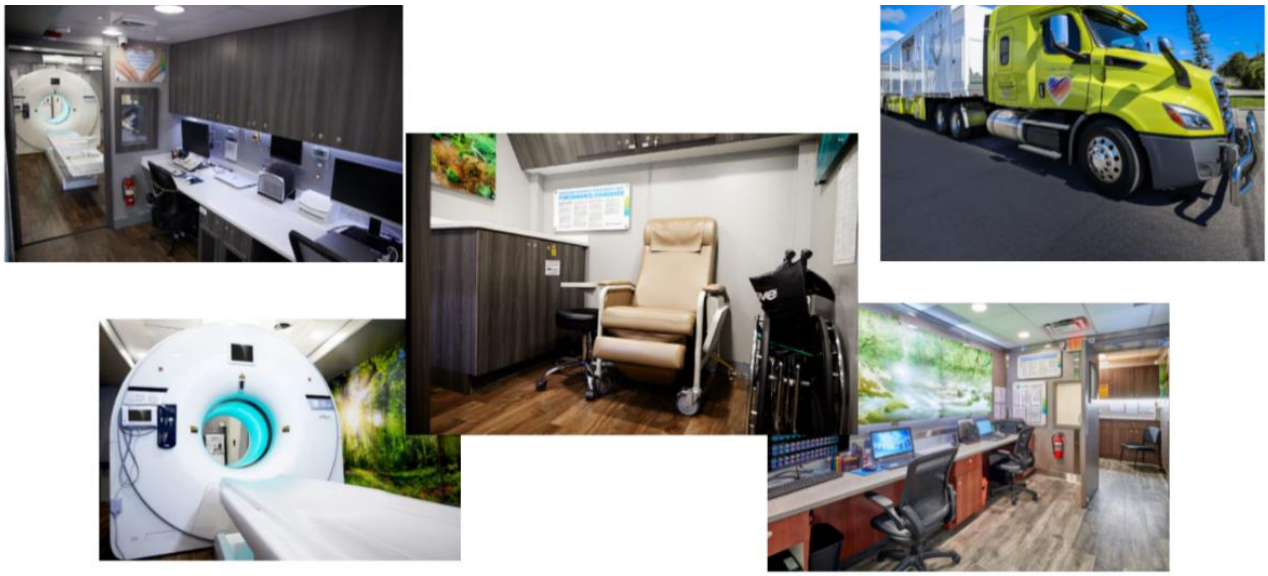

PASSION for CHANGE

©2023 United Imaging Healthcare Co., Ltd. All rights reserved.

If you have any questions about the magazine, or simply wish to reach out to us for any other reasons, you are welcome to contact us at the following email address: uinnovation-global@united-imaging.com